DEVELOPMENT OF MAGNETIC LEVITATION-BASED SENSITIVE ASSAYS

A Thesis Submitted to
the Graduate School of Engineering and Sciences of
Izmir Institute of Technology
in Partial Fulfillment of the Requirements for the Degree of

DOCTOR OF PHILOSOPHY

in Bioengineering

by
Sena YAMAN

July 2020
IZMIR

ACKNOWLEDGEMENTS

First and foremost, I wish to express my sincere gratitude to my supervisor Assist. Prof. Dr. H. Cumhur TEKİN for the guidance, encouragement, and immense knowledge he has provided over four years for my Ph.D. thesis. Also, I wish to express my special thanks to my co-supervisor Assoc. Prof. Dr. M. Cem ERGON for his valuable critics and comments.

I wish to show my great thankfulness to the members of my thesis progress and dissertation committee, Assoc. Prof. Dr. Engin ÖZÇİVİCİ, Assoc. Prof. Dr. Sinan GÜVEN, Assoc. Prof. Dr. Yaşar AKDOĞAN, and Prof. Dr. Haluk KÜLAH, for giving their valuable time, comments, and contributions for this thesis. I would also like to acknowledge the lectures that I have received from the faculty members of the Biotechnology and Bioengineering Department, IZTECH, during this Ph.D. program.

I would like to thank the members of the Laboratory of Biomedical Micro and Nanosystems (LBMS) for creating a very friendly working environment. I thank my colleague Kerem Delikoyun for fabricating the holographic microscopy platform. Also, I wish to thank Müge Anıl İnevi and Öykü Sarıgil from Özçivici Lab for providing tumor cell lines for the magnetic levitation-integrated holographic measurements.

I wish to acknowledge the financial support provided by the Scientific and Technical Council of Turkey (116M298) and the Izmir Institute of Technology Research Fund (2016IYTE68-BAP).

Last but not least, I would like to express my deepest gratitude to my beloved mother, father, and brother for their endless love throughout my life. I always felt their emotional support during the ups and downs of my Ph.D. journey.

ABSTRACT

DEVELOPMENT OF MAGNETIC LEVITATION-BASED SENSITIVE ASSAYS

Magnetic levitation (MagLev), in which an object is levitated with no support other than magnetic force and buoyancy force, is a powerful tool employed in many applications regarding the characterization of materials, biosensing of macromolecules, separation of cells, and monitoring of cellular events. Levitation of an object in MagLev depends on magnetic susceptibility and density of that object relative to its surrounding medium. In this thesis, MagLev-based miniaturized and affordable assay formats for biomolecule detection and cell separation were investigated. In this regard, a novel biomarker method detection in MagLev was developed using polymer microspheres as three-dimensional (3D) assay surfaces to capture target proteins and magnetic nanoparticles to label the captured target on the microspheres. Levitation heights of microspheres conjugated to the protein and magnetic nanoparticles were distinctly different than those of without protein. Thus, levitation height of change of microspheres was precisely measured to convert the magnetic susceptibility change of microspheres into protein concentration. The principle developed for a biotinylated target protein was then investigated by designing sandwich immunoassays using model protein biomarkers: mouse immunoglobulin G and human cardiac troponin I. The developed assays enabled a protein detection range of femtogram-microgram per milliliter. In addition to biomolecule detection, using a lensless holographic microscopy-integrated MagLev platform three different cell lines, bone marrow stem cells (D1 ORL UVA), breast cancer cells (MDA-MB-231), and human monocyte cells (U-937), were distinguished based on their density. The results revealed that the methods developed here could contribute to the MagLev-based sensitive and inexpensive bioanalytical applications.

ÖZET

MANYETİK LEVİTASYON PRENSİBİNE DAYALI ANALİZ YÖNTEMLERİNİN GELİŞTİRİLMESİ

Manyetik levitasyon (MagLev) -bir nesnenin yalnızca manyetik kuvvet ve kaldırma kuvveti aracılığıyla havada askıda tutulması- malzemelerin karakterizasyonu, makromoleküllerin biyo-algılanması, hücrelerin ayrıştırılması ve hücresel olayların izlenmesi ile ilgili birçok uygulamada kullanılmış etkili bir araçtır. MagLev'de bir nesnenin levitasyon yüksekliği, nesnenin içerisinde bulunduğu ortama kıyasla sahip olduğu manyetik duyarlılığa ve özkütleye bağlıdır. Bu tezde, biyomolekül tespiti ve hücre ayrıştırılması için MagLev-tabanlı minyatür ve uygun fiyatlı analiz yöntemlerinin geliştirilmesi araştırılmıştır. Bu bağlamda, hedef proteini üç boyutlu (3B) polimer mikrokürecik yüzeyi üzerinde yakalayarak ve mikrokürecik üzerinde yakalanan proteini manyetik nanoparçacıklar ile etiketleyerek MagLev'de yeni bir biyobelirteç tespit yöntemi geliştirilmiştir. Protein ve manyetik nanoparçacık konjüge edilmiş mikroküreciklerin levitasyon yüksekliği, proteinsiz olanlardan belirgin şekilde farklı bulunmuştur. Bu kapsamda, mikroküreciklerin levitasyon yüksekliği değişimi, mikroküreciklerin manyetik duyarlılık değişimini protein konsantrasyonuna dönüştürmek amacıyla hassas bir biçimde ölçülmüştür. İlk olarak biyotinile edilmiş bir hedef protein için kanıtlanan prensip, sonrasında model protein biyobelirteçleri olan fare immünoglobulin G ve insan kardiyak troponin I molekülleri için tasarlanan immüno tahliller ile araştırılmıştır. Geliştirilen tahlil formatları, mililitre başına femtogram-mikrogram aralığında protein tespitine imkan sağlamıştır. Biyomolekül tespitine ek olarak, lenssiz holografik mikroskopi ile entegre MagLev platformu kullanılarak üç farklı hücre hattı, kemik iliği kök hücresi (D1 ORL UVA), meme kanseri hücresi (MDA-MB-231) ve insan monosit hücresi (U-937), yoğunluklarına göre ayırt edilmiştir. Yapılan çalışmaların sonuçları, bu tezde geliştirilen yöntemlerin MagLev-tabanlı hassas ve ucuz biyoanalitik uygulamalara katkıda bulunabileceğini göstermiştir.

TABLE OF CONTENTS

LIST OF FIGURES

Figure **Page**

Figure **Page**

Figure **Page**

Figure **Page**

LIST OF TABLES

Table **Page**

LIST OF ABBREVIATIONS

s-PMS	Streptavidin-coated polymer microsphere
s-MNP	Streptavidin-coated magnetic nanoparticle
b-BSA	Biotinylated bovine serum albumin
BSA	Bovine serum albumin
CAD	Computer-aided design
CMOS	Complementary metal-oxide-semiconductor
CV	Coefficient of variation
ELISA	Enzyme-linked immunosorbent assay
FBS	Fetal bovine serum
FEM	Finite element modeling
Gd	Gadolinium
HologLev	Lensless holographic microscopy-integrated magnetic levitation
IgG	Immunoglobulin G
LOD	Limit of detection
MagLev	Magnetic levitation
POC	Point-of-care
PBS	Phosphate-buffered saline
PBST	Phosphate-buffered saline containing 1% (v/v) Tween
PBSP	Phosphate-buffered saline containing 1% (w/v) Pluronic
PBSP-BSA	Phosphate-buffered saline containing 1% (w/v) Pluronic and 1% (w/v) BSA
ROUT	Robust Regression and Outlier Removal

CHAPTER 1

INTRODUCTION

A biomarker (or biological marker), which is an identifiable characteristic of a biological process in the body (Balogh et al., 2010), has been the focus of epidemiologists, physicians, and scientists to study human diseases (Brody, 2016; Honardoost et al., 2018; Selleck et al., 2017). The translation of biomarkers into clinical practice has been accelerated over the years (Figure 1.1) (Gosho et al., 2012). The National Institute of Health defines biomarker as "a characteristic used to measure and evaluate objectively normal biological processes, pathogenic processes, or pharmacological responses to a therapeutic intervention" (Biomarkers Definitions Working et al., 2001). In practice, biomarker provides dynamic and powerful insight for i. early diagnosis, ii. monitoring progress, regression and reoccurrence of diseases, and iii. response and resistance to the therapies (Mayeux, 2004). It can be measured on biological media (e.g., blood, cerebrospinal fluid, saliva, or urine) (Timbrell, 1998), or from a recording (e.g., blood

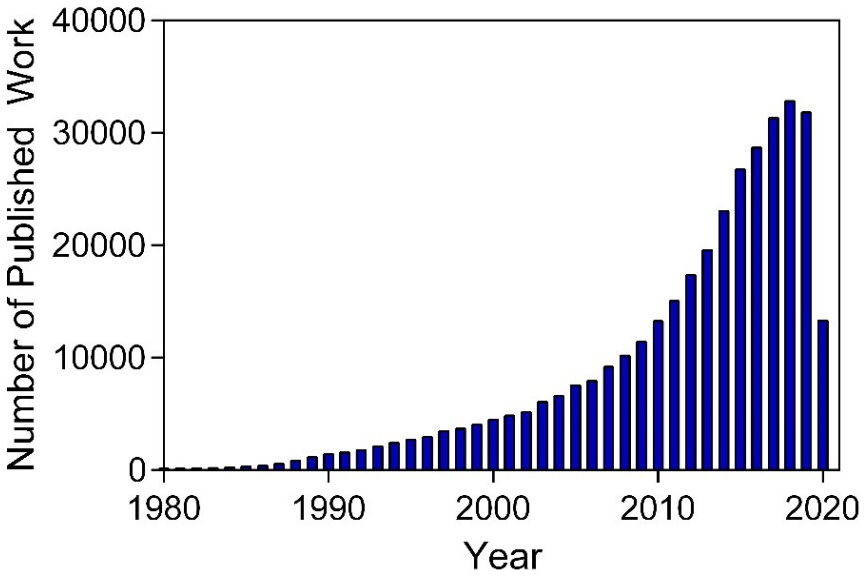

Figure 1.1. The number of published research activity searched with "clinical biomarkers" query in the PubMed database.

pressure) (Desai et al., 2006) or an imaging test (CT scan) (Gorodeski et al., 2011) of a person.

Biomarkers have been proved to be important parameters in showing the severity or presence of diseases in the body, such as cardiovascular diseases (Vasan, 2006), genetic and immunological disorders (Li et al., 2013a), cancer (Henry and Hayes, 2012), infection (Martínez-Sagasti et al., 2018), and exposure to environmental factors (e.g., radiation) (Zeegers et al., 2017). Altered level or activity of a biomarker is often related to a condition in the body. Blood sugar in diabetes (Krentz and Hompesch, 2016), HER2 protein in breast cancer (Gohring et al., 2010), or troponins in cardiovascular dysfunction (Battistoni et al., 2012) are among the well-known and mostly measured disease biomarkers. Clinically relevant protein biomarker detection in centralized laboratories is mostly achieved by enzyme-linked immunosorbent assay (ELISA) (Manole et al., 2018). However, conventional ELISA requires expensive kits, time-requiring washing and incubation cycles, and bulky plate readers (Hosseini et al., 2018) that limit its competency in off -laboratory applications, such as point of care (POC) testing, which should be applied at the bedside of a patient (Ji et al., 2016). On the contrary, novel biochemical analyzers, such as micro-total analysis systems (μTAS) or the so-called 'lab-on-a-chip' (LOC) devices where all steps of an analysis are integrated on a single chip, are strong candidates for being the new generation testing platforms by offering miniaturization, portability, fast and precise measurement, reduced sample/reagent volume, integration, and automation (Castillo-León and Svendsen, 2014). Protein detection based on capturing target molecules onto free-flowing beads that are biofunctionalized with small affinity ligands has evolved as new generation assay strategies in μTAS and LOC devices instead of flat assay surfaces of classical ELISA (Kan et al., 2020). Beads, as solid substrates, offer high surface to volume ratio, high-throughput, high binding capacity, and multiplex measurements. 3D- surfaces of beads enhance sensitivity, lower limits of detection, and ensure obtaining test results in a much shorter time (such as less than an hour) (Chou et al., 2012) compared to ELISA, which may take several hours to 2 days (Rissin et al., 2010).

Apart from detecting disease-related proteins, examining whole cells could provide valuable information regarding the health status of a patient (Seumois and Vijayanand, 2019). For instance, detection of cancer biomarkers circulated in the blood (e.g., circulating tumor cells, circulating tumor DNA, circulating cell-free DNA) serves as “liquid biopsy” (Chen et al., 2019). It is a simple and minimally invasive method that

monitors the patient's blood regarding the tumor and efficiency of the therapeutic strategy (Palmirotta et al., 2018). However, circulating tumor cells as whole-cell biomarkers present at a low abundance in a heterogeneous environment (Lim et al., 2019). Therefore, development of sensitive, easy-to-use, and cost-effective cell separation methods is important for patients to get the most appropriate therapy as well as clinical diagnosis (Wang, 2017). Traditionally, clinically relevant cells are enriched, identified or separated based on surface markers expressed on their cell membrane (e.g., EpCAM and CD34) (Bantikassegn et al., 2015; Wojciechowski et al., 2008). Mostly utilized technologies that target those markers are fluorescent-activated cell sorting (FACS) and magnetic-activated cell sorting (MACS) (Miltenyi et al., 1990). In the case of FACS, bulky, expensive and complex operation scheme is required (Wolff et al., 2003). Although the MACS technique is simple, it may cause the dissociation of cells and non-specific cell capture (Hu et al., 2016). Cell manipulation in miniaturized platforms provides novel functionalities such as controllable transport, separation, analysis, and handling of single cells in microscale (Xia et al., 2005). Besides, label-free techniques in miniaturized systems that distinguish cells based on intrinsic properties of cells (e.g., density, size, shape and compressibility) avoid the use of biochemical markers (Gossett et al., 2010).

Among the various promising technologies used in miniaturized systems for macromolecules and cells, magnetic forces are advantageous as they can provide contactless and power-free manipulation applied with a simple permanent magnet (Yaman et al., 2018). Magnetic levitation is a special case of magnetophoresis where the object levitates in a non -homogeneous magnetic field under the balance of magnetic and buoyancy forces acting on that particle (Ge et al., 2019). Levitation height of an object inside a non-uniform field depends on the relativity of magnetic susceptibility and density of that object compared to the medium it levitates inside (e.g., paramagnetic liquid), and can be tracked at a single-particle level (Tasoglu et al., 2015). So far, magnetic levitation has been successfully utilized in several work regarding the analysis of macromolecules (e.g., plasma proteins (Ashkarran et al., 2020)), cells (e.g., blood and tumor cells (Durmus et al., 2015)) and the bead-based biomarker detection (e.g., Interleukin 6, Syphilis, Hepatitis C and Chagas disease antibodies (Andersen et al., 2017; Castro et al., 2018; Subramaniam et al., 2015)).

In this study, it was aimed to develop sensitive fast, affordable, and miniaturized assays for protein biomarker detection and cell separation/analysis using magnetic levitation technology. For protein detection experiments, polymer microspheres were

designed as mobile assay surfaces to capture target proteins, and magnetic nanoparticles were designed as magnetic labels that significantly increase magnetic susceptibility of protein-microsphere complex compared to no protein- carrying microspheres. Magnetic susceptibility change regarding the magnetic particle attachment was used as a marker to estimate the amount of biomarker present in the sample solution. For cell separation, the changes in density were utilized as a physical biomarker in lensless holographic microscopy-integrated magnetic levitation platform for label-free, portable and low-cost cell analyses. In this regard, following the introduction part and the state of the art of biosensing given in Chapters 1 and 2, respectively, the thesis is structured as follows: In Chapter 3, the magnetic levitation platform was produced and characterized by finite element modeling tool simulations. In Chapter 4, the protein detection in the magnetic levitation platform was characterized using a model target protein, biotinylated bovine serum albumin. Next, the strategy developed for bovine serum albumin was applied for the detection of two clinically relevant biomarkers, immunoglobulin G and human cardiac troponin I, in pure and complex sample matrices by designing magnetic levitation based-sandwich immunoassay formats. In Chapter 5, a washing-free immunoassay was developed and investigated for immunoglobulin G detection following the characterization of the assay with biotinylated bovine serum albumin. In Chapter 6, a holographic microscopy-integrated magnetic levitation platform was tested for portable, label-free separation of bone marrow stem cells (D1 ORL UVA), breast cancer cells (MDA-MB-231), and human monocyte cells (U-937) and the assessment of their viability.

CHAPTER 2

STATE OF THE ART OF BIOSENSING

2.1. What is a Biomarker?

A biomarker, a shortening of biological marker, is an indicator of a pathological condition in a biological system that can be measured reproducibly and accurately (Strimbu and Tavel, 2010). As a term, “biomarker” has been defined in different ways from early times by several authorities. In 1993, the joint venture of the United Nations Environment Program, the International Labor Organization, and the World Health Organization (WHO) defined biomarker as “any substance, structure, or process that can be measured in the body or its products and influence or predict the incidence of outcome or disease”. In the report on the validity of biomarkers, WHO stated the biomarker as “almost any measurement reflecting an interaction between a biological system and a potential hazard, which may be chemical, physical, or biological. The measured response may be functional and physiological, biochemical at the cellular level, or a molecular interaction” (Organization, 1993; WHO, 2001).

Biomarkers are surrogate endpoints; that are used to substitute clinically meaningful endpoints. They can be easily and quickly measured and/or quantified (e.g., blood pressure) than the true endpoints (e.g., stroke). However, not all but only a small subset of biomarkers correlate with clinical endpoints with strong scientific evidence and have surrogate endpoint status (Aronson, 2005).

Biomarkers may be present in several complex biological matrices such as urine, expired air, hair, feces, tear fluid, cerebrospinal fluid, blood, and its components such as plasma and serum (Picó et al., 2019). Most of the biomarkers in clinical practice are single proteins (Kumar and Sarin, 2009). A list of clinically relevant protein biomarkers for tumor diagnosis is presented in Table 2.1.

Table 2.1. Some of FDA approved protein biomarkers for tumor diagnosis (Source: (Füzéry et al., 2013))

Biomarker	Clinical use	Cancer type	Specimen	Methodology	Year first approved
Pro2PSA	Discriminating cancer from benign disease	Prostate	Serum	Immunoassay	2012
OVA1 (multiple proteins)	Prediction of malignancy	Ovarian	Serum	Immunoassay	2009
Fibrin/ fibrinogen degradation product (DR-70)	Monitoring progression of the disease	Colorectal	Serum	Immunoassay	2008
Circulating Tumor Cells (EpCAM, CD45, cytokeratins 8, 18+, 19+)	Prediction of cancer progression and survival	Breast	Whole blood	Immunomagnetic capture/ immune-fluorescence	2005
HER-2/neu	Assessment for therapy	Breast	FFPE tissue	Immunohistochemistry	1998
CA-125	Monitoring disease progression, response to therapy	Ovarian	Serum, plasma	Immunoassay	1997
Free PSA	Discriminating cancer from benign disease	Prostate	Serum	Immunoassay	1997

Selective quantification of protein biomarkers is crucial for molecular diagnosis and approach of treatment (Duffy and Crown, 2008; Overdevest et al., 2009). For instance, the clinical limit of detection for prostate cancer is 0.1 ng/mL for a conventional assay (Giljohann and Mirkin, 2009) and an increased level of PSA (> 4 pg/mL) is related to the disease pathology. On the other hand, in the serum of patients who have undergone

a radical prostatectomy operation, its concentration is usually less than 0.1 ng/mL. However, to assess the disease reoccurrence in those patients, to be able to monitor the low concentrations (< 0.1 ng/mL) of PSA is crucial (Ludwig and Weinstein, 2005). Tumor necrosis factor- α (TNF-α) is another biomarker that is a polypeptide cytokine produced by macrophages and other cell types with respect to an injury, inflammation, or a bacterial infection (Beutler and Cerami, 1988; Tracey and Cerami, 1994). Normally, in the serum of healthy people it is found in very low amounts (~ 1-10 pg/mL) and increased level of this factor reflects pathological situations (Heyman et al., 1994; Kern et al., 1989; Šimúth et al., 2004). These examples indicate that developing immunoassays for rapid and accurate detection of biomarkers at picogram per mL levels is of great clinical importance.

2.2. Immunoassays

2.2.1. Immunoreaction

von Behring -the father of immunology- and Kitasato showed the existence of a neutralizing agent against diphtheria toxin in 1890 (Kaufmann, 2017). After several works, the agent that has the ability to recognize immune substances is referred to as "Antikörper" or antibodies, and the substance that triggers the production of the antibody as "Antisomatogen" and "Immunkörperbildner". These terms gave rise to the term "antigen" (Abbas et al., 2014).

Antibodies, or known as immunoglobulins (Igs), belong to a class of serum proteins called γ-globulins. They are Y-shaped, heterodimeric (a protein containing two polypeptide chains formed by different proteins) glycoproteins synthesized by B-lymphocytes against antigens and foreign substances to mediate immunity (Roberts, 2015). They consist of two heavy (H) and light (L) polypeptide chains which are connected by disulfide bonds (Figure 2.1). The light chain constitutes one constant (C_L) and one variable (V_L) domain whereas heavy chain contains one variable domain (V_H) and three or four constant domains (C_{H1-4}). Each variable region of the antibody has

hypervariable sequences that specially bind antigens. Fc (crystallization fragment) region of antibodies determines the specific binding to Fc receptors on certain cells. Fab region which contains N-terminal domains of light and heavy chain participates in antibody-antigen binding (Schroeder and Cavacini, 2010; Yagiela et al., 2010).

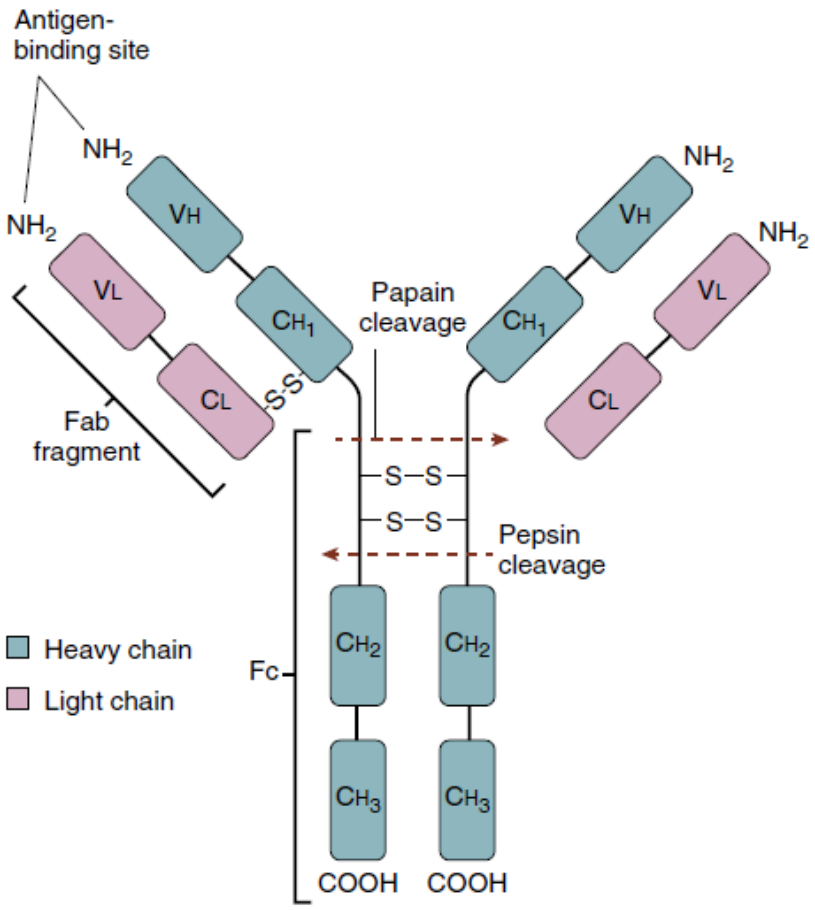

Figure 2.1. Y-shaped structure of an immunoglobulin G antibody with disulfide linkages. (Source: (Yagiela et al., 2010))

2.2.1.1. Classes of Immunoglobulins

Immunoglobulins are categorized into five primary subclasses or isotypes as immunoglobulin A (IgA), immunoglobulin D (IgD), immunoglobulin E (IgE), immunoglobulin G (IgG), and immunoglobulin M (IgM) according to the amino acid

sequence of the heavy chain on the molecule (Table 2.2). This sequence difference determines the number and location of disulfide bonds, number of oligosaccharides on the molecule, number of constant domains, and length of the hinge region (linker between Fab and Fc) (Yagiela et al., 2010).

Table 2.2. Properties and structures of immunoglobulins
(Source: (Yagiela et al., 2010))

Type	Heavy Chain	Property	Molecular weight (kDa)
IgG	gamma-chain	●constitutes 75% of total Igs ●has four subclasses: IgG1, IgG2 (IgG2a and IgG2b), IgG3, IgG4 ●important for phagocytosis and immune response against submucosal antigens ●neutrophils, monocytes, and dendritic cells have Fc receptors for IgG ●half-life: 21 days	150
IgA	alpha-chain	●constitutes 15% of total Igs ●important for the immune response against supramucosal antigens ●has two sub-classes: IgA1 and IgA2 ●most mucosal secretions constitute IgA ● the half-life of IgA1: 5-9 days; half-life of IgA2: 4-5 days	320
IgE	epsilon-chain	●constitutes 0.002% of total Igs ●important secondary exposure responses, initiating acute and chronic inflammation ● half-life: 2 days	200
IgD	delta-chains	●constitutes 0.2% of total Igs ●co-expressed with IgD on the cell surface ●important for protection against parasites ●half-life: 2-3 days	180
IgM	mu-chain	●constitutes 10% of total Igs initial, or primary, immune responses to antigenic compound ●co-expressed with IgD on the cell surface ●half-life: 10 days	900

2.2.2. Concepts and Classifications of Immunoassays

Immunoassays (IA) are tests utilizing the specificity and sensitivity of antibody (Ab)- antigen (Ag) interaction to detect target substances, called analyte, qualitatively or quantitatively (Darwish, 2006). Abs are protein molecules synthesized by the trigger of immunological agents called Ags in animals and humans. Abs are secreted into the blood to neutralize these agents and stimulate further immunological reactions such as cell killing and inflammation (Sörman et al., 2014). Abs have unique structures that recognize relevant antigens by a lock-and-key mechanism and this specific interaction of Ab-Ag is called immunoreaction (Eisen and Chakraborty, 2010). IAs exploit this specific interaction to measure the presence of a target analyte. Target analytes of IAs can be categorized into two groups: i. immune substances, such as antigens, cells, antibodies, cell adhesion molecules, cytokines, alexins; ii. trace molecules, such as proteins, hormones, enzymes, and cyclic drugs (Liu and Jiang, 2017). Following its use in the 1950s for the detection of hormones (Yalow and Berson, 1960), the use of immunoassays has been adopted as the primary bioanalytical method for quantification of proteins or other small molecules in a variety of fields such as clinical diagnosis, food safety, environmental tests, pharmaceutical analyses, and biochemical research (Bojorge Ramírez et al., 2009; Candlish, 1991; Darwish, 2006).

IAs are based on highly specific molecular recognition between an antibody and its corresponding antigen/analyte (Lin et al., 2010). This antibody-analyte interaction is converted to a measurable signal and correlated with the analyte concentration. To read-out the measured analyte quantity, labels such as are fluorescent, chemiluminescent, or colorimetric are commonly used (Hosseini et al., 2018).

IA formats can be dived into two categories as “homogeneous” and “heterogeneous” according to where the immunoreaction takes place (Self and Cook, 1996). In heterogeneous IAs, antibodies (or antigens) which are immobilized on a solid support (e.g., microplate), and interaction with the target analyte occurs at the liquid-solid interface. Unbound antigens (or antibodies) and other substances are then removed by washing (Nistor and Emnéus, 2005). Homogeneous IAs are realized by the interaction of antibodies and antigens in the solid phase, and bound and unbound antibodies are distinguished with a chemical or physical change upon binding (Nistor and Emnéus,

2005). Heterogeneous IA format generally offers a high level of sensitivity due to the high surface to volume ratio (Johannsson, 1991). On the other hand, homogeneous IA format enables quick and multiplex analysis (Liu et al., 2016). Homogeneous and heterogenous IAs can be further dived into competitive and non-competitive IAs (Nistor and Emnéus, 2005). In competitive IAs, unlabeled target Ags compete with exogenously labeled Ags for binding to a limited number of Ab-binding sites. The detection signal is inversely proportional to the analyte concentration: the signal decreases with the increase in unlabeled target Ag concentration. In non-competitive format Ags are captured with excess antibodies first, then detected with labeled secondary antibodies (Lin et al., 2010). This format forms a "sandwich immunoassay" where the detection is directly proportional to the analyte concentration (Zhou et al., 2016a).

2.2.2.1. Enzyme-Linked Immunosorbent Assay (ELISA)

The ELISA technique was conceptualized by Peter Perlmann for the quantification of IgG in rabbit serum (Engvall and Perlmann, 1971). ELISA is a type of plate-based immunoassay in which the target antigens are captured directly onto the solid surface or indirectly with a capture antibody. It consists of antibodies linked with a reported enzyme, and the assay is developed with the addition of a colorimetric substrate that results in a measurable product (Wild, 2005). Depending on the type of the assay, sample, and analyte, ELISA can be performed in i. direct, ii indirect, and iii sandwich formats (Figure 2.2) (Hosseini et al., 2018; Salazar et al., 2017). In indirect ELISA, the target analyte is attached to the solid surface of the plate. Next, the enzyme-linked antibodies are added to the assay. Then, the substrate and stopping solution are introduced. This type of ELISA requires the use of purified samples since non-target proteins may interact with the solid phase (Akamizu et al., 2005). In indirect ELISA, an additional (secondary) antibody is used when compared to the direct (Laborde et al., 2017). In sandwich format, the target analyte is retained between the primary and secondary antibody. This format requires the immobilization of the primary antibody onto the solid surface and provide better control in terms of specificity (Katsurada et al., 2007). However, undesired attachment between the primary and secondary antibody may occur

in the absence of the target analyte. This situation results in false-positive signals. The approximate lengths of assays are 3h 10 min, 4h 10 min, and 4 h10 min in direct, indirect, and sandwich assay formats (Hosseini et al., 2018).

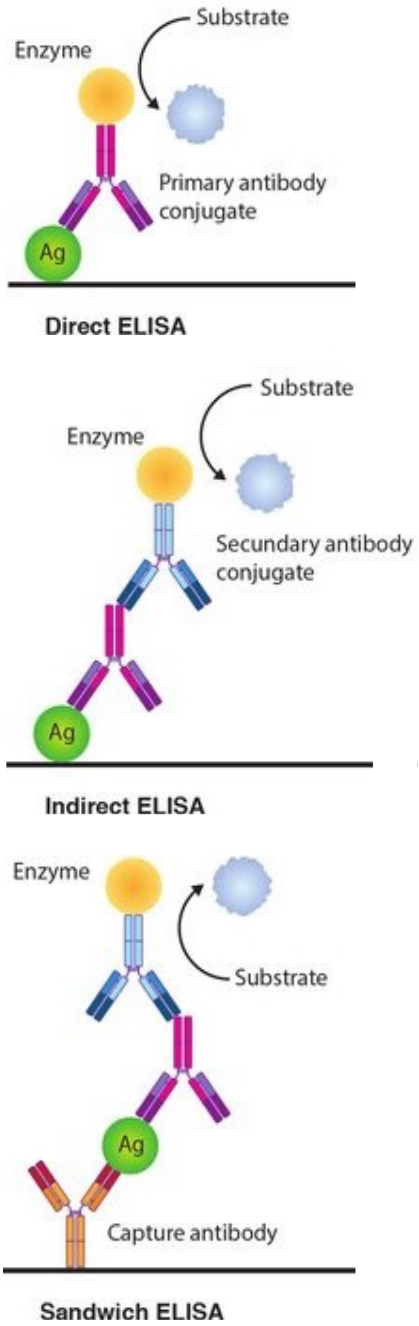

Figure 2.2. The mostly used ELISA formats for the detection of antigens or antibodies. (Source: (Salazar et al., 2017))

2.2.3. Immunoassays in Miniaturized Systems

ELISA offers high sensitivity and specificity; however conventional ELISA requires a series of washing, incubation steps that are prone to errors. Also, it works with a large volume of sample and reagents (Tongdee et al., 2020). Miniaturization of immunoassays into micro-devices provides immense opportunities including i. reduced sample volumes, .ii. enhanced sensing, iii. minimized human error and contact with harmful reagents, iv. short diffusion distance, and therefore decreased analysis time per number of tests, and v. automation (Hosseini et al., 2015; Hosseini et al., 2018; Kharisov et al., 2016; van der Wal et al., 2014).

2.2.3.1. The Use of Micro- and Nanoparticles

To overcome the limitations of current biosensing technologies, the use of micro- and nanoparticles in immunoassays has gained great importance. These particles (i.e., beads) are functionalized through bio-conjugation with detector molecules (e.g., DNA, RNA, antibodies and antigens) and used as 3D immunoassay surfaces (Otieno et al., 2016). The main advantages of the micro/nanoparticles in immunoassays can be stated as follows: i. larger surface to the volume compared to the 2D surfaces of conventional assays, ii. spatial freedom for capturing the analyte, and iii. possibility of multiplex tests (Elshal and McCoy, 2006).

Polymer microspheres, magnetic nanoparticles (MNPs), silver nanoparticles (AgNPs), and gold nanoparticles (AuNPs) are exploited in many biosensing applications for biomarkers (Dai et al., 2013; Raez et al., 2007; Tomás et al., 2019; Zhao et al., 2017).

MNPs (e.g., Fe_3O_4 and γFe_2O_3) can be easily manipulated under an applied magnetic field (Urusov et al., 2017). So that, they have been utilized in magnetic field-induced protein biomarker detection efforts either as labels and/or assay surfaces (Tekin and Gijs, 2013). For instance, Jin et al. used clustered MNPs as magnetic labels to quantify prostate-specific antigen (PSA) (Figure 2.3 a) (Jin et al., 2009). In the assay, PSA

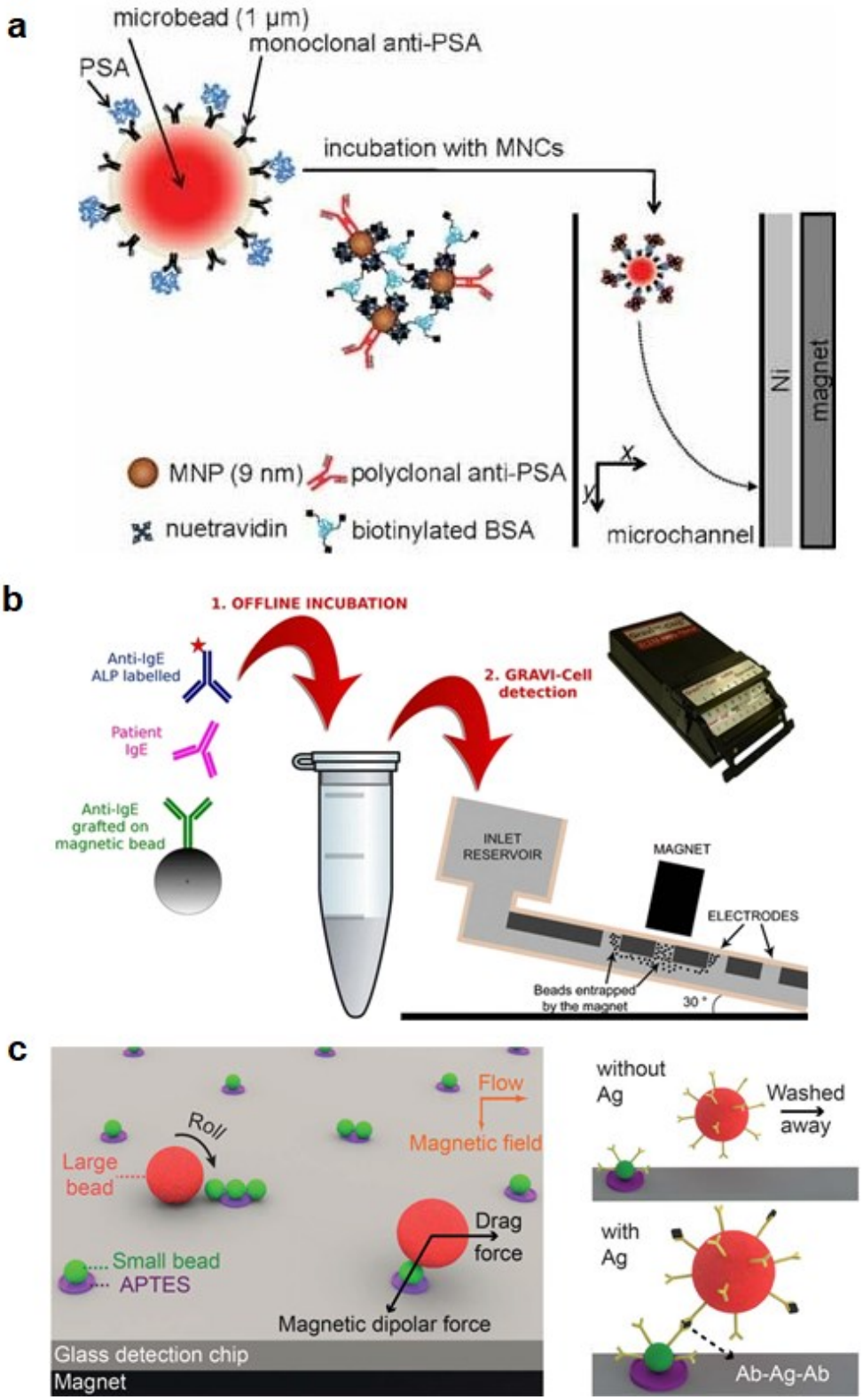

Figure 2.3. Examples of magnetic nanoparticle-based immunoassays. (a) Detection of PSA using clustered MNPs. (Source: (Jin et al., 2009)), (b) Detection of IgE in serum. (Source: (Proczek et al., 2012)), (c) Surface coverage assay using magnetic nanoparticles. (Tekin et al., 2013)

was incubated with anti-PSA antibody bearing microbeads first. Then the complex formed upon binding of PSA to the microbead was labeled using MNP clusters. By analyzing MNP-associated microbeads in terms of deflection velocity under a magnetic-field gradient, 45 fg/mL of PSA could be detected in phosphate-buffered saline (PBS). Similarly, Hall et al. used MNPs as labels in a giant magnetoresistive (GMR) biosensor which is capable of detecting magnetic tags very sensitively and reached 5 fM detection levels of carcinoembryonic antigen (CEA) in serum (Hall et al., 2010). Proczek et al. developed an immunoaffinity capillary electrophoresis system where they used MNPs as "mobile substrates" to capture IgE in serum samples (Figure 2.3 b) (Proczek et al., 2012). Under electrochemical detection, a limit of detection (LOD) value of 17.5 ng/mL was achieved. Using antibody-coated MNPs as mobile substrates and labels at the same time, Tekin et al. introduced a magnetic surface coverage assay for tumor necrosis factor-α (TNF-α), and reached down to 1 fg/mL detection levels in serum (Figure 2.3 c) (Tekin et al., 2013).

Non-magnetic beads that are produced from polymers are also utilized in many miniaturized immunoassays due to their well-known characteristics. One of the most used polymer beads is made up of polystyrene. For instance, Ko et al. developed a multiplex electro-immunoassay in a chip that could simultaneously detect cancer biomarkers alpha-fetoprotein (AFP), CEA, and PSA (Figure 2.4 a) (Ko et al., 2008). In the assay, antibody-immobilized polystyrene beads are fixed on the chip surface. After the addition of antigens, AuNPs were added for labeling and a silver enhancer was used for amplification of the measurement signal. The working range of the chip was 10^{-3} to 10^{-1} μg/mL. Using superporous agarose beads as a solid support, Yang et al. developed a colorimetric sandwich immunoassay with a large surface area for increased sensitivity (Yang et al., 2008). The method enabled the detection of 100 pg/mL goat IgG in PBS. In addition, a commercial multiplex bead-based immunoassay in a microplate format has been developed as "The Luminex™ xMAP (multi-analyte profiling)" (Figure 2.4 b). In the assay, fluorophore-labeled 5.6 μm polystyrene microspheres that are also coated with detection antibodies are used for the quantitative analysis of multiple analytes. After capturing the analytes, beads are transferred into a flow cytometry device and excited by two different laser beams (i.e., green and red) (Dunbar, 2006).

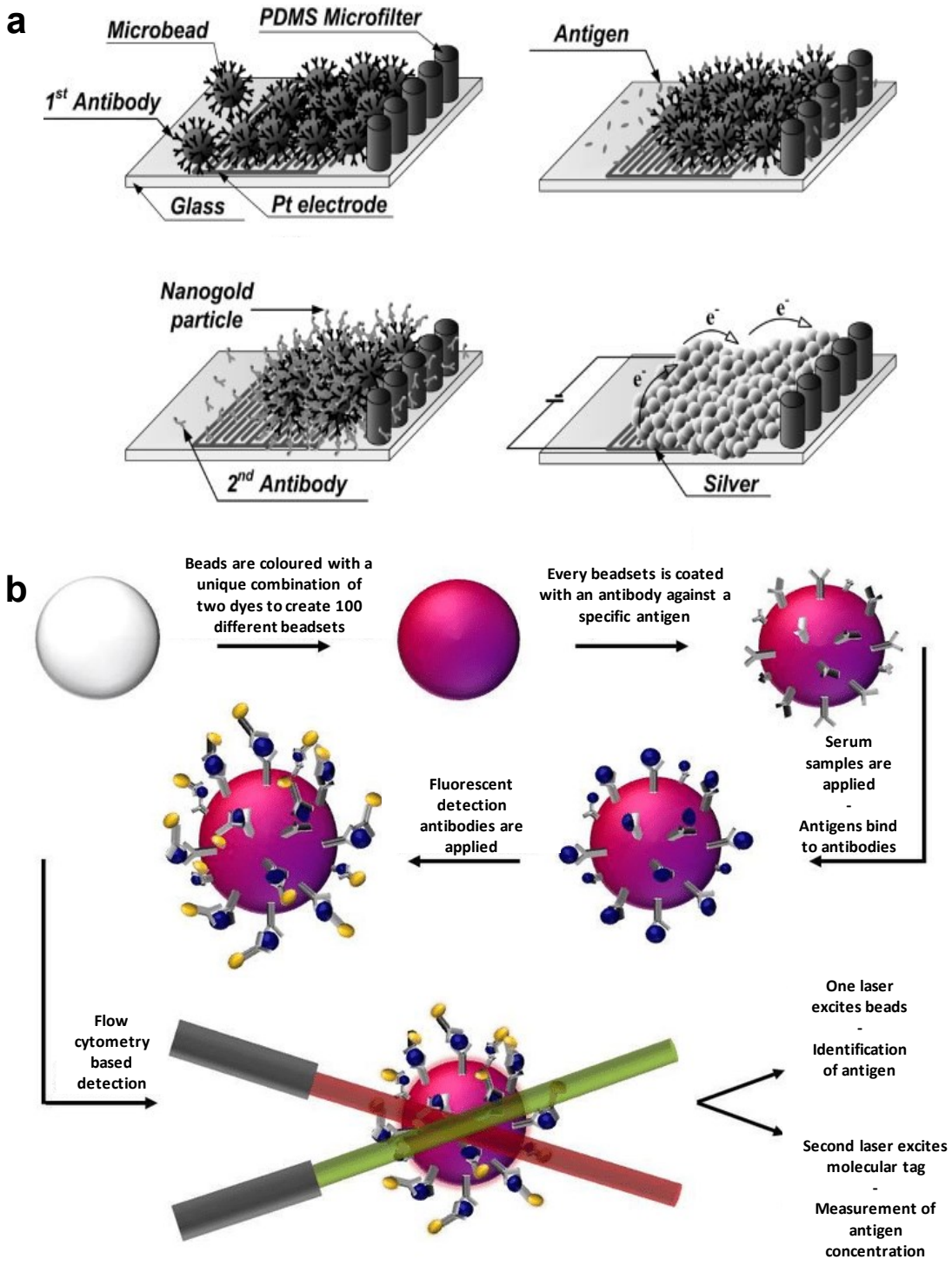

Figure 2.4. Examples of non-magnetic beads-based immunoassays. (a) The use of polystyrene beads as solid support onto the chip. (Source: Ko et al., 2008). (b) The use of beads for multiplexed detection of analytes. (Source: (Ramsey, 2015)

2.3. Model Biomarkers Used in the Assays Developed in This Study

2.3.1. Immunoglobulin G

Immunoglobulin molecules have diagnostic significance as their abnormal concentration in blood is a good indicator of several diseases. In certain cases, serum Igs offer better stability and higher concentration at primary stages when compared to the disease-causing virus, cells, or antigens. Therefore, many bacterial, fungal, or viral infections (Kamat et al., 1999; Li et al., 2013b; Luzza et al., 1995), autoimmune disorders (e.g., lupus and rheumatoid arthritis) (Aho et al., 1997; Arbuckle et al., 2003), certain types of cancer (Tan et al., 2009), and congenital or neonatal infections (Neto et al., 2004) can be diagnosed by a serological test that monitors immunoglobulin levels in the patient's blood. For instance, in the SARS-CoV-2 outbreak which occurred towards the end of 2019 and affected thousands of people worldwide, serological analysis based on detecting IgG and IgM against the nucleocapsid protein of the virus has been developed to prevent false-negative cases that can be seen by polymerase chain reaction (PCR) (Jacofsky et al., 2020). Among the antibodies listed in Table 2.2, IgG (Figure 2.5) has the highest half-life, and therefore can be detected for a long time after infection.

2.3.2. Cardiac Troponin I

Cardiovascular diseases (CVDs) -blood vessel and heart related disorders- are the most frequent cause of death in many countries (Jamison et al., 2006). The most important and clinically relevant biomarkers of cardiac infarction (Table 2.3) are cardiac troponins (cardiac troponin I (cTnI), cardiac troponin T(cTnT)), myoglobin, C-reactive protein (CRP), lipoprotein-associated phospholipase, interleukins (interleukin-6 (IL-6) and interleukin (IL-1)), tumor necrosis factor-alpha (TNF- α), and myeloperoxidase (MPO)

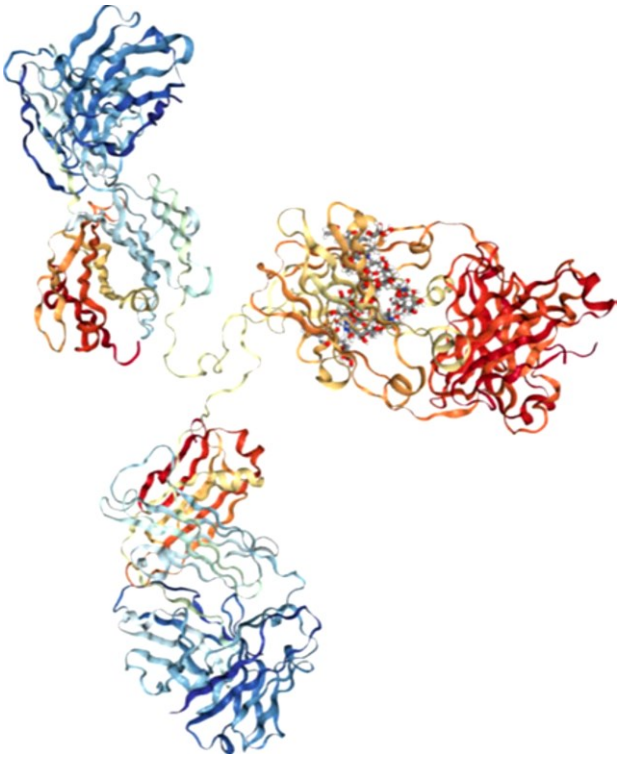

Figure 2.5. 3D structure of Immunoglobulin G.
(Source: (Hosseini et al., 2018))

(Qureshi et al., 2012). Over the last 50 years, the use of cardiac biomarkers has evolved for diagnosis and prevention of acute myocardial infarction (AMI), and risk assessment for heart failure (HF) (Mair et al., 2015). With the development of radioimmunoassay in the 1970s, AMI diagnosis using creatine kinase (CK) activity and myoglobins were investigated (Roberts et al., 1976; Stone et al., 1975). Due to the necessity of more specific biomarkers related to cardiac damage, cardiac troponins were searched for their translation from research into routine practice in the 1980s (Cummins et al., 1987; Katus et al., 1989).

Cardiomyocytes are cells that are responsible for generating contraction in myocardial tissue. Cardiac troponins C, I, and T are regulatory proteins of cardiomyocyte contractility (Figure 2.6). Troponin T is found in cardiac and skeletal muscle and connects the troponin complex to the tropomyosin (Filatov et al., 1999). Troponin I binds to actin and inhibits the contraction in the absence of Ca^{2+} (Chan and Rainer, 2013). Troponin I and T of cardiac muscle differ from that of skeletal muscle (Dzoyem et al., 2014). Troponin C is responsible for binding Ca^{2+} ions to regulate contraction (Christenson et al., 1997).

Table 2.3. Clinically important cardiac biomarkers
(Source :(Qureshi et al., 2012))

Cardiac biomarker	Cut-off levels	Specificity	MW (kDa)	Initial elevation	Time to peak	Return to normal	POC test availability
Troponin I (cTnI)	0.01–0.1 ng mL^{-1}	High	23.5	4–6 h	12–24 h	6–8 days	Yes
Troponin T (cTnT)	0.05–0.1 ng mL^{-1}	High	37	4–6 h	12-12 h	7–10 days	Yes
Myoglobin	70–200 ng mL^{-1}	Low	18	1–3 h	6–12 h	24–48 h	Yes
C-reactive protein (CRP)	$<10^3$ ng mL^{-1} low risk ; 1–3 $\times 10^3$ ng mL^{-1} intermediate risk ; >3–15 $\times$ 10^3 ng mL^{-1} high risk	High	125	ND*	ND	ND	Yes
Creatine kinase MB subform (CK-MB)	10 ng mL^{-1}	Medium	85	4–6 h	12–24 h	3–4 days	Yes
N-terminal pro-B-type natriuretic peptide (NT-proBNP)	0.25–2 ng mL^{-1}	High	8.5	ND	ND	ND	Yes
Myeloperoxidase (MPO)	>350 ng mL^{-1} stratification risk	Medium	150	ND	ND	ND	Yes
Heart fatty acid binding protein (H-FABP)	≥6 ng mL^{-1} stratification risk	Low	15	2–3 h	8–10 h	18–30 h	Yes
TNF-α	<0.0036 ng mL^{-1} low risk; ≥0.0036 ng mL^{-1} high risk	ND	ND	ND	ND	ND	ND
Interlukin-6 (IL-6)	Low < 0.0013 ng mL^{-1} ; Mid 0.00138–0.002 ng mL^{-1} ; High > 0.002 ng mL^{-1}	ND	ND	ND	ND	ND	ND
Fibrinogen	Low < 3.58 × 10^6 ng mL^{-1} ; Mid 3.58–4.20 × 10^6 ng mL^{-1} ; High > 4.20 × 10^6 ng mL^{-1}	ND	ND	ND	ND	ND	ND

*ND: not defined

The diagnosis of cardiovascular diseases is made according to the three criteria defined by the World Health Organization (WHO) (Yang and Min Zhou, 2006): i. chest pain, ii. electrocardiogram (ECG), and iii. increased biomarker levels in the blood. However, half of the patients with CVD shows no symptoms on ECG (Yusuf et al., 1984). Therefore, reducing the time of cardiac biomarker measurement tests, usually less than 60 min, is of great importance (Novis et al., 2004).

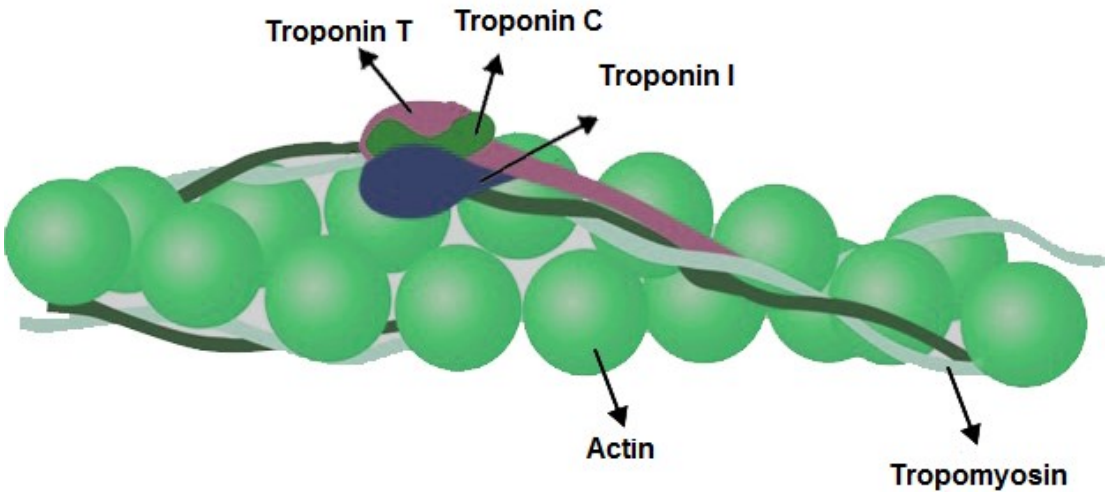

Figure 2.6. The structure of Troponins in muscle cells. The three subunits of the troponin molecule regulate actin and myosin interaction. (Source: (Negahdary et al., 2016))

2.4. Live Cells as Biomarkers

Separation, enrichment, and purification of cell subpopulations are vital for research, therapeutic, and diagnostic purposes (Recktenwald, 1997). Historically, cell populations were thought to be homogeneous (Altschuler and Wu, 2010). Now, it is known that cell-to-cell variability in terms of genetic, functional, and morphological does exist in multicellular organisms (Islam et al., 2014). Even seemingly homogeneous cell populations may contain diverse cells with unique properties (Yuan et al., 2017).

Heterogeneity between genetically identical cells is closely related to the metastasis, resistance to drugs, and cell differentiation (Bauwens et al., 2008; Gao et al.,

2019a; Turner and Reis-Filho, 2012). Traditional techniques such as filtration (Vogel and Kroner, 1999), and centrifugation (Axelsson, 2009) are bulk-scale methods lacking single-cell accuracy. The average response obtained by these techniques does not represent the small but informative subpopulation of cells (Hu et al., 2016). Discrimination of cells based on cell-surface markers such as epithelial cell adhesion molecule (EpCAM) is one of the most widely applied techniques (Armstrong et al., 2011). However, populations with the same surface marker expression may also have hidden cell-to-cell variations (Strzelecka et al., 2018). Therefore, to be able to separate and analyze cells at single-cell-resolution is of big advantage instead of measuring a pooled population of cells, especially for in-depth research of neurons, cancer, stem cell differentiation, and embryos (Del Ben et al., 2016; Nathamgari et al., 2015; Sikorski et al., 2015; Zhou et al., 2016b).

Flow cytometry (FM)/fluorescent-activated cell sorting (FACS) (Figure 2.7 a) has been the most utilized affinity-based single-cell separation technique for a long time (Shields et al., 2015). FACS offer automated, high throughput, robust and multiplex detection of single cells (Hu et al., 2016). For example, Jones et al. used the FACS system to separate mesenchymal progenitor/stem cells (MPCs) in human bone marrow. (Jones et al., 2002). However, the FACS system has a complex, expensive, and bulky instrumentation and an increased risk of contamination during the measurement (Shields et al., 2015). More importantly, loss of function or lowered viability may occur at the end of the process (Kumar and Bhardwaj, 2008).

Magnetically-activated cell sorting (MACS) is another most common affinity-based technique used to separate magnetically-labeled cells from the unlabeled under an external magnetic field (Miltenyi et al., 1990) (Figure 2.7 b). For instance, using an immunomagnetic separator (MagSweeper), Talasaz et al. enriched labeled circulating epithelial cells in the peripheral blood of cancer patients (Talasaz et al., 2009). MACS is cost-effective compared to the FACS; however, final purity may not be satisfactory and cells are only separated into positive and negative populations (Hu et al., 2016).

Laser capture microdissection (LCM) and manual cell picking (MCP) (Figure 2.7 c, d) are other sensitive techniques for selective separation of single cells e.g., individual neuron cells (Eberwine et al., 1992; Kummari et al., 2015); they work with low throughput, though.

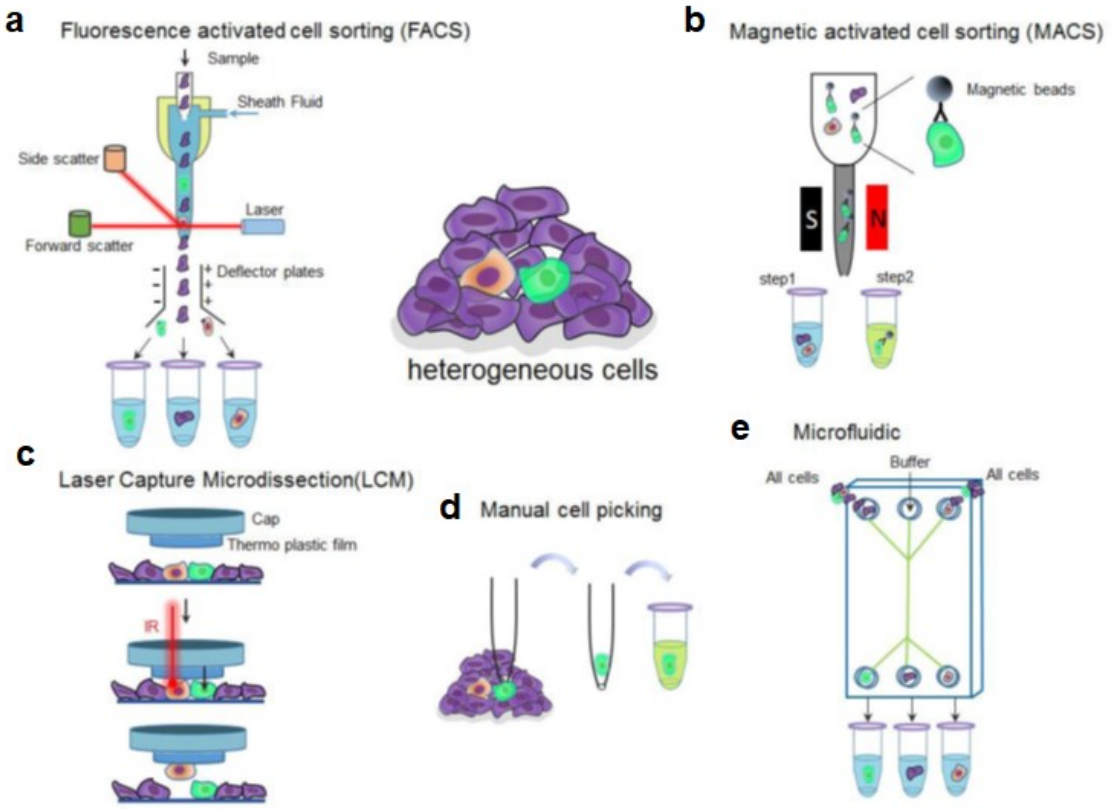

Figure 2.7. Single-cell separation techniques. Schematic representation of (a) FACS in which labeled cells pass in a stream from a laser at a single-cell level. Depending on the fluorescent characteristics of cells, which are measured by the detector, they are collected at different tubes. (b) MACS in which cells labeled with antibody-coated magnetic particles are collected under an external magnetic field. (c) LCM exploits a laser to melt the thermoplastic film on the cap and separate cells of interest that adhere to the melted membrane under microscopic visualization. When the cap is evacuated, the captured cells are removed, undesired cells are left behind. (d) Manual cell picking with a glass micropipette under the microscope (e) Microfluidic techniques to separate different cells. Green, purple, and yellow cells represent different cell types. (Source: (Hu et al., 2016))

The integration of cell sorting into miniaturized devices (Figure 2.7 e) enables rapid and simple processing, reduced human intervention, and precise controlling of sample fluids in the range of μL to pL (Chin et al., 2007; Hu et al., 2016). Among the diverse manipulation technologies, methods utilizing intrinsic properties of cells, such as size (Davis et al., 2006), density (Sarigil et al., 2019), deformability (Byun et al., 2013), polarizability (Çağlayan et al., 2020), and magnetic susceptibility (Kim et al., 2016), are great alternatives to biochemical labels. Even though some intrinsic properties, such as size, may vary from cell-to-cell, the density is tightly controlled within a cell type. The

change in cytoplasm density is often associated with division, growth, state, differentiation, and apoptosis of cells (Grover et al., 2011; Neurohr and Amon, 2020), making the density an important physical biomarker of cell tests.

2.5. Forces Used in Miniaturized Platforms to Manipulate Particles and Cells

For manipulation of single cells or particles in miniaturized platforms, the use of optical tweezers (Grier, 2003), dielectrophoretic (Qian et al., 2014), acoustic (Barani et al., 2016), and magnetic forces (Zborowski et al., 2017) are extensively investigated. Dielectrophoresis is used to manipulate particles with distinct dielectric properties under non-uniform electric fields. In optical tweezers, the force exerted by a laser beam is focused on the particle for the manipulation. In acoustophoresis, particles are manipulated by acoustic forces depending on their size, density, and compressibility relative to the surrounding medium. Yet, acoustic waves are generated by costly experimental setups. Amongst, the use of the magnetic forces is advantageous since it enables the manipulation of objects by a simple magnet located externally (without a direct contact with the sample fluid). Unlike electrophoresis-based techniques, magnetic manipulation is not disturbed by surface charges, pH, temperature, or ionic concentrations (Ozefe and Yildiz, 2020). The theory of magnetic forces and magnetophoretic manipulation is discussed further in Chapter 3.

CHAPTER 3

MODELLING, PRODUCTION, AND CHARACTERIZATION OF MAGNETIC LEVITATION PLATFORM

In this chapter, the development of magnetic levitation based sensitive assay platform is focused. In this regard, first, the theoretical background of magnetism and magnetic levitation are presented at the beginning of the chapter.

The model platform was designed in computer-aided design (CAD) software. The components of the magnetic levitation platform were assembled on a body produced by 3D printing technology. Afterwards, the magnetic force resulted from the magnets in the built platform was modeled using a finite element modeling software, and the levitation of microspheres was simulated and experimentally tested. Lastly, the measurement sensitivity of the platform was characterized by the levitated microspheres.

3.1. Fundamentals of Magnetism

The magnetic field is produced by an electrical charge in motion; by an electron in its orbit around the nucleus or by electric current flowing through a circular wire (Cullity and Graham, 2011; Oersted, 1820). The units of important magnetic quantities used throughout the thesis are presented in Table 3.1.

Permanent magnets, the earliest of which were used in the compasses, are described by two magnetic poles which are called “north” and “south” (Figure 3.1). A magnetic pole creates a magnetic field that produces a magnetic force on the nearby pole (Bozorth, 1947). .The strength of this magnetic field is proportional to the magnetic field strength, **H** (Spaldin, 2010). The magnetic field can be expressed by the contributions of

Table 3.1. Important magnetic quantities with their symbols and units (Source: (McElhinny and McFadden, 1999; Spain and Venkatanarayanan, 2014; Spaldin, 2010))

Magnetic Quantity	Symbol	Unit (SI)
Magnetic field strength	H	$A\ m^{-1}$
Magnetic induction	B	T
Magnetic flux	Φ	Wb
Magnetic permeability	μ	$H\ m^{-1}$
Relative permeability	μ_r	unitless
Magnetic susceptibility (per unit mass)	χ_{mass}	$m^3\ kg^{-1}$
Magnetic susceptibility (per unit mole)	χ_{mole}	$m^3\ mol^{-1}$
Magnetic susceptibility	χ	unitless
Magnetization (per unit volume)	M	$A\ m^{-1}$
Magnetic moment	m	$A\ m^2$

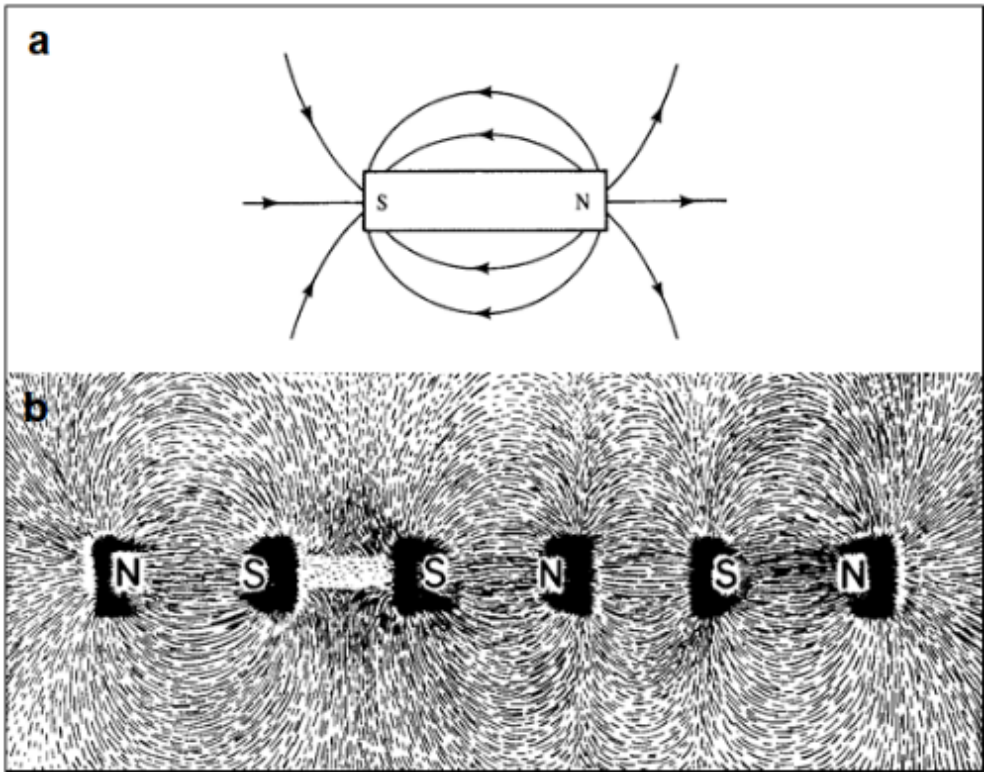

Figure 3.1. Magnetic field lines originate from N to S poles, by convention. (a) Field lines around a bar magnet. (Source:(Cullity and Graham, 2008)) (b) Field lines of bar magnets revealed by iron filings. (Source:(Bozorth, 1947))

two vectors: magnetic induction or magnetic field density, **B** and magnetization, **M** (Yamaguchi et al., 2006):

$$\boldsymbol{B} = \mu_0(\boldsymbol{H} + \boldsymbol{M}) \tag{3.1}$$

,where μ_0 is the permeability of free space (a vacuum), and **B** represents the total number of magnetic field lines crossing a given area. Therefore, **B** can be can also be expressed by dividing the amount of magnetic (flux) field lines, **Φ**, that passes through a defined area (A), as follows (Cullity and Graham, 2011):

$$\boldsymbol{B} = \boldsymbol{\Phi}/A \tag{3.2}$$

Magnetization can be expressed as a magnetic moment per unit volume (Cullity and Graham, 2011):

$$\boldsymbol{M} = \frac{\boldsymbol{m}}{V} \tag{3.3}$$

,where **m** is the magnetic moment showing the tendency of a material to interact with an external magnetic field, and V is the volume.

Magnetization can also be expressed as (Cullity and Graham, 2011):

$$\boldsymbol{M} = \chi \boldsymbol{H} \tag{3.4}$$

,where $\boldsymbol{\chi}$ is termed as magnetic susceptibility, a quantity that indicates how a material responses to an applied magnetic field. Volumetric susceptibility is a unitless

proportionality constant in SI units. Magnetic susceptibility can also be expressed by per unit mole (χ_{mole}), per unit mass (χ_{mass}) (Table 3.1).

Another magnetic quantity is magnetic permeability, μ, which is the ratio of **B** to **H** (Spaldin, 2010) :

$$\mu = \frac{\boldsymbol{B}}{\boldsymbol{H}} \tag{3.5}$$

μ shows how permeable a material is to the applied magnetic field. For instance, materials with high permeability allow magnetic flux to pass through easily. If one combines Equation 3.1 and 3.3 another ratio which is called relative magnetic permeability (μ/μ_0 *or* μ_r) can be obtained as follows (Coey, 2010):

$$\frac{\mu}{\mu_0} = 1 + \chi \tag{3.6}$$

μ_r is a unitless quantity that represents the ratio of the permeability of a material to the permeability of a vacuum.

3.2. Magnetism and Materials

Materials can be classified as diamagnetic, paramagnetic, and ferromagnetic depending on their behavior to an applied magnetic field (Yaman et al., 2018).

Diamagnetism is the weakest form of magnetism. The change in the orbital motion of electrons occurs due to the presence of an external magnetic field (McElhinny and McFadden, 1999). All materials have diamagnetism; however, it is so weak that it can only be observed in the materials that do not show other magnetic properties. The atoms in diamagnetic (e.g., water) materials have closed-shell electron structures and do

not have a net magnetic moment due to the absence of unpaired electrons (Spaldin, 2010). When exposed to external magnetic fields, negative magnetization is observed. Diamagnetic materials have negative and very small χ on the order of 10^{-5} (McElhinny and McFadden, 1999). Paramagnetic (e.g., aluminum and magnesium) materials have unpaired electrons (Spain and Venkatanarayanan, 2014). The magnetic moments of atoms start to align at a certain degree with the applied magnetic field and they have susceptibility slightly greater than zero (10^{-3}-10^{-5}) (McElhinny and McFadden, 1999). Upon removal of the external magnetic field, magnetic moments return to their disordered arrangement. Therefore, both diamagnetic and paramagnetic materials do not retain magnetism when the magnetic field is removed (Spain and Venkatanarayanan, 2014). Ferromagnetic (e.g., iron) materials have great positive magnetic susceptibility values and large net magnetization (Coey, 2010). They have small regions called domains in which all magnetic moments are aligned in parallel in the presence of the external field (Bozorth, 1947). Even after the removal of magnetic field magnetization persist to some extent (McElhinny and McFadden, 1999).

3.2.1. Magnetism in Nanoparticles

Magnetic nanoparticles are a class of magnetic particles with a typical diameter of less than 100 nm (Issa et al., 2013). When the size of a particle is decreased, it gains novel properties (e.g., physical, chemical and mechanical) different than the bulk material (Podaru and Chikan, 2017). The magnetic behavior of a nanoparticle is controlled by its size. By reduction of particle diameter, single-domain particles are formed. Below some critical radius, the magnetization of particles is spontaneously reversed by the thermal energy. This type of magnetism is called superparamagnetism (Petracic, 2010). Superparamagnetic nanoparticles have 0 net magnetizations in the absence of an external magnetic field. When the magnetic field is applied, they have a net alignment (Li and Wu, 2013). This type of particles act like paramagnetic materials; however, the magnetic moment originates from the single domain (10^5 atoms) instead of single atoms in paramagnetic materials (Podaru and Chikan, 2017). Therefore, the superparamagnetic

materials exhibit larger magnetization than paramagnetic materials and become aligned with smaller magnetic fields (Li and Wu, 2013).

3.2.2. Magnetophoresis

Magnetophoresis is a term describing the motion of a particle in a magnetic field gradient (Chalmers et al., 1999). Magnetophoresis enables contact-free manipulation of microparticles or cells using either simple permanent magnets (Hejazian and Nguyen, 2016) or electromagnets (Zhu et al., 2014), while other contact-free manipulation techniques for biological applications (e.g., thermophoresis, acoustophoresis and electrophoresis) require complex instrumentation for the generation of heat (Piazza, 2008), sound waves (Xu et al., 2011), and electricity (Yamada et al., 2009).

Typically, it can be achieved in two forms by utilizing the difference in magnetic susceptibility properties of particles/cells and their surrounding medium: i. negative magnetophoresis (or diamagnetophoresis), and ii. positive magnetophoresis. Negative magnetophoresis is a label-free technique in which the diamagnetic particles or cells suspended in a paramagnetic solution (e.g., gadolinium (Gd (III)), manganese (Mn (II)) salts) (Xiao et al., 2016) or a ferrofluid (e.g., magnetite (Fe_3O_4)) (Rosenweig, 1985) are pushed away from the magnet by the magnetophoretic force (Liang and Xuan, 2012). In positive magnetophoresis, magnetic particles inside a diamagnetic medium migrate towards the higher magnetic field (Gómez-Pastora et al., 2019). Moreover, biological particles or cells which are diamagnetic (except deoxygenated red blood cells and magnetotactic bacteria) can be specifically labeled with magnetic micro-and nanoparticles and manipulated under positive magnetophoresis (Castillo-León et al., 2011).

3.2.2.1. Magnetic Liquids

Cell/particle manipulation in magnetic force-based miniaturized systems include the use of either a ferrofluidic or paramagnetic salt solution.

Ferrofluidic liquids: Ferrofluidic liquids contain the colloidal suspensions of magnetic nanoparticles, such as Fe_3O_4 or Fe_2O_3, having diameters of 10 nm (Rosenweig, 1985).

Paramagnetic liquids: Paramagnetic salt solutions have relatively low magnetic susceptibility and magnetization values in general. They are obtained with paramagnetic metals such as (Mn^{2+}) or (Gd^{3+}) and an organic chelating agent. Due to their unpaired inner shell electrons, paramagnetic liquids create magnetic moment under magnetic field.

Gadolinium molecules are commonly preferred in the bioimaging applications that include contrast-enhancing, such as magnetic resonance imaging (MRI), due to their high magnetic moments and high stability (Garcia et al., 2017). However, free Gd^{3+} ions have toxic effects on biological organisms (Ersoy and Rybicki, 2007). To inhibit the toxicity of Gd^{3+}, gadolinium-based contrast agents (GBCAs), which are Gd^{3+} molecules chelated with the incorporation of either linear or macrocyclic ligands, have been developed (Xiao et al., 2016).

GBCAs are extensively preferred in protein and cell studies (Anil-Inevi et al., 2019; Sarigil et al., 2019; Shapiro et al., 2012a; Shapiro et al., 2012b) as they are cheap, non-protein-denaturating, and readily available as magnetic resonance imaging (MRI) contrast agents. Gadavist (Bayer AG) (or Gadobutrol) (Figure 3.2) is one of the

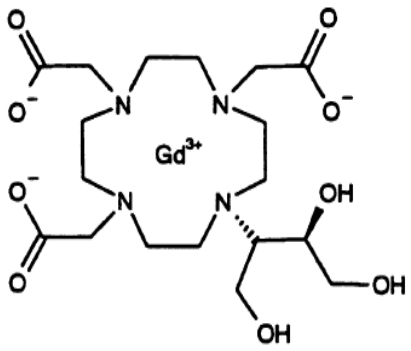

Figure 3.2. The chemical structure of Gadobutrol.
(Source: (Tombach and Heindel, 2002))

most used macrocyclic GBCAs to obtain paramagnetic solutions for magnetic applications. Paramagnetic liquids are preferred in the separation of different objects according to their density (magnetic susceptibility is also possible) in static-flow systems. These types of density-based separations are reported in the literature as magnetic levitation or “MagLev”.

3.2.2.2. Magnetic Levitation

Magnetic levitation (or MagLev) is a case of magnetophoresis where the object inside an nonhomogeneous magnetic field is levitated under the effect of a magnetic field. A simple magnetic levitation can be achieved by placing two permanent magnets at the opposing configuration. Diamagnetic particles or living cells can be trapped between the permanent magnets. The magnetic force exerted on diamagnetic particles (or cells) in a magnetic medium under the magnetic field is represented by Equation 3.7 (Weston et al., 2010):

$$\boldsymbol{F}_{magnetic} = (\boldsymbol{m}.\nabla).\boldsymbol{B} \tag{3.7}$$

,where ∇ is the del operator, B is the magnetic induction, and m is the magnetic moment which can be calculated as follows (Gijs, 2004; Pamme, 2006):

$$\boldsymbol{m} = (V\Delta\chi/\mu_0)\,\boldsymbol{B} \tag{3.8}$$

,using V: the volume of the particle, $\Delta\chi$: the magnetic susceptibility difference between the particle and paramagnetic medium ($\chi_m - \chi_p$), and μ_0: the permeability of the free space.

During the levitation, magnetic force ($F_{magnetic}$), buoyancy force ($F_{buoyancy}$), and drag force (F_{drag}) act on particles as they gain velocity, v (Durmus et al., 2015):

$$\boldsymbol{F}_{magnetic} + \boldsymbol{F}_{buoyancy} + \boldsymbol{F}_{drag} = 0 \tag{3.9}$$

$\boldsymbol{F}_{drag}$ is represented by $\boldsymbol{F}_{drag} = 6\,\pi\,R\,\eta\,f_D\,v$ for spherical objects (Bhuvanendran Nair Gourikutty et al., 2016) where R is the radius of the particle, η is the dynamic viscosity of the paramagnetic medium, and f_D is the drag coefficient that is equal to 1 when the object is far away from the channel walls (Durmus et al., 2015).

$\boldsymbol{F}_{buoyancy}$ can be represented as $\boldsymbol{F}_{buoyancy} = V\,\Delta\rho\boldsymbol{g}$, where $\boldsymbol{g}$ is the gravitational acceleration (9.8 ms^{-2}) in the z-direction, and $\Delta\rho$ is the volumetric density difference between the object and the paramagnetic medium ($\rho_m - \rho_p$).

Objects levitate on the y plane until the $\boldsymbol{F}_{magnetic}$ and $\boldsymbol{F}_{buoyancy}$ balance each other (Durmus et al., 2015):

$$\boldsymbol{F}_{magnetic} + \boldsymbol{F}_{buoyancy} = 0 \tag{3.10}$$

If the expressions in Equation 3.7, 3.8, and 3.10 are expanded and arranged, one can obtain:

$$\frac{V\Delta\chi}{\mu_0}(\boldsymbol{B}.\nabla)\boldsymbol{B} - V\,\Delta\rho\boldsymbol{g} = 0 \tag{3.11}$$

When Equation 3.11 is rearranged, volume terms are canceled out. This indicates that magnetic levitation is independent of the volume of the particles (or cells).

$$\frac{\Delta\chi}{\mu_0}(\boldsymbol{B}.\nabla)\boldsymbol{B} = \Delta\rho\boldsymbol{g} \tag{3.12}$$

$(\boldsymbol{B}.\nabla)\boldsymbol{B}$ can be written for the Cartesian coordinate system as follows (Yaman et al., 2018):

$$(\boldsymbol{B}.\nabla)\boldsymbol{B} = \begin{pmatrix} Bx\frac{\partial Bx}{\partial x} & By\frac{\partial Bx}{\partial y} & Bz\frac{\partial Bx}{\partial z} \\ Bx\frac{\partial By}{\partial x} & By\frac{\partial By}{\partial y} & Bz\frac{\partial By}{\partial z} \\ Bx\frac{\partial Bz}{\partial x} & By\frac{\partial Bz}{\partial y} & Bz\frac{\partial Bz}{\partial z} \end{pmatrix} \tag{3.13}$$

As one can see from the final Equation 3.12, magnetic levitation of particle is independent of the volume of the particle and only dependent on two characteristics, i. density and magnetic susceptibility under the same magnetic field and paramagnetic medium. Particles with positive magnetic susceptibility (e.g., paramagnetic and ferromagnetic) are attracted by the magnetic force and gather where the magnetic field lines are denser whereas particles with negative susceptibility (e.g., diamagnetic) are repelled by the magnetic force and levitates where the magnetic field is at minimum. Depending on the magnetic susceptibility and density of the object relative to its surrounding environment ($\chi_m - \chi_p$), it comes to an equilibrium position after some time ($t_{equilibrium}$) where the magnetic forces are balanced by the buoyancy forces (Figure 3.3).

3.2.2.3. MagLev Designs for Bioanalytical Applications

Up to now, several designs and improvements have been made for the magnetic levitation platform. Some of the configurations of magnetic levitation setups for bioanalytical applications are given in Figure 3.4. A “standard” magnetic levitation setup consists two block magnets at opposing configurations (Durmus et al., 2015; Mirica et

al., 2009; Shapiro et al., 2012a; Shapiro et al., 2012b). In the "tilted" magnetic levitation setup, the platform is tilted to the gravitational axis to increase the range of the density measurement (Nemiroski et al., 2016). An "axial" magnetic levitation setup consists of ring magnets at the opposing configuration to yield a linear magnetic field between the magnets and to enhance sensitivity and operational space (Ge and Whitesides, 2018; Zhang et al., 2020). MagLev was also designed for "high-throughput" measurements with the integration of a 96-well plate and a flatbed scanner to the platform (Ge et al., 2018).

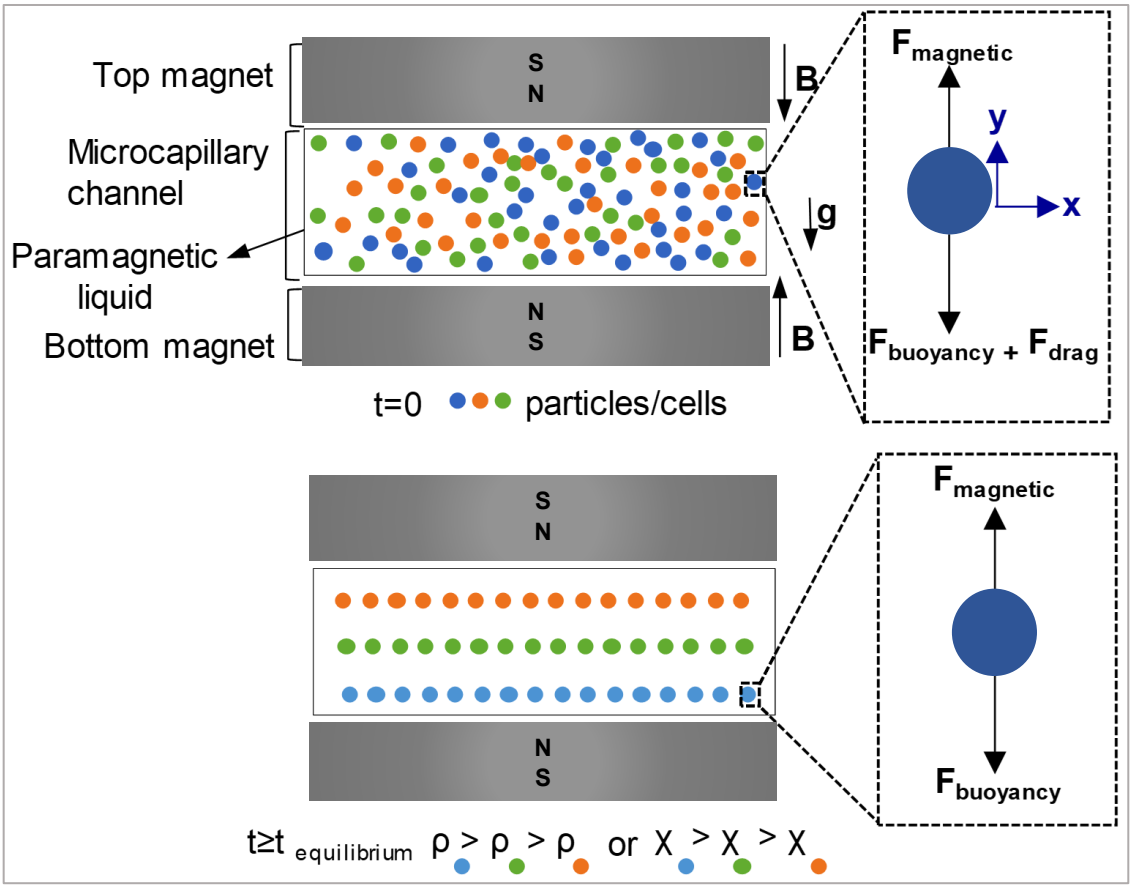

Figure 3.3. Schematic illustration of the MagLev principle. Particles (or cells) dissolved in a paramagnetic liquid inside a magnetic field gradient come to a unique equilibrium point under the following forces: Magnetic force (Fmagnetic), buoyancy force ($F_{buoyancy}$) and drag force (F_{drag}) After a certain time, the particles come to an equilibrium position and levitate under the balance of magnetic force and buoyancy force. B, g, ρ, and χ represent magnetic induction, gravity, density, and magnetic susceptibility, respectively.

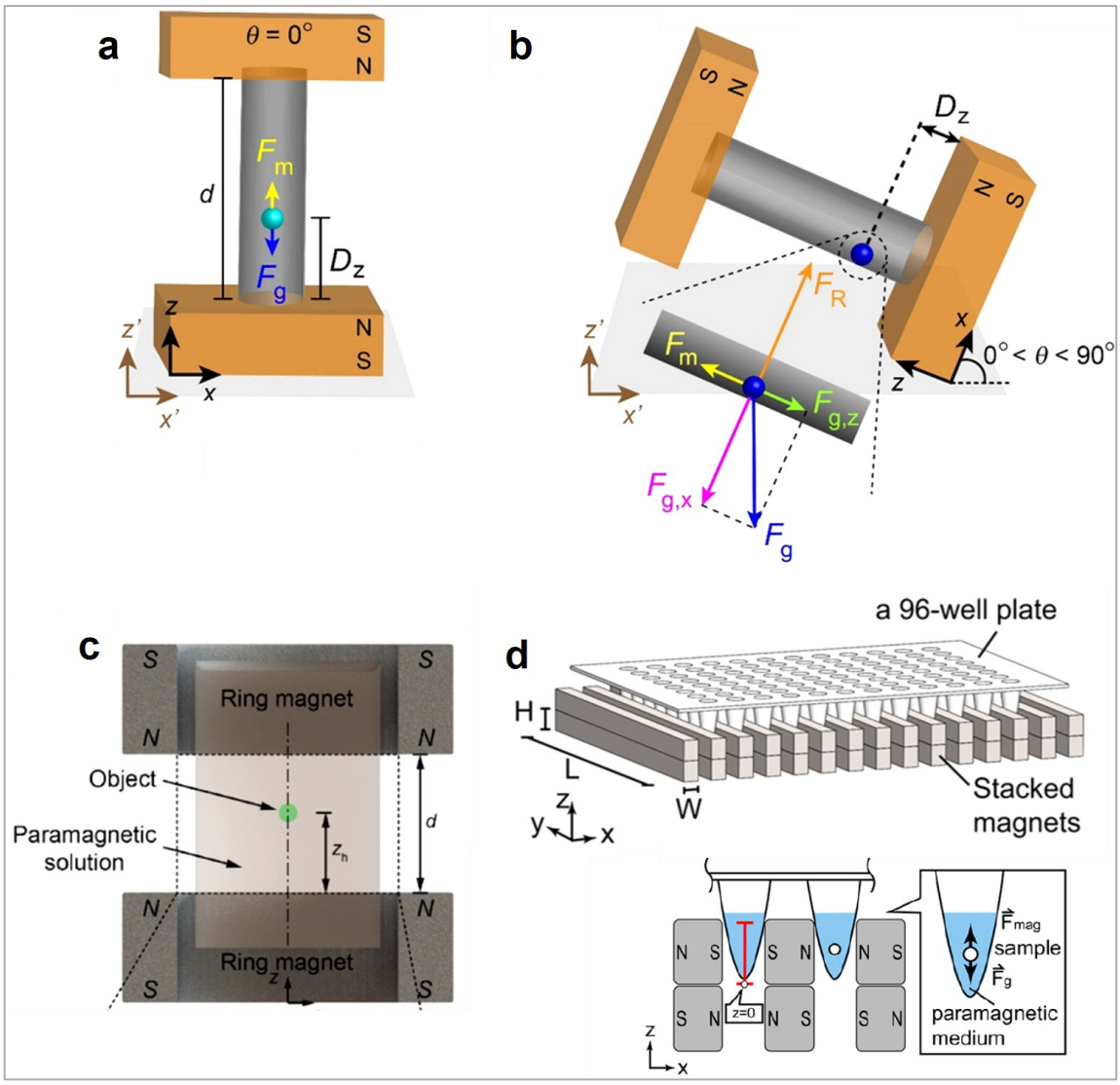

Figure 3.4. Review of the magnetic levitation-based bioanalytical applications. (a) a standard MagLev setup, (Source: (Nemiroski et al., 2016)) (b) a tilted MagLev setup for sensitivity enhancement, (Source: (Nemiroski et al., 2016)) (c) an axial MagLev setup, (Source: (Zhang et al., 2020)) (d) a high-throughput" MagLev setup (Source: (Ge et al., 2018)). F_m/F_{mag} and F_g represent magnetic and buoyancy forces, respectively. The abbreviations D (in a and b) and Z (in c and d) are the distances from height zero.

3.3. Development of Magnetic Levitation Platform

In this study, the magnetic levitation platform was designed in a standard configuration with two permanent block magnets. To build the platform the main components, which are i. two N52 grade neodymium-iron-boron (NdFeB) magnets with

5 mm height x 2 mm width x 50 mm length, ii. a glass capillary channel with 1 mm height x 1 mm width x 50 mm length and 0.2 mm wall thickness, and iii. two aluminum mirrors with 12.7 mm height x 12.7 length x 3.2 mm width, were assembled using a holder produced by 3D printing technology. In this context, the studies were started with the building of the holder in "AutoCAD (2016) software". After the technical drawing (Figure 3.5 a), the file was saved in .STL format for printing via a 3D printer (Formlabs Form 2). Then, using "PreForm software" the platform body was rotated in 3D and the support extensions were added accordingly for the printing process (Figure 3.5 b). Then, the drawing file with support extensions (.FORM) was sent to the 3D printer and the printing was achieved by stereolithography technique using photo-reactive resin "Clear v2 FLGPCL02" at a resolution of 0.025 mm. Upon completion of the printing, the holder was scraped off the surface of the printer with a suitable apparatus. The printed part was shaken for 30 seconds in a reservoir containing isopropyl alcohol (2-propanol) and kept in the reservoir for 10 minutes. Next, the process in the first step was repeated by taking the parts into a second reservoir containing fresh isopropyl alcohol. After the second treatment with isopropyl alcohol, the print was dried with filter paper, cut with a pair of pliers from the support parts, and made suitable for assembly.

N52 grade NdFeB magnets were chosen in the platform since they are cheap, commercially available, and capable of providing high magnetic fields (~0.4 T at the surface). During the assembly, the magnets were placed in the platform in anti-Helmholtz configuration (SN---NS configuration). The mirrors were attached at a 45^{o} angle to image the distance between the magnets using an inverted microscope (Figure 3.5 c, d). The sample solution was inserted into the glass microcapillary channel that was placed between the magnets before each measurement (Figure 3.5 c).

3.3.1. Modeling of the Magnetic Field

For simulations, COMSOL Multiphysics software was used as the finite element modeling (FEM) tool. Modeling geometry was constructed by measuring the dimensions of the produced platform. In this regard, the magnets were separated at a-1800 µm-

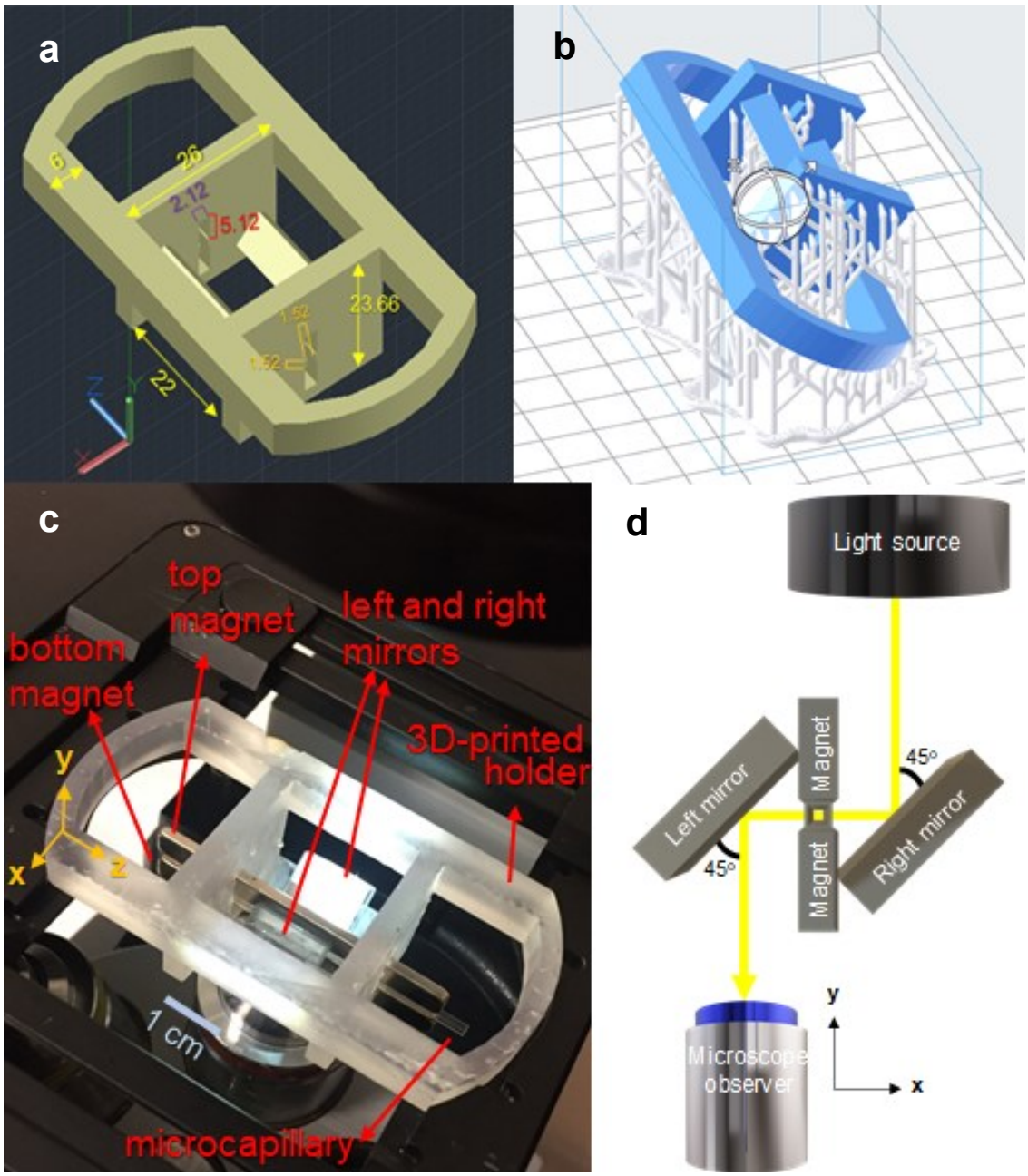

Figure 3.5. Magnetic levitation platform developed in this study. (a) 3D drawing of the platform body in the CAD software. The lengths are in -mm scale. (b) Image of the platform in Preform software after the body was rotated at an appropriate angle and support extensions were added for printing procedure. (c) The photograph of the assembled platform that inserted onto the inverted for microscopy measurements. (d) Schematic illustration of imaging the capillary channel using an inverted microscope. The side mirrors attached at a 45^{o} angle reflects the light coming from the light source of the microscope and illuminates the capillary channel. Then, the light passes through the capillary is reflected to the observer of the microscope.

distance, and the microcapillary channel was inserted at the center in the model (Figure 3.6). The magnetic induction was modeled according to B = μ_0 (H + M) formula, where M: the magnetization of two permanent NdFeB 52 grade magnets were taken as 1150kA/m, and μ_0 : the permeability of free space was taken as 1.2566×10^{-6}

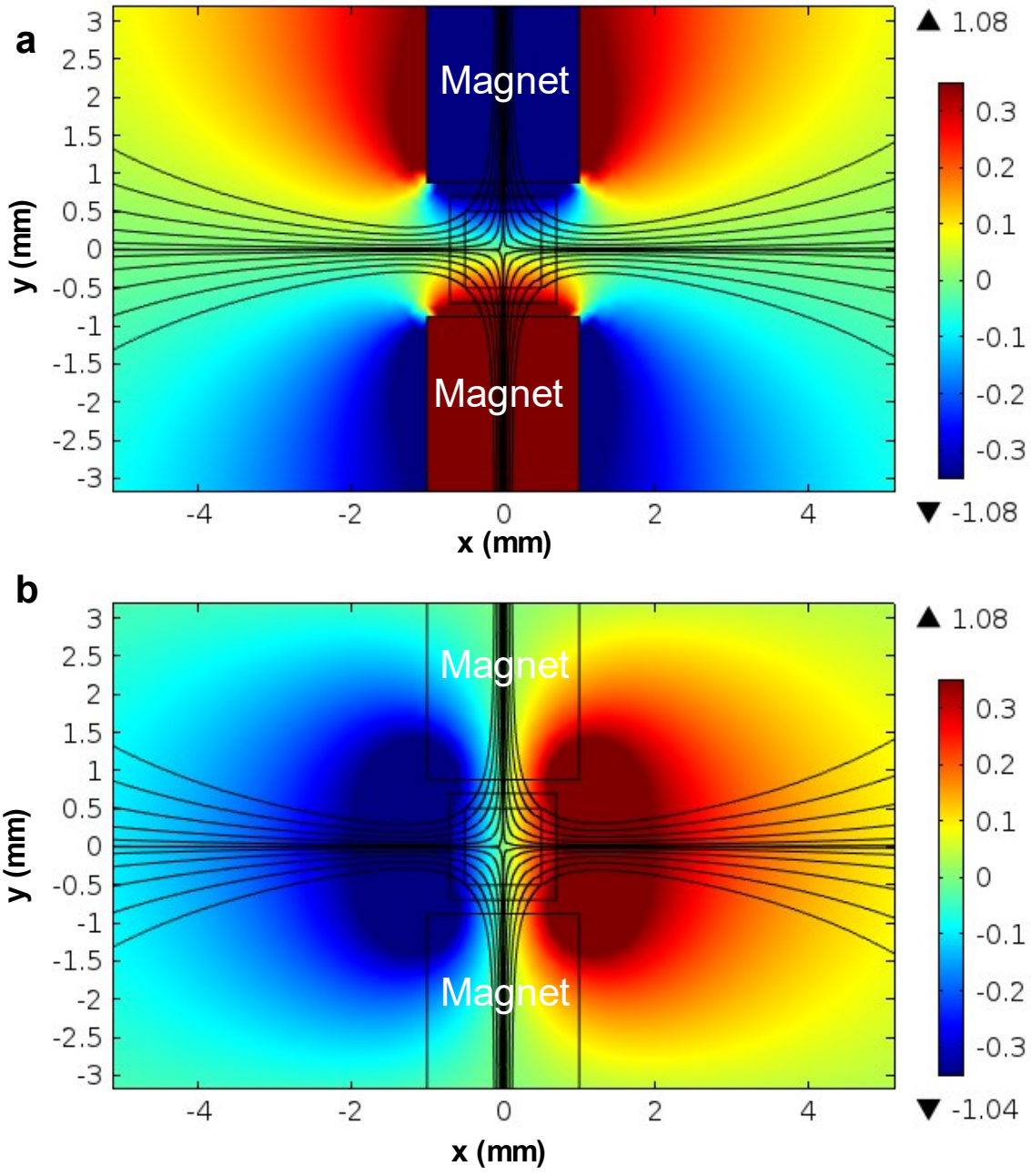

Figure 3.6. 2D simulation results of magnetic flux density (T) along the capillary channel. (a) Surface: Magnetic induction at y-direction (By), Streamlines: Total magnetic induction (By+Bx). (b) Surface: Magnetic induction at x-direction (By), Streamlines: Total magnetic induction (B_y+B_x).

$kg \cdot m \cdot A^{-2} \cdot s^{-2}$. μr: the relative permeability of air was taken as 1. Simulation results revealed that the magnetic field is at its maximum near the magnets whereas the magnetic field on the centerline plane between the magnets is at its minimum.

From the FEM simulation, magnetic induction term for the levitation in y-direction was determined from Equation 3.14 by neglecting $\vec{B}z\frac{\partial \vec{B}y}{\partial z}$ component since the magnets were long enough when compared to its width:

$$(\vec{B}.\nabla)\vec{B} = \vec{B}x\,\frac{\partial \vec{B}y}{\partial x} + \vec{B}y\,\frac{\partial \vec{B}y}{\partial y} + \vec{B}z\frac{\partial \vec{B}y}{\partial z} \tag{3.14}$$

$\vec{B}x\,\frac{\partial \vec{B}y}{\partial x} + \vec{B}y\,\frac{\partial \vec{B}y}{\partial y}$ estimated from the FEM data with respect to the interspace between the magnets by taking the top surface of the bottom magnet as height zero (Figure 3.7).

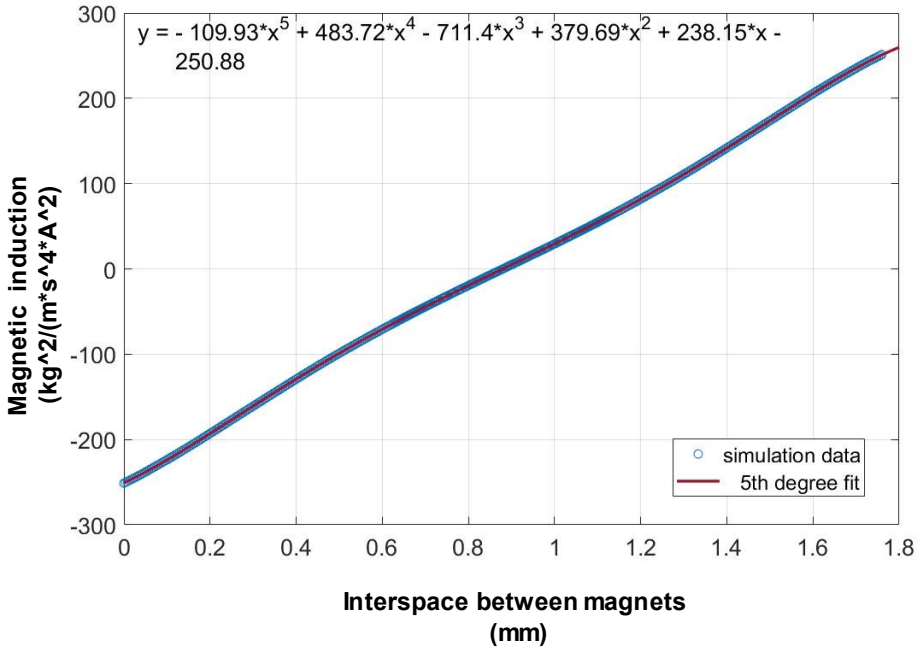

Figure 3.7. Magnetic induction distribution along the interspace between magnets. The data of $(\vec{B}.\nabla)\vec{B} = \vec{B}x\,\frac{\partial \vec{B}y}{\partial x} + \vec{B}y\,\frac{\partial \vec{B}y}{\partial y}$ obtained with COMSOL are fitted into a 5th-degree curve using MATLAB software.

3.3.2. Simulation of Microsphere Levitation for Paramagnetic Solution and Magnetization

Here, using the $(\vec{B}.\nabla)\vec{B}$ obtained in the FEM tool, levitation of diamagnetic polymer microspheres in a paramagnetic medium with different concentrations of Gadolinium ions (Gd^{3+}) were simulated in terms of Gd^{3+} concentration and magnetization of permanent magnets (M) using a custom-coded MATLAB file. According to Equation 3.12, it was expected to observe microspheres at higher heights with increasing Gd^{+3} concentration and magnetization of magnets since both of them increase the magnetic force applied to the microspheres. During the simulations, the density of polymer microspheres was taken as 1.050 g/mL and the molar magnetic susceptibility of the Gd^{3+} solution was taken as 3.2×10^{-4} M^{-1} (Durmus et al., 2015). As the polymer microspheres are diamagnetic, they are assumed to have a 0 magnetic susceptibility. The densities of 10, 30, 60, and 90 mM Gd^{3+} solution prepared with PBS and 1% (v/v) Tween 20 (PBST) were estimated as 1009.63, 1016, 1024, and 1033.00 g/mL using the reported density of 1M Gadavist solution at 37ºC. Then, the polymer microspheres were tested at those Gd^{3+} concentrations. The results of simulations and experiments data are presented in terms of their distance from the centerline plane (the mid-distance between the magnets: ~ 900 μm) (Figure 3.8). The experimental results revealed that the model could predict the magnetic levitation of microspheres for all Gd^{3+} concentrations. Both experimental and simulation results were in agreement with Equation 3.12 since microspheres came closer to the centerline place (the distance decreased) by increasing Gd^{3+} concentration. As expected, increasing Gd^{3+} concentrations increased the magnetic susceptibility change between the paramagnetic medium and microspheres so that they levitated at higher heights with less deviation from the centerline plane.

The levitation of microspheres was also simulated by changing the magnetization of permanent magnets. The results revealed that the magnetization value of magnets has a significant influence on the levitation of microspheres. Low magnetization values (i.e., 500, 600, 700, and 600 kA/m) was not enough to levitate polymer microspheres at 10 mM Gd^{3+} concentration (Figure 3.9 a). Because microspheres at this concentration deviated from the centerline plane as much as the distance equal to the height of the

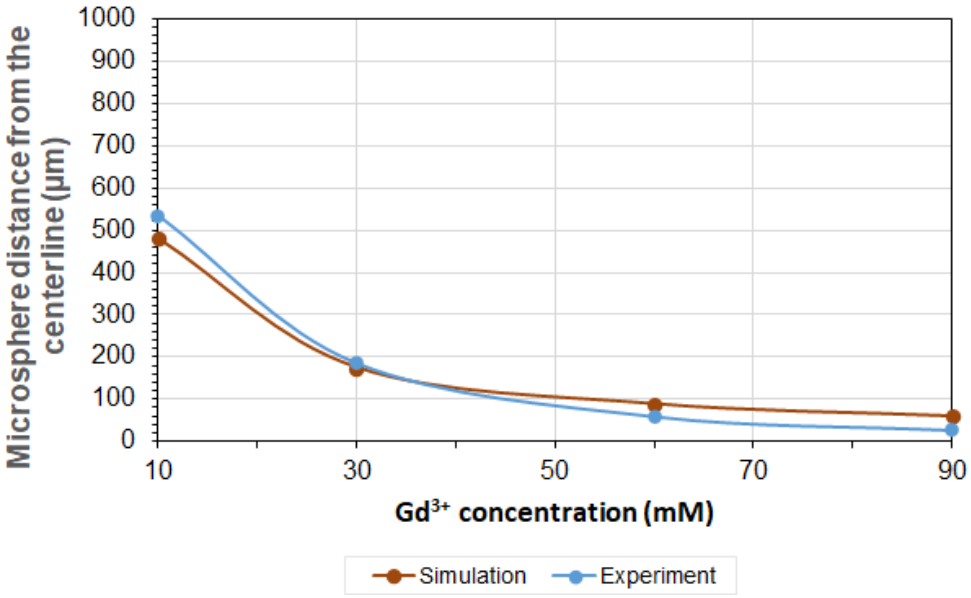

Figure 3.8. Simulation and experimental data of polymer microsphere levitation under different Gd^{3+} concentrations using M=1150 kA/m magnetization value.

centerline plane (~ 900 µm). Simulations and experimental data also revealed that increasing Gd^{3+} concentration decreases the distance of microspheres from the centerline plane for all magnetization values. High Gd^{3+} (i.e., ≥ 30 mM) brought microspheres closer to the centerline since they were able to levitate at higher positions. Other simulations were made using M=1150 kA/m for different paramagnetic medium densities. According to the results, increasing the density of the paramagnetic medium also decreases the distance of microspheres from the centerline position. This enables focusing microspheres at higher heights (Figure 3.9 b). The change in microsphere position is bigger for lower Gd^{3+} concentrations with respect to an increase in density. These results indicate that to be able to obtain a better sensitivity, a lower Gd^{3+} concentration could be used if a denser levitation medium is prepared. Therefore, increasing the density of the paramagnetic medium using additives (e.g., Ficoll and dextran) could be an alternative way for sensitivity enhancement.

The assays developed in this work were designed to be performed at room temperature. However, one should note that changes from an ambient temperature affect the magnetic field strength created by the magnets. High-temperature grades cause misalignments in the magnetic domains of the magnets that decrease the magnetic field strength (Callister and Rethwisch, 2018). For instance, the NdFeB magnet loses 0.11%

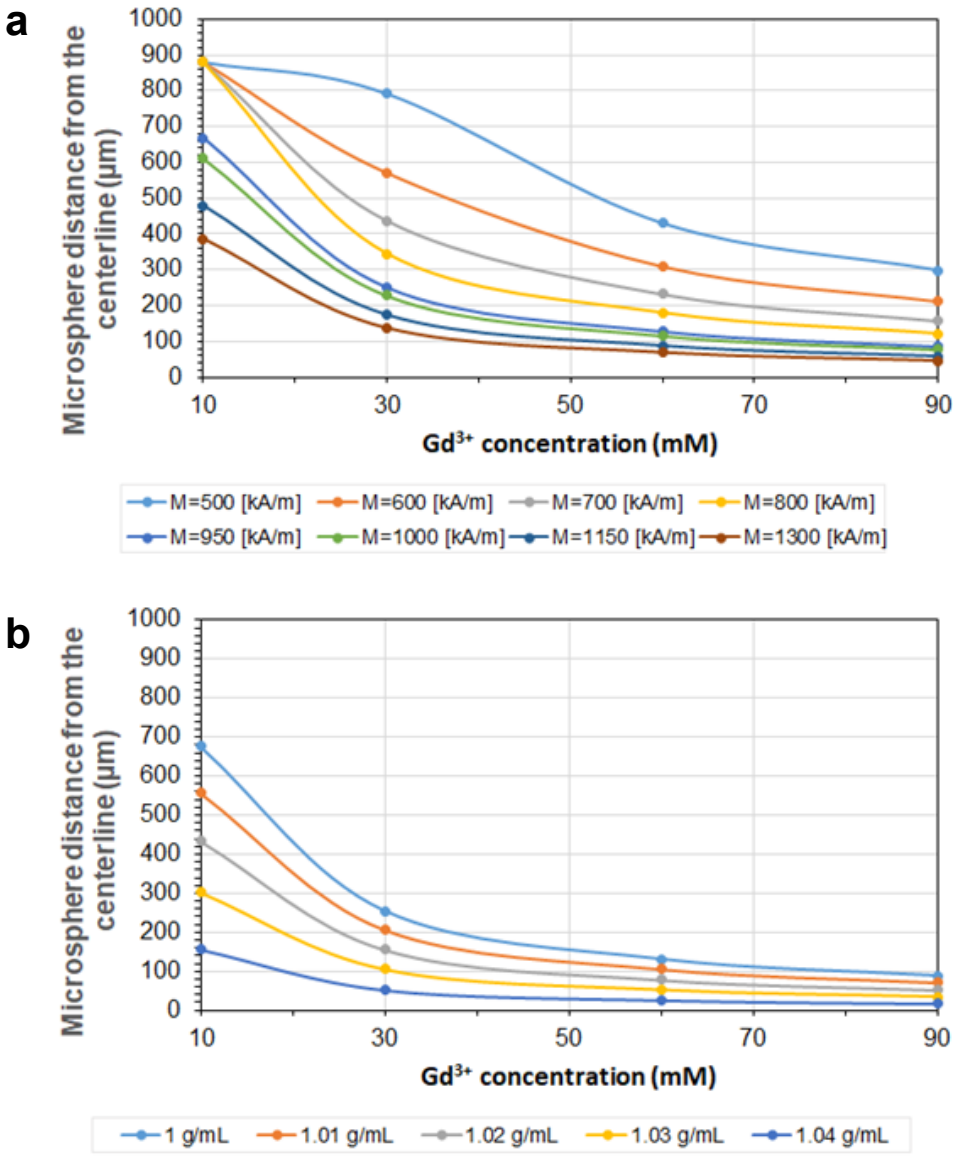

Figure 3.9. The modeling levitation of polymer microspheres. (a) Simulated levitation of microspheres with respect to Gd^{3+} and magnetization (M). (b) Simulated levitation of microspheres with respect to Gd^{3+} and paramagnetic medium density with M=1150 kA/m magnetization.

of its performance per degree Celsius rise (Popescu et al., 2013). On the other hand, when compared to heat, cold environment provides better performance for permanent magnets with an increase in magnetic field strength since the atoms in the material move less randomly, creating a better alignment (Callister and Rethwisch, 2018). It has been reported that magnetic levitation is not significantly affected by temperature changes in the range of 28−36 °C (Anil-Inevi et al., 2018). Nevertheless, using the platform for the applications to be performed at different temperatures, it may be necessary to maintain

the temperature constant with the integration of temperature sensors and heating/cooling modules (You et al., 2014) to the platform in the future. Another option could be the use of electromagnets instead of permanent magnets to adjust the magnetic field strength (Stern et al., 2019). However, electromagnets would increase the size of the platform and demand electricity to operate when compared to the permanent magnets (Sliker et al., 2015).

3.3.3. Measurement Sensitivity of the Platform

Lastly in this chapter, the measurement sensitivity of the platform was demonstrated. In this thesis two characteristic heights, i. levitation height and ii. deviation height were calculated and used for the analysis. Levitation height represents the distance of the microspheres from the top surface of the bottom magnet whereas deviation height represents the distance of the polymer microspheres from the middle of the magnets (centerline). Measurements were done using Image J software and are shown in Figure 3.10. Since the position of capillary channel changes within the experiments, two images are captured using the inverted microscope by i. focusing magnets (Figure 3.10 a) and by focusing ii. microspheres (Figure 3.10 b). Measurement accuracy was examined choosing one random bead in 3 different capillaries. N=4 measurements were done by resetting and setting x, y, and z stages of the microscope (Table 3.2). According to the results, the standard deviation between deviation height measurements was for three randomly selected microspheres were 0.7, 2.5, and 4.4 µm.

Table 3.2. Investigation of measurement accuracy for deviation height determination

# of measurement	**Deviation Height (µm)**		
	1st microsphere	**2nd microsphere**	**3rd microsphere**
1	223.7	186.4	181.7
2	224.5	189.8	183.7
3	224.9	186.9	181.6
4	225.7	192.5	172.3
	SD= ± 0.7 µm	SD= ± 2.5 µm	SD= ± 4.4 µm

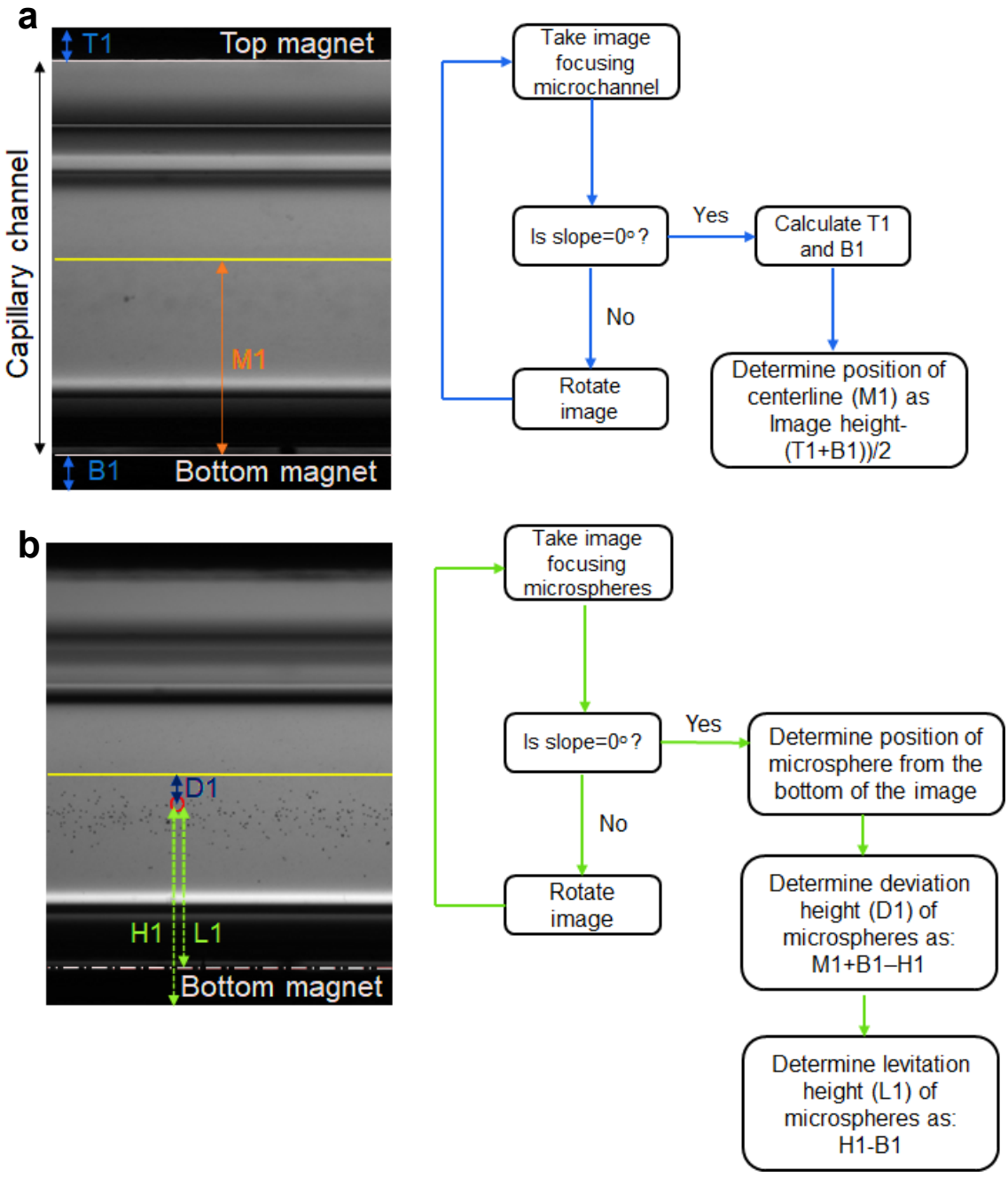

Figure 3.10. Determining deviation heights of polymer microspheres. Micrographs optically focused on (a) magnets and (b) microspheres. Yellow line: centerline plane, T1, B1: the observable of top and bottom magnet thicknesses, M1: the distance of centerline plane to the top surface of the bottom magnet (half of the distance between two magnets, which is equal to (Image height-(T1+B1))/2), H1: height of the microsphere measured from the bottom of the image, L1 and D1: levitation and deviation height of the microsphere.

3.4. Conclusion

In this chapter of the thesis, modeling, production, and characterization of the magnetic levitation platform for bioanalytical measurements were done. A 3D printed-body was produced with a commercial 3D printer for rapid prototyping of the MagLev platform. The miniaturized platform with all its components cost less than $30.

According to the simulation results, the model developed here predicted the levitation of microspheres in agreement with the experimental data for 10, 30, 60, and 90 mM Gd^{3+} based levitation medium. Two characteristic heights were defined for further analysis. According to the measurement sensitivity test, the produced platform can measure the height of polymer microspheres with an error of less than 5 μm between the measurements.

The benefits and difficulties related to the produced magnetic levitation platform for bio-diagnostic applications are summarized as follows: i. The platform can be operated using simple and inexpensive permanent NdFeB magnets without electricity requirement. Since the NdFeB magnets offer high stability, they do not require replacement for a long period. ii. The system works with biocompatible agents; therefore, the process is non-toxic to the environment, iii. The microsphere levitation is dependent on the concentration and density of the paramagnetic media. This enables tuning of the sensitivity of the measurements according to the needs. iv. Since the volume of the glass capillary channel is ~50 μL, it requires less sample and produces less waste per number of tests. Lastly, v., even though the platform is miniaturized and compact, the use of the platform is limited to the equipped laboratories since the measurement is based on a bench-top microscope. Therefore, it requires further improvements for being a completely portable and self-contained setup.

CHAPTER 4

SENSITIVE BIOMOLECULE DETECTION USING MAGNETIC LEVITATION TECHNOLOGY

4.1. Background

Magnetic levitation, which is a magnetic phenomenon of levitating particles suspended in a paramagnetic liquid under a non-uniform magnetic field, is a powerful tool for determining densities and magnetic properties of micro- and nanoparticles. The levitation height of particles in the magnetic field depends on the magnetic susceptibility and density difference between the object and the surrounding liquid. Here, a magnetic susceptibility-based protein detection scheme was developed in a low-cost and miniaturized magnetic levitation setup consisting of two opposing magnets to create a gradient of a magnetic field, a glass capillary channel to retain the sample, and two side mirrors to monitor inside the channel. The method includes the use of polymeric microspheres as mobile assay surfaces and magnetic nanoparticles as labels. The assay was realized by capturing the target protein to the polymer microspheres. Then, magnetic nanoparticles were attached to the resulting microsphere-protein complex creating a significant difference in the magnetic properties of polymer microspheres compared to those without protein. The change in the magnetic properties caused a change in the levitation height of the microspheres. The levitation heights and their distribution were then correlated to the amount of target protein. The method enabled a detection limit of ~110 fg/mL biotinylated BSA (b-BSA) in serum. With the sandwich immunoassay developed for mouse immunoglobulin G (IgG), detection limits of 1.5 ng/mL and >10 ng/mL were achieved in buffer and serum, respectively. This approach sensed the minute changes in the volume magnetic susceptibility of the microspheres with a resolution of 4.2×10^{-8} per 1 μm levitation height change.

4.2. Introduction

Protein biomarkers in blood serve as molecular signatures of complex diseases, such as cancer (Kristiansen, 2012; Lam et al., 2014; Tran et al., 2012), cardiovascular disorders (Signorelli et al., 2014), and other pathological situations (Araujo and Doi, 2017; Blennow and Zetterberg, 2015). Hence, sensitive and rapid detection of proteins provides valuable information about the presence and course of a disease that could improve the survival rate of patients. However, a biomarker may be present at very low levels (e.g., sub-ng/mL) in the blood, which requires large volumes of samples and long processing time for classical biomarker analysis techniques (e.g., enzyme-linked immunosorbent assay (ELISA)). In addition, the lack of portability hinders the applicability of traditional techniques in resource-limited settings (Sharma et al., 2015). Therefore, novel sensing methods or devices detecting a low amount of proteins directly from a complex mixture, such as human serum, have the potential to advance conventional diagnostics techniques to further levels.

Over the years, magnetic force-based detection techniques have gained much attention as ideal candidates for biomarker analysis due to their contactless control on biological samples, ease of operation, low energy requirement and simple design (Alnaimat et al., 2018; Tekin and Gijs, 2013; Yaman et al., 2018). Magnetic force-based protein detection technologies have focused on the use of magnetic nanoparticles (MNPs) which are typically made of a magnetic core (e.g., Fe_3O_4 and γFe_2O_3) and a surrounding shell (e.g., dextran and silica) (Jamshaid et al., 2016). Labeling of biological particles lacking magnetic property in nature with MNPs makes them susceptible to the magnetic field and so they can be controlled by a simple magnet. In magnetic force-based biosensing applications, MNPs can be exploited as either magnetic labels, or assay substrates on which the protein of interest is captured, or both (Tekin and Gijs, 2013). In several studies (Hall et al., 2010; Jin et al., 2009; Proczek et al., 2012; Tekin et al., 2013), these particles allowed high- sensitive detection of proteins using microfluidic devices. Since these studies require precise control of microfluidic flow rates and sophisticated experimental schemes, they could not offer easy-to-use and low-cost detection protocols.

Magnetic levitation, which is levitating of objects under an inhomogeneous magnetic field based on the balance of magnetic and buoyancy forces, has inspired many

applications including sorting of numerous materials (Andres, 1976; Mirica et al., 2010; Nemiroski et al., 2016), the association of proteins and ligands (Benz et al., 2012; Mirica et al., 2008; Shapiro et al., 2012a; Shapiro et al., 2012b), cell measurement/detection (Andersen et al., 2017; Andersen et al., 2019; Durmus et al., 2015; Felton et al., 2016; Knowlton et al., 2015a; Sarigil et al., 2019; Tasoglu et al., 2015), and 3D-assembly of living cells (Anil-Inevi et al., 2018; Haisler et al., 2013; Mishriki et al., 2019), and biomarker detection (Castro et al., 2018; Subramaniam et al., 2015). Lately, this technology has been emerged to provide high-throughput (Ge et al., 2018), compact, and portable analysis of microparticle and cell densities (Amin et al., 2017; Felton et al., 2016; Knowlton et al., 2017a; Knowlton et al., 2015b; Knowlton et al., 2015a). Fundamentals and applications of magnetic levitation are well-documented in recent review articles (Gao et al., 2019b; Ge et al., 2019; Turker and Arslan-Yildiz, 2018).

A simple-designed magnetic levitation setup consists of two magnets whose same poles face each other. A particle suspended in a paramagnetic liquid is levitated between these magnets at an equilibrium position determined by its density and magnetic susceptibility relative to the surrounding liquid. Briefly, measuring the levitation height of an object reveals the density and magnetic susceptibility information. So far, density-change regarding the binding of proteins onto the beads is measured by monitoring the levitation height change in the magnetic levitation system and correlating to the amount of proteins bound onto the beads (Andersen et al., 2017; Castro et al., 2018; Shapiro et al., 2012a; Subramaniam et al., 2015). One of those is a multiplex detection of antibodies against syphilis and hepatitis C by observing the height change of levitating polystyrene beads upon binding of antibodies and subsequent deposition of metal nanoparticles (Subramaniam et al., 2015). Recently, the levitation height of two different-density polymethylmethacrylate microspheres has been tracked for the quantification of interleukin-6 (IL-6) (Andersen et al., 2017). These antibody-coated microspheres conjugate in the presence of IL-6 and reach a density value between those of two types of microspheres. The technique can detect 10 pg/mL (corresponds to ~ 0.5 pM) of IL-6 in phosphate buffered saline (PBS) samples. Moreover, the quantification of Chagas disease-related anti-*Trypanosoma cruzi* antibodies in blood samples have been achieved with a detection limit of 5 μg/mL (corresponds to ~ 30 μM) (Castro et al., 2018).

Here, apart from density-based techniques used the magnetic levitation principle, a magnetic susceptibility-based protein detection method using polymer microspheres as mobile assay surfaces and MNPs as labels was presented. Labeling protein conjugated-

polymer microspheres with MNPs changed the magnetic susceptibility of the conjugate, and in the magnetic levitation system, the equilibrium height of the complex was significantly altered compared to no protein-conjugated microspheres. ~ 110 fg/mL (~ 1.6 fM) b-BSA could be detected in serum. With the developed sandwich immunoassay, detection limits for mouse IgG in pure buffer and serum were 1.5 ng/mL (~ 10 pM) and > 10 ng/mL, respectively. The assay required 200 µL of sample and reasonably short analysis time (~ 50 min for assay preparation steps off the platform and ~ 30 min for levitation on the platform). The results suggested that magnetic levitation-based assays hold a great promise for sensitive and rapid protein analysis in serum samples.

4.3. Materials and Methods

4.3.1. Experimental Setup

The protein assay was performed in a magnetic levitation platform composed of (i) two magnets (N52 grade neodymium, 50 mm length × 2 mm width × 5 mm height, supermagnete.de) with polarization through their heights, (ii) two mirrors (1/2" square protected aluminum mirror, 3.2 mm thick, Thorlabs) tilted at 45^{o} to monitor the channel along its height using an inverted microscope, and (iii) a glass microcapillary channel (50 mm length × 1 mm width × 1 mm height, vitrocom.com) with a wall thickness of 0.2 mm placed between the magnets (Figure 3.5 c). The glass capillary has a tolerance of ±10% for its inner dimensions. The parts of the platform were assembled in a 3D-printed body which was produced by stereolithography technique using photo-reactive resin “Clear v2 FLGPCL02” at a resolution of 25 µm (Kecili and Tekin, 2020) (Formlabs, Form2 3D printer).

4.3.2. Design and Characterization of the Magnetic Levitation-Based Protein Assay Using b-BSA

The assay for b-BSA detection included streptavidin-coated fluorescent polystyrene microspheres (s-PMS) (Streptavidin Fluoresbrite HG 6 μm polystyrene beads, Polysciences, Inc.), streptavidin coated-magnetic nanoparticles (s-MNP) (MACS Streptavidin-coupled microbeads, 50 nm, #130-048-102, Miltenyi Biotec), and biotinylated-BSA (b-BSA) (Sigma Aldrich, # A8549-10MG) as a model protein. Gd-BT-DO3A (Gadavist, Gadobutrol (Gd^{3+})), which is a non-ionic paramagnetic medium with weak protein binding properties (Staks et al., 1994), was used to increase the magnetic susceptibility difference between microspheres and the medium. Cell viability tests also revealed that this medium showed good biocompatibility up to 200 mM concentration levels (Anil-Inevi et al., 2018; Yaman et al., 2018).

In brief, the protein detection protocol starts with the incubation of s-PMS at two different concentrations (i.e., 10^5 or 10^6 particles/mL) with the sample solution (200 μL) for 30 min on a vortex mixer. As a sample, b-BSA was spiked either in PBS (Gibco, pH=7.4) or in dialyzed fetal serum albumin (FBS) (Sigma-Aldrich). Prepared FBS samples were diluted either 1:10 (v/v) with PBS (Gibco, pH=7.4) containing 1% (v/v) Tween 20 (Sigma-Aldrich) or 1:1 (v/v) with 1% (w/v) Pluronic F127 (Sigma-Aldrich). Then, the mixture was centrifugated at 13500 rpm (DAIHAN Scientific CF-10) for 5 min and the supernatant was discarded. Finally, b-BSA bound s-PMS were re-suspended in 200 μL of a levitation buffer (i.e., PBS (pH=7.4) containing either 1% (v/v) Tween or 1% (w/v) Pluronic F-127) and incubated with 1 μL of s-MNP stock solution for 15 min. After it was mixed with 1M Gd^{3+} stock solution (having a volume of 0.4, 1.2, 2.4, and 3.6 μL to get 10, 30, 60, and 90 mM Gd^{3+} in the final solution, respectively), the final mixture (40 μL) was loaded into the microcapillary channel using an automatic micropipette. For each experiment, a new microcapillary treated with an air plasma for 4 min at 0.5 mbar and 100 W (Diener Plasma Cleaner) was used. After sample loading, one end of the microcapillary channel was sealed by immersing it into the Critoseal (Leica Microsystems, Germany). The center part of the channel was monitored under the inverted microscope (Zeiss Axio Observer Z1, 5 × objective) equipped with a camera (AxioCam ICm1). A single micrograph of the microcapillary was used to analyze

microsphere positions for each experiment. Distance measurements on the images were conducted using Image J Software (Section 3.3.3, Table 3.2). In a single micrograph, 100-120 microspheres could be analyzed at a concentration of 10^6 microspheres/mL.

4.3.3. Application of the Assay for the Measurement of IgG Levels

The proof of concept developed for b-BSA was tested for the detection mouse IgG (Sigma-Aldrich, I5381) spiked in buffer and serum as the target protein biomarker.

4.3.3.1. Biofunctionalization of the Microspheres and Magnetic Nanoparticles

Biofunctionalization of streptavidin polymer microspheres and magnetic nanoparticles with biotinylated goat anti-mouse IgG (Sigma-Aldrich, B7264) was achieved by coupling biotinylated Ab onto the bead surfaces via streptavidin-biotin interaction. In this regard, both s-PMS and s-MNP were biofunctionalized with biotinylated goat anti-mouse IgG antibodies as follows:

1. 1 µL stock solutions of s-PMS and s-MNP were dissolved in a dilution buffer (Buffer 1: PBS containing 1% (w/v) of Pluronic (PBSP) or Buffer 2: PBS containing 1% (w/v) Pluronic and BSA (Sigma-Aldrich) (PBSP-BSA)) in separate Eppendorf tubes.

2. 1 µL and 0.08 µL of biotinylated anti-mouse IgG antibodies (0.5 mg/mL) were added to s-PMS and s-MNP, respectively.

3. The solution volume in each Eppendorf tube was completed to 100 µL with the dilution buffer and the Eppendorf tubes were agitated for 30 min on a vortex.

4. The non-occupied streptavidin molecules on the beads were blocked with biotin (Sigma-Aldrich) to avoid non-specific interactions. 1 µL and 0.08 µL of 1 mg/mL biotin solutions were added to the tubes for s-PMS and s-MNP, respectively.

5. After 30 min of mixing with biotin, both microspheres and magnetic nanoparticles were centrifugated and washed twice using dilution buffer.
6. Lastly, microspheres and magnetic nanoparticles were resuspended in the dilution buffer at their initial stock concentration.

4.3.3.2. Optimization of the Dilution Buffer

All IgG experiments were conducted in PBS and FBS diluted 1:1 (v/v) with PBS (pH = 7.4) containing 1% (w/v) Pluronic F-127 and 1% (w/v) BSA according to the optimization studies. In the optimization, two different dilution buffers were tested to dilute sample solution for IgG experiments. These buffers were also used in biofunctionalization and levitation of particles.

4.3.3.3. Optimization of the Magnetic Nanoparticle Concentration

The amount of anti-mouse IgG magnetic nanoparticles was also tested to find a suitable amount for the sensitive detection of IgG. This approach was tested in PBS and FBS samples by comparing the deviation height differences between the reference (0 g/mL IgG) and 1 µg/mL IgG.

4.3.3.4. Measurement of IgG Concentration in Pure and Complex Media

The incubation and levitation procedures performed in b-BSA tests were also applied for IgG. For IgG detection experiments, the microspheres were added to the dilution buffer at a concentration of 10^6 particles per mL. The sample solution (200µL) for both PBS and FBS experiments were diluted 1:1 (v/v) using the dilution buffer and

incubated with anti-mouse IgG microspheres for 30 min. Then, the solution is centrifugated and resuspended in 200 µL of dilution buffer. Anti-mouse IgG magnetic nanoparticles (1µL/3µL) were added to the solution and incubated for 15 min. Later, the solution is mixed with 1M Gadolinium solution having a volume of 1.2 µL to achieve 30 mM Gd^{3+} in the final loading solution of 40 µL.

4.3.4. Statistical Analysis

All experiments were repeated three times unless stated, using a new capillary channel for each experiment. The data are presented as mean ± standard deviation (SD) from the mean values of triplicates. Statistical significance was determined by one-way analysis of variance (ANOVA) corrected for multiple comparisons and t-test with Welch's correction. The coefficient of variation (CV) (%) was calculated as (standard deviation of population/mean of the population) × 100. Statistical outliers in data were detected and removed under the integrated Robust Regression and Outlier Removal (ROUT) Method (Motulsky and Brown, 2006) for different maximum desired false discovery rate (Q) values (i.e., 0.5, 1, 2, and 5 %) for CV(%)-based analysis. These analyses were conducted using GraphPad Prism (version 6.0). The mean values of experimental data were fitted into linear curves (i.e., semilog lines) to obtain standard equations for deviation height/CV versus protein concentration.

4.4. Results and Discussion

The magnetic levitation platform includes two permanent neodymium magnets at the opposing configuration (i.e., same magnetic poles face each other), a glass microcapillary channel inserted between the magnets (50 mm length × 1 mm width × 1 mm height), two tilted mirrors at 45º to monitoring inside the channel using an inverted microscope and 3D-printed holder to maintain these pieces (Figure 4.1 a). In this platform, magnetic flux density (**B**) modulus reaches its maxima near the magnets and its

minima at the midpoint between the magnets (Figure 4.1 b). When diamagnetic microspheres spiked in a non-ionic paramagnetic medium, they come into an equilibrium position along with the channel height and levitate where the magnetic force ($\vec{F}_M$) is counterbalanced with the buoyancy force ($\vec{F}_B$). Under the same magnetic field conditions, the steady-state levitation height of a microsphere depends purely on the magnetic susceptibility (χ) and density (ρ) difference between the microsphere and the paramagnetic medium. For instance, if the microspheres have high magnetic susceptibility or density (e.g., magnetic nanoparticles), they levitate close to the magnets whereas diamagnetic particles (e.g., polymer microspheres) are repelled by the applied magnetic field and levitate close to the midpoint between the magnets.

4.4.1. Characterization of Magnetic Levitation-Based Protein Measurement

The method detects b-BSA by monitoring levitation heights of streptavidin-coated polystyrene microspheres (s-PMS). The deviation height of microspheres (h_D) is calculated as the distance of microspheres from the centerline plane between magnets in the absence and presence of b-BSA and streptavidin-coated MNP (s-MNP). In the assay (Figure 4.1 c), b-BSA molecules are captured on s-PMS surfaces, and the captured b-BSA are labeled with s-MNP due to the strong molecular affinity between streptavidin and biotin molecules (K_a = ~2.5 × 10^{13} M^{-1} (Deng et al., 2013)). These aggregations alter the net magnetic susceptibility and density of s-PMS, and so they significantly change the deviation height of s-PMS compared to s-PMS without b-BSA (Figure 4.1 d). The assay monitors two parameters for protein detection: (i) average deviation height of microspheres and (ii) deviation height distribution of microspheres, as explained in Chapter 3.

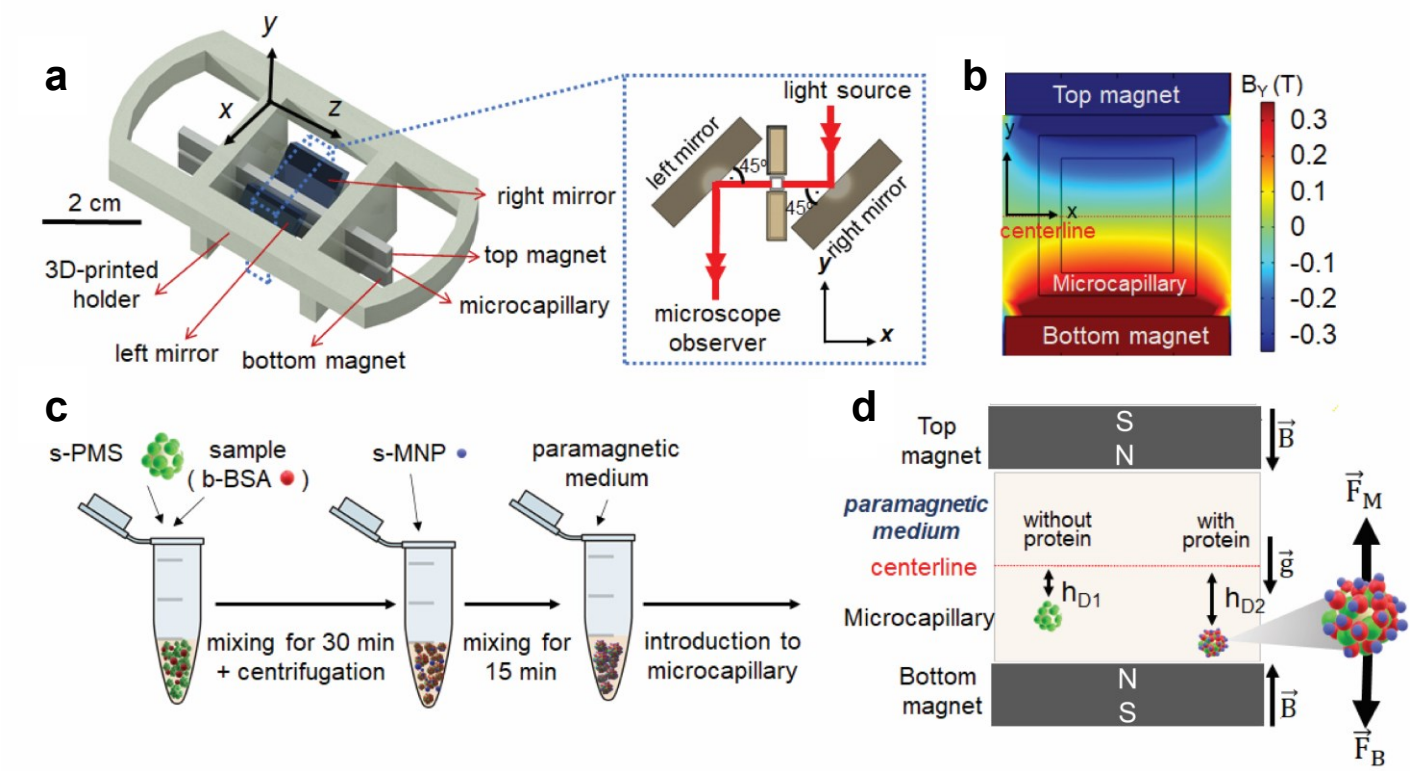

Figure 4.1. Principles of the magnetic levitation-based protein assay. (a) Illustration of the setup. A 3D-printed holder is used to assemble mirrors, magnets and a glass microcapillary. Two tilted side mirrors are attached onto the 3D-printed holder to monitor inside the capillary. (b) Magnetic induction in the y direction (B_y). Magnets are separated 1800 µm from each other, and the microcapillary with a channel height of 1000 µm and a channel wall thickness of 200 µm is placed between the magnets. (c) Schematic representation of offline incubation steps (d). Schematic representation of the protein detection principle. Due to magnetic induction (**B**) and gravity (**g**), microspheres inside the capillary channel levitate where the magnetic force ($\vec{F}_M$) is balanced by the buoyancy force ($\vec{F}_B$). Upon binding of protein (b-BSA) and s-MNP onto the s-PMS, the complex gains magnetic susceptibility and levitates significantly different than the no-protein condition (reference test). h_D represents the deviation distance of the microspheres from the centerline plane.

4.4.2. Modelling and Design of Assay Protocol

Using Equation 3.12 and magnetic induction ($\vec{B}$) values generated by two N52 grade NdFeB magnets in FEM simulations (Chapter 3), equilibrium positions of polystyrene microspheres were simulated for magnetic nanoparticle attachment with an in-house developed MATLAB file. Magnetic susceptibility of microspheres loaded with magnetic nanoparticles was calculated by solving Equation 3.12 for χ_p using the $\vec{B}$ data at the levitation position of the microsphere along with the channel height. The number of MNPs made the change in the magnetic susceptibility of the microspheres was then estimated with the calculated χ_p. In the calculations, the magnetic susceptibility of MNP and microspheres (without any MNPs) were taken as 1.4×10^{-2} (Zhang et al., 2005) and 0, respectively.

In the levitation platform, the behavior of the diamagnetic microsphere with a density of 1.050 g/mL and a diameter of 6 μm and 60 μm, and the magnetic nanoparticle with a density of 1.800 g/mL and diameter of 50 nm are shown in Figure 4.2. The magnetic nanoparticle is attracted by the magnet and gets no levitation under the applied magnetic field. On the other hand, the polymer microsphere is repelled by the magnets and magnetic levitation is achieved. In the presence of magnetic nanoparticle conjugation, the diamagnetic microsphere tends to levitate closer to the bottom magnet due to the increase in overall magnetic susceptibility. Aggregated microspheres (D: 60 μm) can levitate to the same height as single microspheres (D: 6 μm) if their magnetic properties are the same and the levitation height is independent from the volume (Equation 3.12 and Figure 4.2).

For the reference condition (no b-BSA) diamagnetic microspheres (s-PMS) tend to migrate towards the centerline plane where magnetic field is minimum (Figure 4.1 b) and become stationary where the magnetic force and the buoyancy force acting on those particles are equal to each other. For two particles having the same magnetic susceptibility, the particle with a higher density levitates close to the lower magnet. On the centerline plane (i.e., the middle plane between top and bottom magnets), particles having nearly the same density as the levitation medium are gathered. Since s-PMS (i.e., 1.050 g/mL) is denser than the paramagnetic levitation medium (i.e., calculated as ~1.016 g/mL), it levitates below the centerline (Figure 4.2).

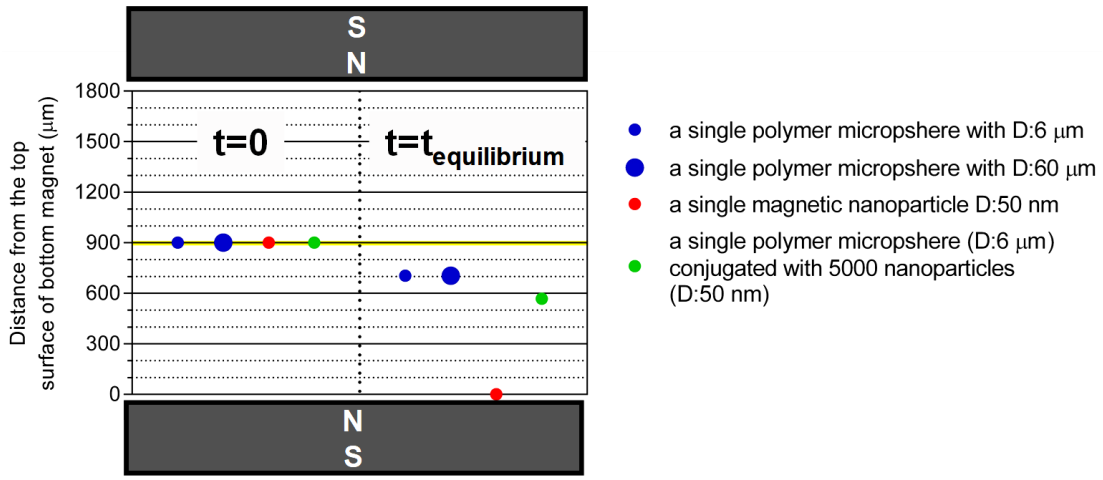

Figure 4.2. The behavior of four different particles in the magnetic levitation setup. case (i): a single diamagnetic microsphere (6 μm), case: (ii) a single polymer microsphere (60 μm), case (iii): a single magnetic nanoparticle (50 nm) , and case: (iv) a single diamagnetic microsphere (6 μm) conjugated with 5000 magnetic nanoparticles (50 nm). The graph shows initial (t=0) and final (t=equilibrium) positions of the particles spiked in 30 mM Gd^{3+}. Yellow line: centerline.

The levitation of diamagnetic s-PMS to show the deviation height change of a single s-PMS in case of binding of three different particles in Gd^{3+} based paramagnetic levitation medium was simulated (Figure 4.3): (i) diamagnetic nanoparticle with 50 nm diameter, 1.8 g/mL density and 0 volumetric magnetic susceptibility, (ii) magnetic nanoparticles with 50 nm diameter, 1.8 g/mL density and 1.4×10^{-2} volumetric magnetic susceptibility, and (iii) b-BSA molecules with ~69.4 kDa molecular weight and 0 volumetric magnetic susceptibility. According to the simulation results in 30 mM Gd^{3+}, the significant change in the deviation height of a s-PMS occurred due to magnetic nanoparticle attachment (Figure 4.3 a). For example, the deviation height of s-PMS changed by 10.2% compared to the initial case (i.e., without magnetic nanoparticles) due to the attachment of 10^3 magnetic nanoparticles. On the other hand, 1.23% and 0.0034% changes were observed for 10^3 diamagnetic nanoparticles and 10^3 BSA molecules, respectively. Hence, the magnetic nanoparticles can change s-PMS heights due to their strong magnetic properties, and density changes on s-PMS have only a small influence on the s-PMS heights. Simulations were also conducted to evaluate the deviation height of s-PMS with 10^3 magnetic nanoparticles for different Gd^{3+} concentrations (Figure 4.3b).

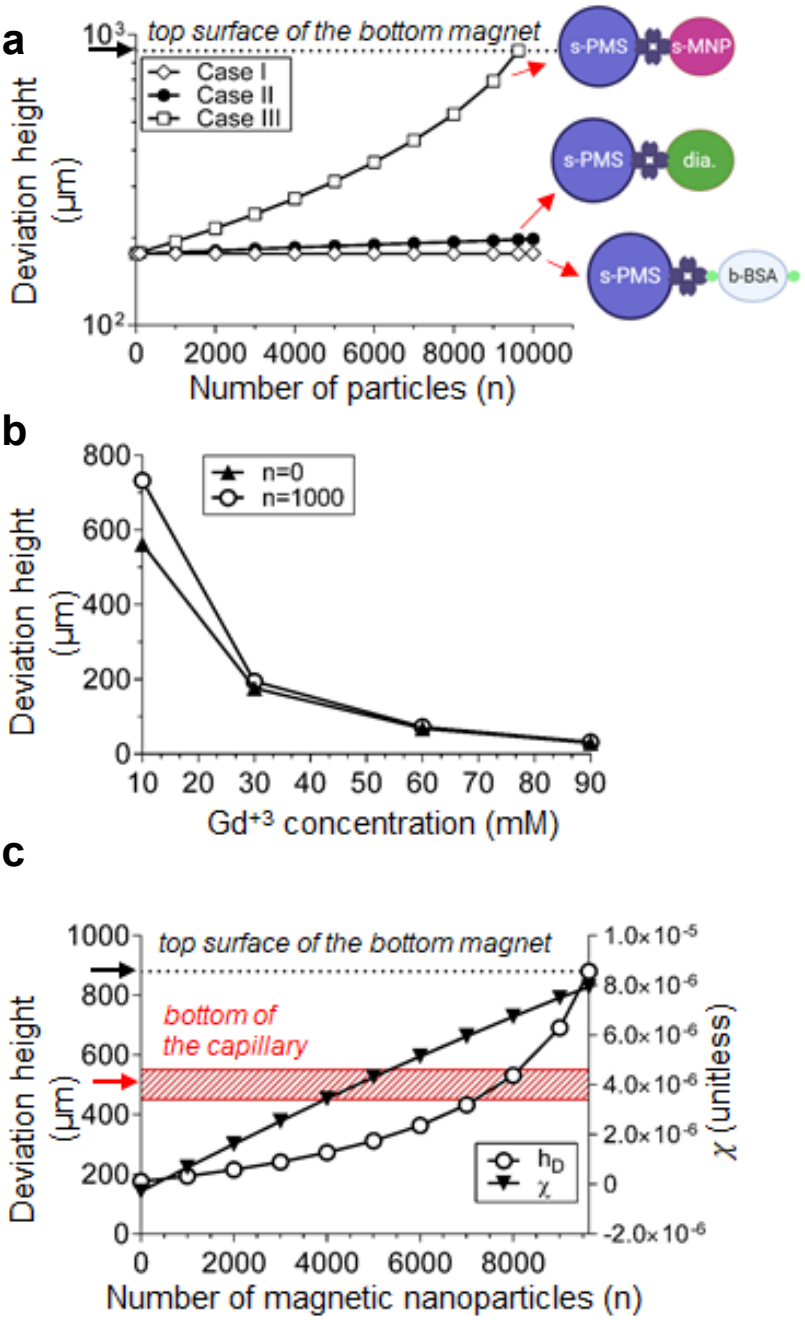

Figure 4.3. Simulation of assay sensitivity for binding of different particles onto polystyrene microspheres. (a) Deviation heights of microspheres when covered with b-BSA molecules, magnetic nanoparticles, and diamagnetic nanoparticles at different numbers (n). The dashed line represents the top surface of the bottom of the magnet. The simulation is performed for a 30 mM Gd^{3+}-based paramagnetic medium. (c) Modeling of deviation heights of microspheres in case of binding of magnetic nanoparticles for n = 0 and n = 1000 with 10 mM, 30 mM, 60 mM, and 90 mM Gd^{3+}-based levitation medium. (d) Modeling of deviation heights of microspheres and the corresponding magnetic susceptibility in case of binding of magnetic nanoparticles at different numbers. The dashed line represents the top surface of the bottom of the magnet. The red shaded area is the range of microcapillary bottom surface distances (450-550 μm) from the centerline.

According to the results, increasing Gd^{3+} concentration decreases the deviation height change of s-PMS upon magnetic nanoparticle attachment. In other words, the lower the concentration of Gd^{3+} is, the higher the detection sensitivity is achieved. For example, the deviation height change for 90 mM Gd^{3+} is increased only by 5.5%, whereas it is increased by 6.1%, 10.2% and 30.4% for 60 mM, 30 mM and 10 mM Gd^{3+}, respectively, due to the attachment of 10^3 magnetic nanoparticles (Figure 4.3 b). Even though 10 mM Gd^{3+} concentration gives the highest sensitivity in terms of deviation height change, s-PMSs come to the equilibrium at very close heights to the bottom of the capillary with a channel height of 1000 μm, which prevents observing them in the channel. Lastly, the change of a magnetic susceptibility and deviation height of s-PMS is simulated upon the attachment of magnetic nanoparticles at different numbers in 30 mM Gd^{3+} levitation medium (Figure 4.3 c). Magnetic susceptibility values increase linearly with the number of the attached magnetic nanoparticles whereas deviation height values increase sharply with the magnetic nanoparticles. With 30 mM Gd^{3+}, up to ~4×10^{-6} (SI units), magnetic susceptibility changes corresponding to ~4×10^3 magnetic nanoparticle binding on the s-PMS can be observable in the capillary channel with a height of 1000 μm ± 100 μm.

Next, the levitation profile of s-PMS spiked in 30 mM Gd^{3+} with (i) no b-BSA, (ii) 1.05 ng/mL b-BSA, and (iii) 1.05 ng/mL b-BSA and s-MNP was experimentally tested (Figure 4.4). Similar to the simulation results in Figure 4.3, the significant change in the levitation of s-PMS occurs in the presence of s-MNP (Figure 4.4 b). Most of proteins are diamagnetic and owe very small magnetic susceptibility (e.g., χ_{BSA}: -0.826×10^{-6} (CGS units)(Luo et al., 2010) and e.g., χ_{water}: -0.719×10^{-6} (CGS units) (Spees et al., 2001)). Hence, there was no significant change in the density and magnetic susceptibility of s-PMS upon the binding of b-BSA, and consequently, the deviation height of s-PMS was not altered. On the other hand, s-MNP attached to the s-PMS and b-BSA complex changed the overall magnetic susceptibility (χ_p) of the complex and set a new levitation height for s-PMS, which is closed to the bottom magnet. Later, the magnetic susceptibility change due to the attachment of 1.05 ng/mL b-BSA was calculated to be 2.7×10^{-6} (SI units) from Figure 4.4 c by fitting the deviation height versus magnetic susceptibility data shown in Figure 4.3.

In routine operations, superconducting quantum interference device (SQUID) magnetometry (Cukauskas et al., 1974), vibrating sample magnetometer (VSM) (Foner, 1959), and nuclear magnetic resonance (NMR) (Frei and Bernstein, 1962) are widely used

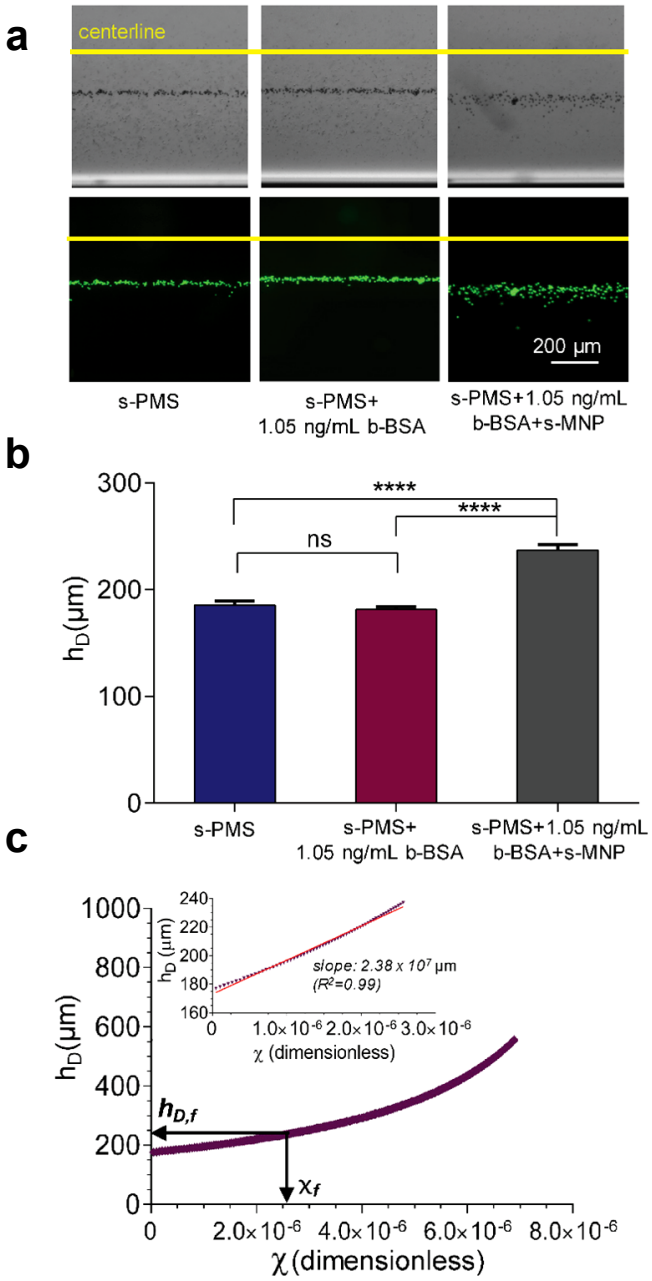

Figure 4.4. The sensitivity of the protein assay in the presence and absence of magnetic nanoparticles for detection of 1.05 ng/mL b-BSA. (a) Bright-field and fluorescent microscopy images of s-PMS after 30 min of levitation in the 30 mM Gd^{3+}-based paramagnetic medium. Micrographs correspond to the reference (no b-BSA), s-PMS with 1.05 ng/mL b-BSA, and s-PMS with 1.05 ng/mL b-BSA and s-MNPs experiments, respectively. (b) Quantitative deviation height analysis of microspheres shown in a. Data are presented as mean deviation height ±SD. Data are compared with each other using a one-way ANOVA. **** represents $P < 0.0001$ and ns represents not significant. (c) Magnetic susceptibility versus deviation height simulation for s-PMS. The final magnetic susceptibility (χ_f) of s-PMS in the presence of 1.05 ng/mL b-BSA and s-MNPs can be determined from the distinct deviation height ($h_{D,f}$) of s-PMS. Zoomed plot and linear fit to the data with a coefficient of determination (R^2) are shown in the figure.

techniques for sensitive magnetic susceptibility measurements of materials. However, they include a hard-to operate and expensive scheme that is not optimized for single-particle measurements. To overcome these limitations, the magnetophoretic motion of particles in a non-homogeneous magnetic field has been used for measuring volumetric susceptibilities of both non-labeled cells ($\chi_{\text{HeLa tumor cells}}$: -0.5136×10^{-6} (CGS units)) (Kashevskii et al., 2006) and labeled cells ($\chi_{\text{yeast, liver and carcinoma cells}}$: $13\text{-}20 \times 10^{-6}$ (SI units)) (Russell et al., 1987). In this study, a magnetic levitation strategy to measure target proteins captured on microspheres with a change in the magnetic susceptibility of microspheres was used. The method can distinguish a volumetric magnetic susceptibility of a single microsphere with a resolution of 4.2×10^{-8} (SI units) per 1 μm deviation height change in a 30 mM Gd^{3+} based paramagnetic liquid (Figure 4.4 c).

4.4.3. Levitation Profile of s-PMS in Paramagnetic Medium

The sensitivity of magnetic levitation-based measurement can be adjusted by changing paramagnetic agent concentration as shown in the simulations (Figure 4.3). Different Gd^{3+} concentrations (i.e., 10, 30, 60 and 90 mM) were tested to levitate s-PMS with a diameter of 6 μm suspended in PBS buffer with 1% (v/v) of Tween 20 surfactant during 30 min (Figure 4.5). As expected from simulation results (Figure 4.3 c), s-PMS reached the bottom of the capillary channel ($h_D = 500 \pm 50$ μm) for 10 mM Gd^{3+}, which was not capable to levitate s-PMS in the channel and could not be used for protein detection experiments.

Moreover, increasing the amount of Gd^{3+} resulted in levitating s-PMS at higher positions closed to the centerline plane, which was the middle plane between magnets. Microspheres reached their equilibrium levitation heights faster for higher Gd^{3+} concentrations (Figure 4.5 b). For instance, deviation height values of s-PMS were remained constant after 25 min for 10 mM Gd^{3+}, whereas this equilibrium was reached only after 10 min for 60 mM of Gd^{3+}. For protein detection experiments in different Gd^{3+} concentrations, the levitation could be conducted for 30 min to ensure a steady-state deviation height profile.

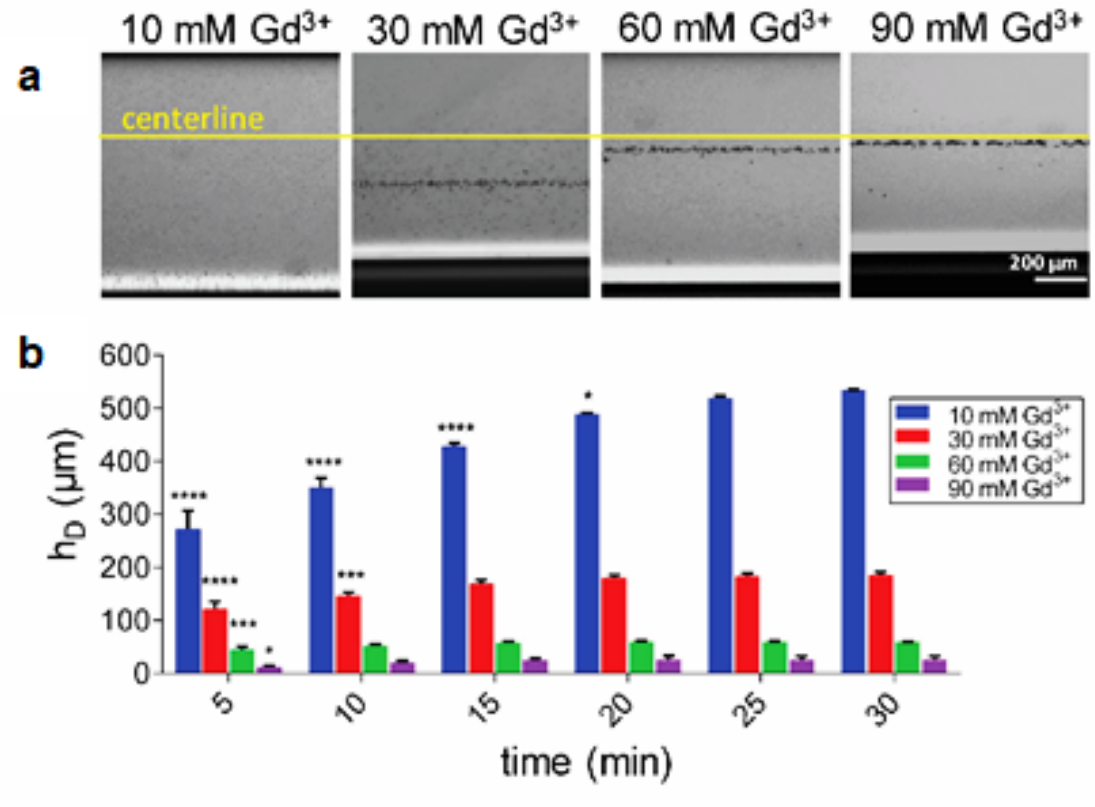

Figure 4.5. Levitation of s-PMS with s-MNP under different Gd^{3+} concentrations without b-BSA. (a) Micrographs of s-PMS, after 30 min levitation with 10, 30, 60, and 90 mM of Gd^{3+}. The yellow line represents the centerline plane. (b) Deviation height analysis of microspheres. Data are shown as the mean of three replicates with error bars (±SD). Data for each Gd^{3+} concentration are compared with the final levitation value (i.e., the deviation profile after 30 min of levitation) at that concentration value using a one-way ANOVA. ****, ***, and * represent $P < 0.0001$, $P < 0.001$, and $P < 0.05$, respectively.

4.4.4. Levitation of s-PMS in the Presence of b-BSA Spiked in PBS

Detection of b-BSA with the presented assay method was conducted in 30 mM, 60 mM, and 90 mM Gd^{3+}. The average deviation heights of s-PMS for various b-BSA concentrations are shown in Figure 4.6. Limit of detection (LOD) signal was calculated as adding three standard deviations to the mean of the reference signal (0 g/mL b-BSA) (Shrivastava and Gupta, 2011). Experimental results were fitted into a linear curve since the linear fitting of experimental data provided a sufficient coefficient of determination (R^2=0.92) compared to sigmoid and exponential fits presented in Figure 4.7. Since the

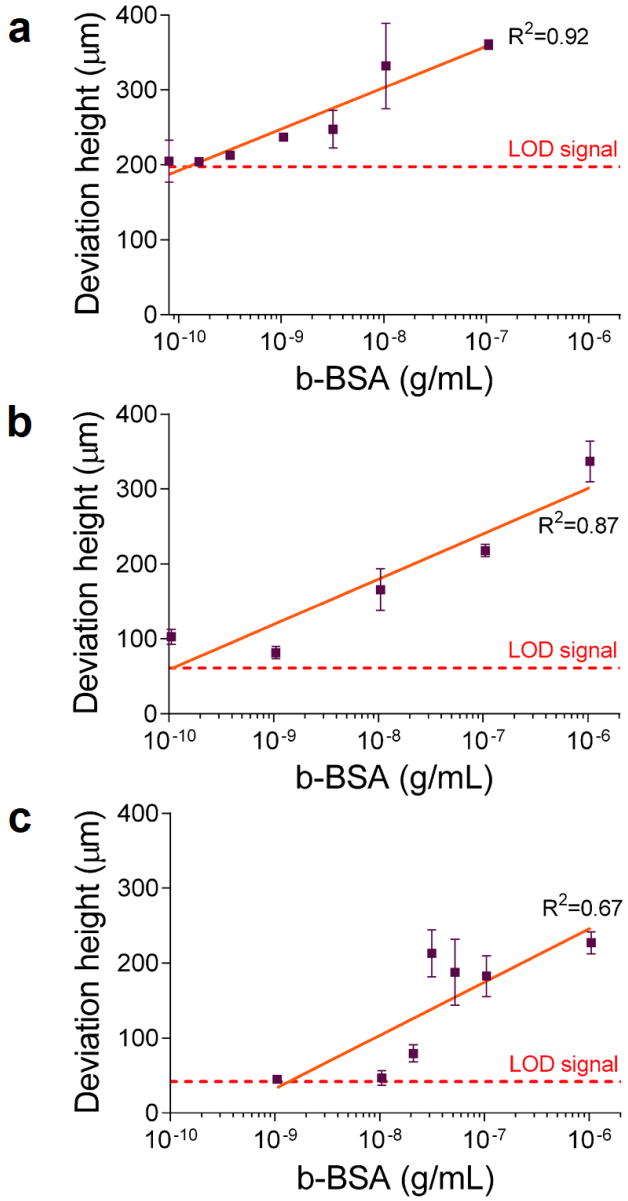

Figure 4.6. Levitation of s-PMS in b-BSA-spiked PBS samples. Deviation heights with (a) 30 mM, (b) 60 mM, and (c) 90 mM Gd^{3+}-based paramagnetic medium are presented. Data are shown as mean of three replicates with error bars (±SD). Linear fits to the data with coefficient of determination (R^2) are shown as solid lines.

linear regression is commonly preferred in bead-based assays and detection platforms (Gaster et al., 2009; Rissin et al., 2010; Tekin et al., 2013), linear fits for the estimation of detectable protein concentrations were preferred to use. Lowest detected protein concentration values were calculated as the intersection of these linear curves and the LOD signal. For a protein concentration above and near the LOD line of 30 mM Gd^{3+}

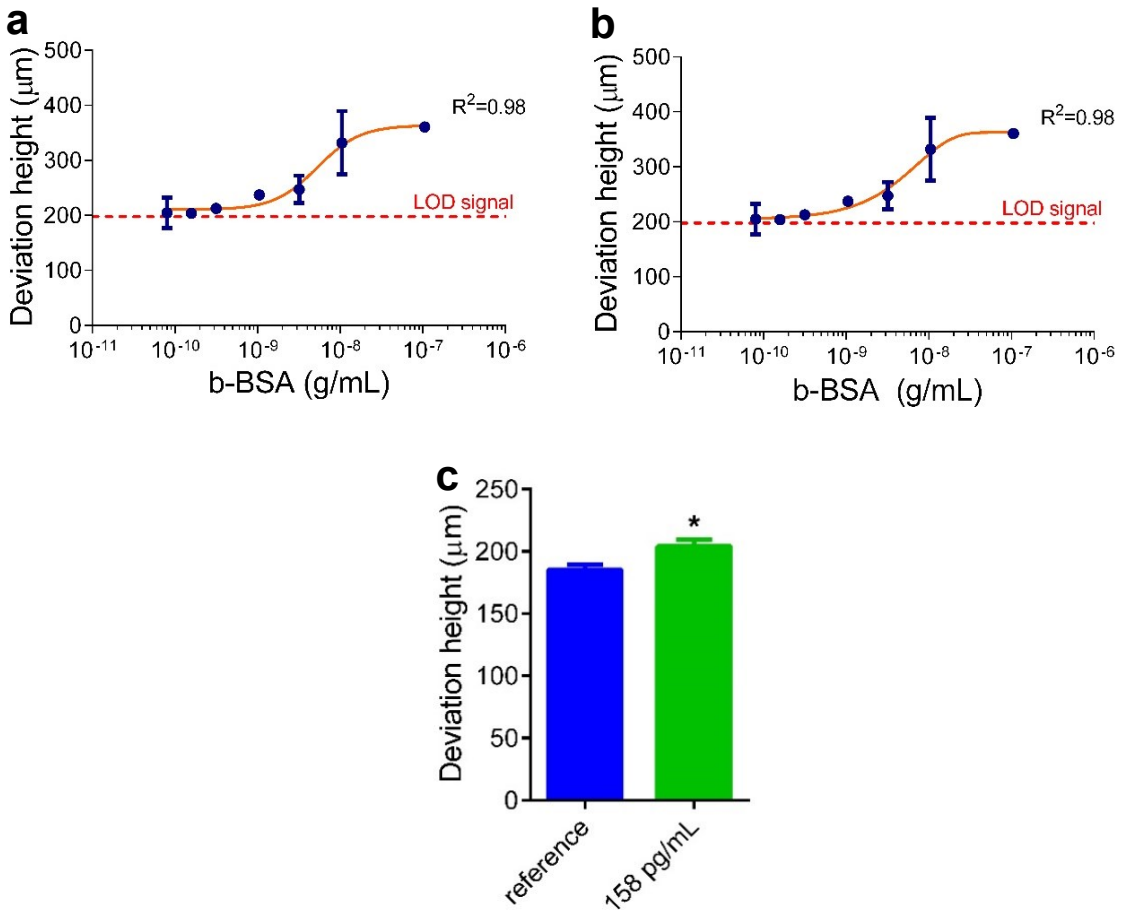

Figure 4.7. The fitting of the experimental data for PBS-30 mM Gd^{3+} experiments. (a) A sigmoidal and (b) an exponential fit. LOD signals were calculated by adding 3 × SD of the reference signal (0 g/mL) to the mean of the reference signal. (c) A tested b-BSA concentration above and near the LOD line in PBS for 30 mM Gd^{3+} was also compared to the reference with an unpaired t-test with Welch's correction. Statistical significance (*) was determined as $p<0.05$.

(i.e., 158 pg/mL), the deviation height was also statistically different ($p < 0.05$) compared to the reference (Figure 4.7 c). LOD values of > 0.1 ng/mL were obtained in 30 mM and 60 mM Gd^{3+} solutions for b-BSA whereas a > 1 ng/mL LOD value was reached in 90 mM of Gd^{3+} solutions. As shown in simulations (Figure 4.3), experimental results also revealed that the detection the sensitivity of the assay was improved with the decrease in Gd^{3+} concentration. The LOD value in PBS experiments using 30 mM Gd^{3+} (i.e., 0.12 ng/mL, ~2 pM) requires ~1.0×10^4 b-BSA available molecules per microspheres in the solution. This corresponds to a 1×10^{-6} increase in the average magnetic susceptibility of the microspheres (Figure 4.4 c), which is due to the attachment of more than 1.2×10^3 s-MNPs (Figure 4.3c) per microspheres. Since microspheres started to reach the boundary

of the capillary channel for 1 µg/mL b-BSA at 30 mM Gd^{3+}, deviation height values of microspheres would be saturated beyond this concentration. The points including the reference condition (no b-BSA) are also presented in Figure 4.8.

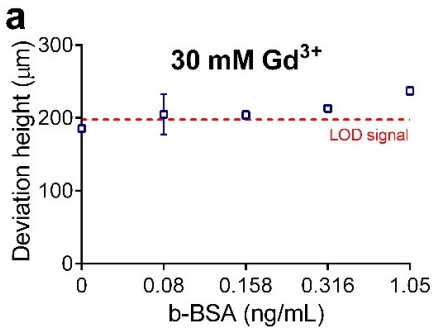

b-BSA (ng/mL)	Average height in Test 1 (µm)	Average height in Test 2 (µm)	Average height in Test 3 (µm)	Average height in all tests (µm)	± SD (µm)
0	179.8	189.4	186.9	185.4	4.1
0.08	198.4	241.8	174.6	204.9	27.8
0.158	210.4	204.8	196.9	204.1	5.5
0.316	214.9	207.7	216.0	212.9	3.7
1.05	230.1	239.6	242.0	237.2	5.2

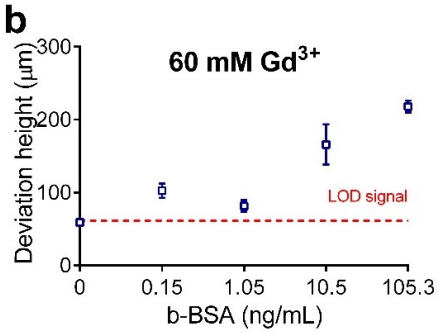

b-BSA (ng/mL)	Average height in Test 1 (µm)	Average height in Test 2 (µm)	Average height in Test 3 (µm)	Average height in all tests (µm)	± SD (µm)
0	58.8	60.2	58.7	59.2	0.7
0.15	90.6	102.4	115.1	102.7	10.0
1.05	70.6	89.6	84.8	81.6	8.1
10.5	128.9	173.4	195.6	166.0	27.7
105.3	229.2	210.1	214.4	217.9	8.2

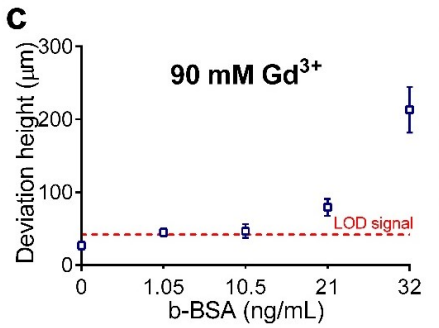

b-BSA (ng/mL)	Average height in Test 1 (µm)	Average height in Test 2 (µm)	Average height in Test 3 (µm)	Average height in all tests (µm)	± SD (µm)
0	21.7	33.7	24.9	26.8	5.1
1.05	43.7	52.3	38.3	44.8	5.7
10.5	38.0	42.0	60.0	46.7	9.6
21	66.4	77.0	94.5	79.3	11.6
32	170.3	225.8	243.6	213.2	31.2

Figure 4.8. Data with zero concentration for PBS samples using different b-BSA concentrations with (a) 30 mM Gd^{3+}, (b) 60 mM Gd^{3+} and (c) 90 mM Gd^{3+}.

4.4.5. Levitation of s-PMS in the Presence of b-BSA Spiked in FBS

Direct examination of biological molecules in the blood serum of a patient is of great importance in diagnostic assay development strategies. In this regard, s-PMS and s-MNP were suspended in FBS without b-BSA and used as a reference test first. However,

all s-PMSs were collected at the bottom of the capillary probably due to the non-specific adsorption of serum proteins and s-MNP onto the s-PMSs, and causing microspheres to settle down to the bottom of the channel (Figure 4.9). To eliminate non-specific adsorption of proteins, Tween 20 and Pluronic F-127 as non-ionic surfactants were used (Boxshall et al., 2006). PBS with 1% (v/v) of Tween 20 solution (PBST) and PBS with 1% (w/v) of Pluronic F-127 (PBSP) were used to dilute the FBS sample. For 1:1 (v/v) dilution of sample solution with PBST (1%) buffer, still no microsphere was observed in the glass microcapillary during the levitation which was probably due to the continuing effect of non-specific bindings. Later, the dilution ratio was increased to 1:10 (v/v) and

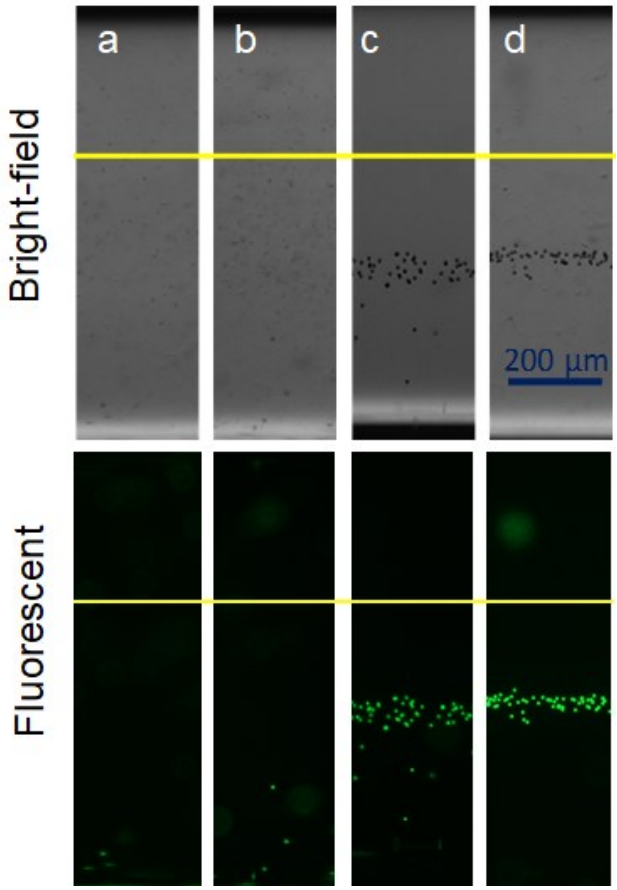

Figure 4.9. The bright-field and fluorescent micrographs of the microcapillary channel for the reference of serum experiments. (a) without diluting the sample, (b) with diluting the sample 1:1 with PBST buffer (PBS containing 1% Tween 20 (v/v)), (c) with diluting the sample 1:10 with PBST buffer, and (d) with diluting the sample 1:1 with PBSP buffer (PBS containing 1% Pluronic F-127 (w/v)). The sample contained dialyzed FBS without b-BSA. Experiments were conducted with a 30 mM Gd^{+3}-based levitation medium. Yellow line: centerline of the magnets

microspheres could be levitated in the glass capillary. In the case of PBSP (1%), a 1:1 (v/v) ratio sample dilution worked for microspheres. Then, the detection capacity of the magnetic levitation-based assay in the serum sample composed of FBS spiked with b-BSA was tested. For b-BSA spiked FBS tests, the sample was diluted with either 1:10 (v/v) using PBST or 1:1 (v/v) using PBSP. Experiments conducted with the 30 mM Gd^{3+}-based levitation medium revealed that deviation heights of s-PMS were increasing with b-BSA concentration and a LOD value of >1 ng/mL was obtained for b-BSA in FBS using both PBST and PBSP dilutions (Figure 4.10 a, b). However, s-PMSs were less dispersed in the capillary channel with PBSP dilution than in that with PBST dilution for the reference test (Figure 4.9). The distribution profile of s-PMS was also increasing with b-BSA concentrations in FBS diluted with PBSP.

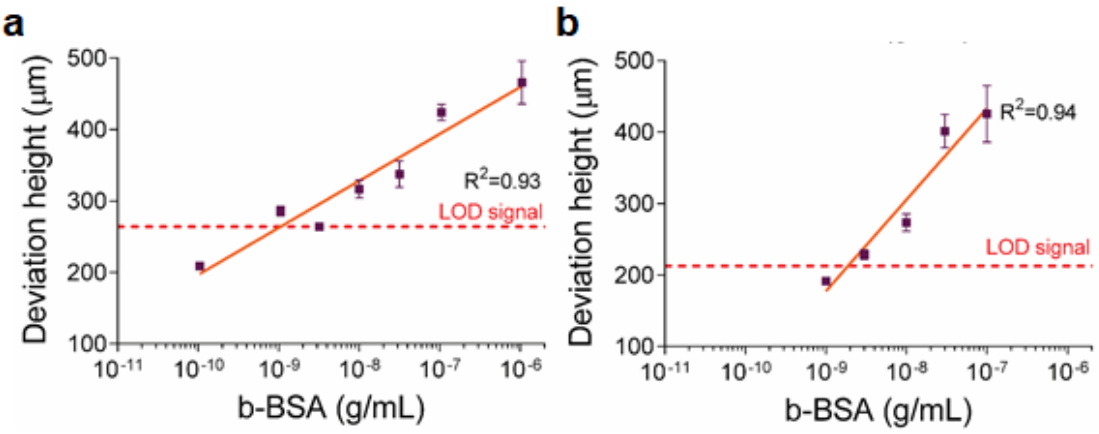

Figure 4.10. Levitation of s-PMS in b-BSA-spiked FBS samples under 30 mM Gd^{3+}-based levitation medium. The FBS samples were diluted using either (a) PBST or (b) PBSP, respectively.

Distribution profile of s-PMS for different b-BSA was also analyzed since not all microspheres would end up with the attachment of the same number of magnetic nanoparticles due to the differences in their binding capacities. CV (%) statistically includes the relative dispersion of data points around the mean value. Because of that, CV (%) was incorporated into the analysis as an indicator of s-PMS distribution within the channel.

CV values of reference tests with 0 g/mL b-BSA were not statistically different even from high b-BSA concentration (i.e., 30 ng/mL) since there could be non-specific

bindings on s-PMS surfaces in serum samples (Figure 4.11). In order to eliminate s-PMS distribution due to non-specific bindings, outlier s-PMSs were statistically determined and removed using the ROUT Method (Motulsky and Brown, 2006). For different maximum desired false discovery rate (Q) values (*i.e.* 0.5-5 %), CV values were calculated (Figure 4.12). Experimental data before and after removing identifiers with Q=1 for serum samples of b-BSA are also presented (Figure 4.13 a-d). With this method, CV values of reference tests became statistically different for various b-BSA concentrations. Furthermore, increasing Q value (Q>0.5%) did not affect CV values of reference tests (Figure 4.13 e, f). Since choosing Q more than 1 increases the risk of getting falsely identified outliers (Motulsky and Brown, 2006), CV analyses were made with removing outliers under the ROUT method with Q=1% value.

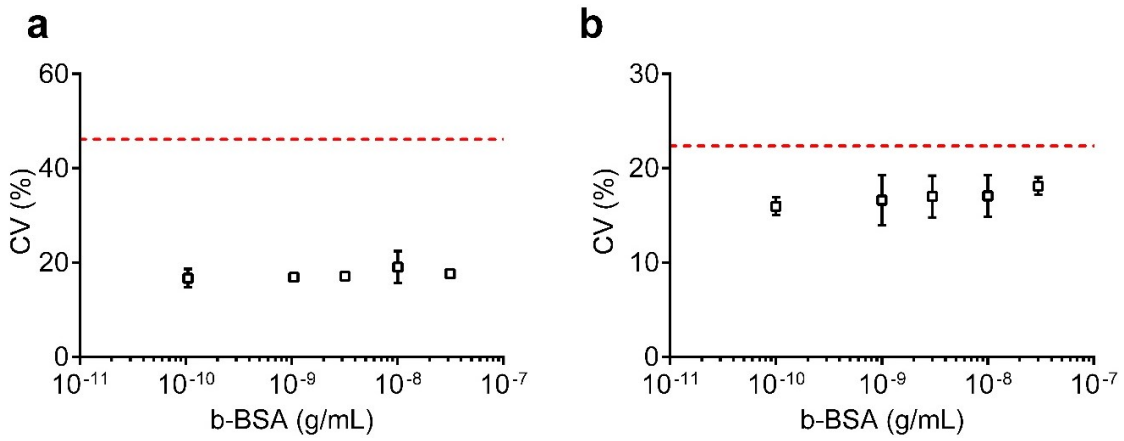

Figure 4.11. Distribution analysis of FBS samples with respect to b-BSA concentration diluted with (a) PBST and (b) PBSP. Data are presented as mean of three replicates with error bars (±SD). Dashed lines represent LOD signal (LOD is calculated as mean CV (%) of reference plus three times of ±SD). CV values of reference tests for PBST and PBSP were 25.2 ± 7.0 and 17.7 ± 1.5, respectively. 30 ng/mL data of both buffers were compared with reference using a t-test with Welch's correction and no significance was observed.

s-PMS with b-BSA showed a more distributed deviation height profile within the microcapillary channel compared to the s-PMS without b-BSA (Figure 4.13). However, the average deviation height-based analysis does not include this distribution.

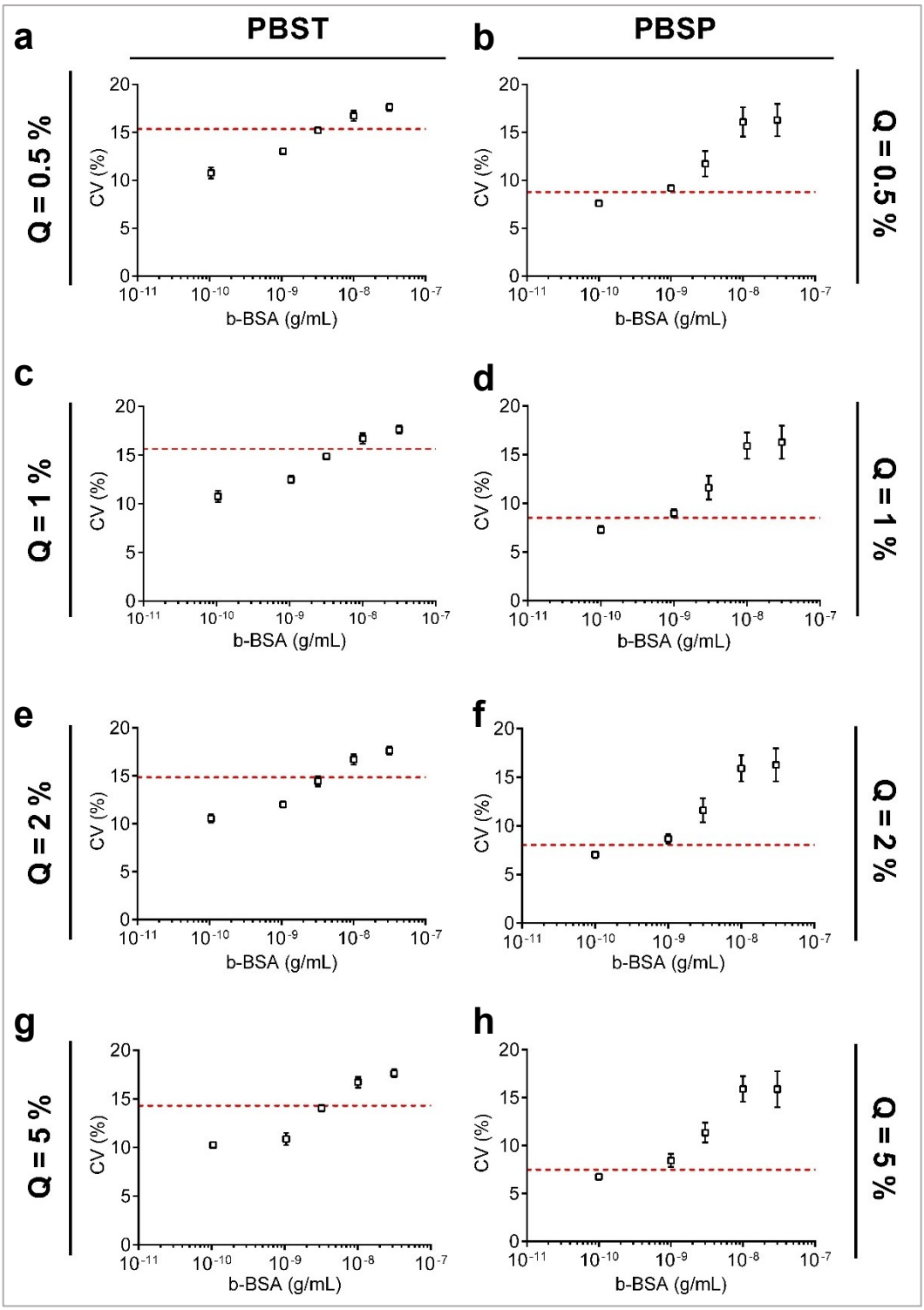

Figure 4.12. CV (%) of serum samples under different Q values. The samples are diluted with (a, c, e, g) PBST and (b, d, f, h) PBSP after outliers were removed with ROUT analysis under Q = 0.5, 1, 2, and 5 %. Data are presented as the mean of three replicates with error bars (±SD). Dashed lines represent LOD (LOD is calculated as mean CV (%) of reference plus three times of ±SD).

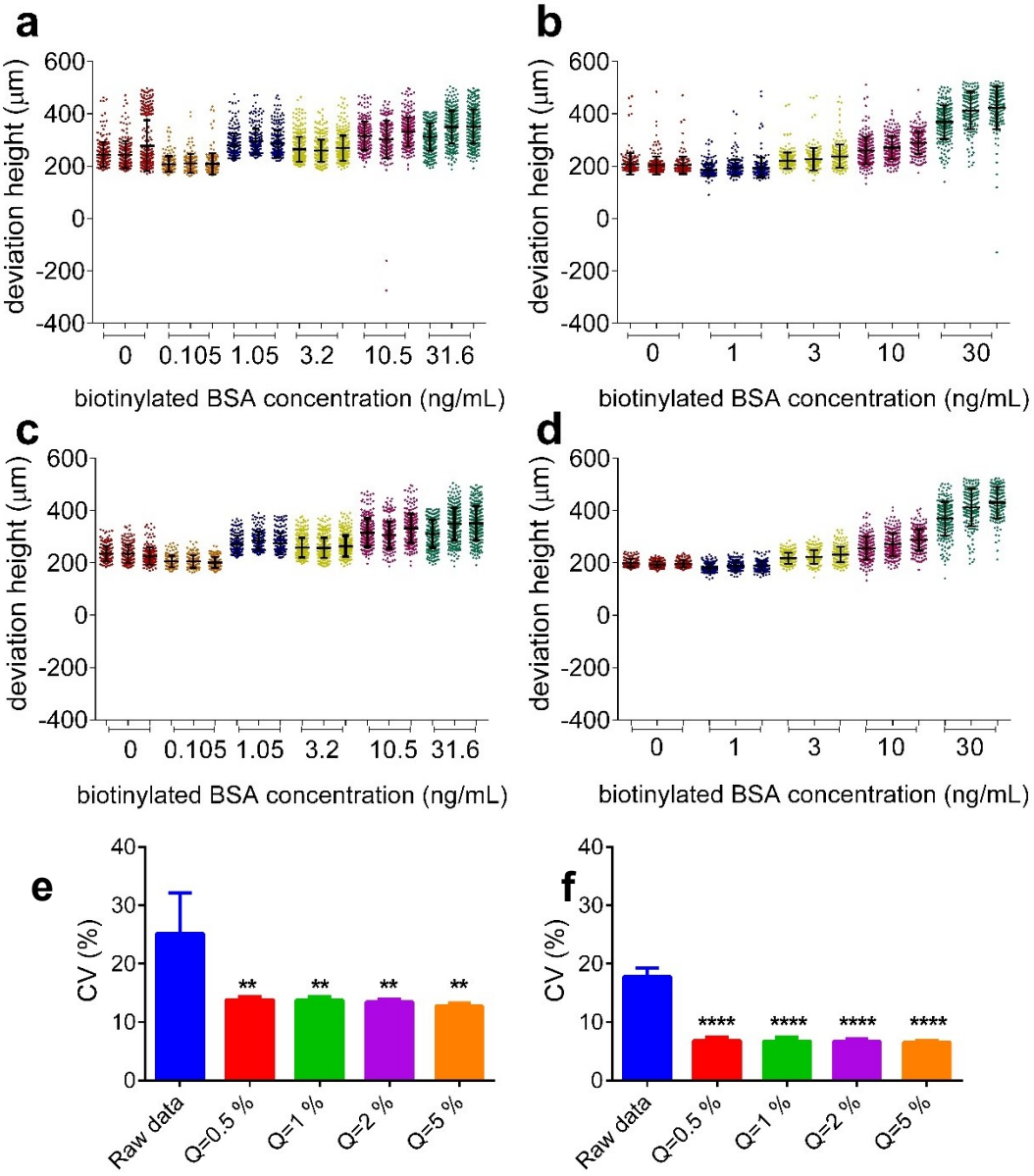

Figure 4.13. The deviation of each microsphere in FBS samples with respect to b-BSA concentration, (a) with diluting the sample 1:10 (v/v) with PBST buffer (PBS containing 1% Tween 20 (v/v)) (b) with diluting the sample 1:1 (v/v) with PBSP buffer (PBS containing 1% Pluronic (w/v)), (c) with diluting the sample 1:10 (v/v) with PBST buffer and eliminating the outliers under ROUT method (Q=1), (d) with diluting the sample 1:1 (v/v) with PBSP buffer and eliminating the outliers under ROUT method (Q=1). Distribution analysis of reference tests (i.e., 0 g/mL b-BSA) in serum samples diluted with (e) PBST and (f) PBSP before and after removing outliers with ROUT for different Q values. Data are presented as the mean of three replicates with error bars (±SD). Data were compared to the raw data of 0 ng/mL b-BSA using a one-way ANOVA for both PBST and PBSP. ** and **** represent $P < 0.01$ and $P < 0.0001$, respectively (n=3).

Due the distributed profile of s-PMS, the change in CV (%) was greater than the change in average deviation height in the presence of b-BSA (Figure 4.14). As shown in Figure 4.15, there was a high distribution in the s-PMS profile for reference tests (CV ≅ 14%) using PBST dilution. On the other hand, for the dilution with Pluronic, s-PMSs in reference tests were not widely distributed (CV ≅ 7%). Hence, in the assay protocol, Pluronic in dilution buffer could eliminate better non-specific bindings on s-PMS surfaces than Tween. CV analysis revealed that detectable b-BSA concentrations could be slightly improved only for the experiments conducted with Pluronic. This approach reduced the LOD down to ~715 pg/mL levels for b-BSA in FBS samples diluted 1:1 (v/v) with Pluronic. However, it should be noted that CV (%) of s-PMS is influenced by the number of analyzed particles. Therefore, s-PMS number in the channel should be kept constant in all experiments.

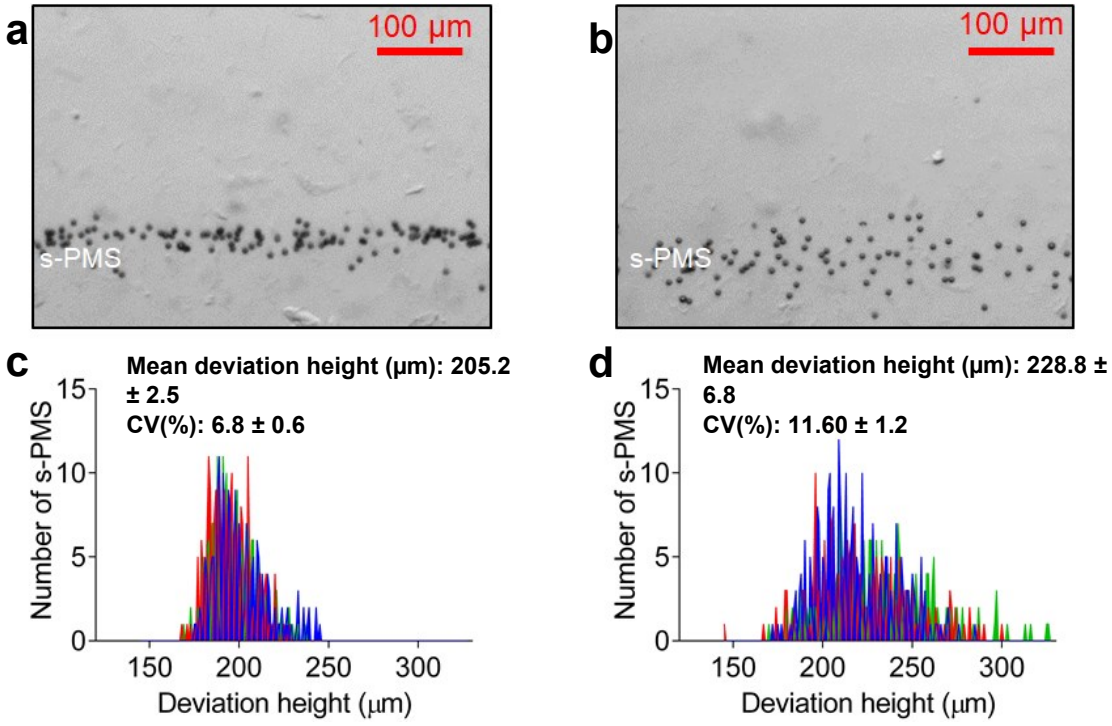

Figure 4.14. Levitation profile of s-PMS in the absence and presence of b-BSA in serum samples diluted with PBSP under 30 mM Gd^{3+} concentration. Micrographs of s-PMS (a) without b-BSA and (b) with b-BSA (3 ng/mL). Distribution analysis of s-PMS (c) without b-BSA and (d) with b-BSA. In the presence of b-BSA, CV was increased 1.7-fold and, on the other hand, the average deviation height was increased 1.1-fold compared to no b-BSA case. Experimental data in c and d were presented as blue, red, green colors for three replicates with statistically removed outliers (Q=1%).

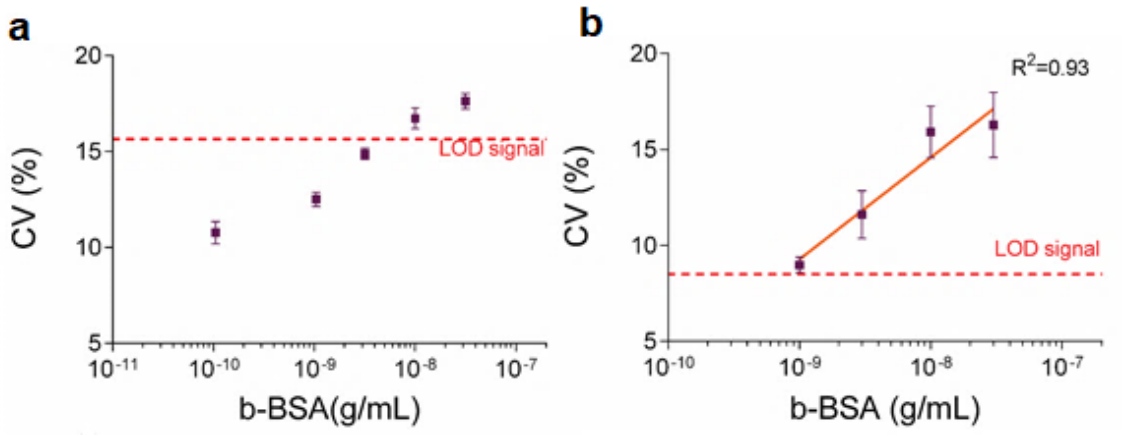

Figure 4.15. CV (%) analyses of the deviation height profiles with respect to b-BSA concentration. The dilution of FBS sample with (a) PBST and (b) PBSP, respectively. Data are shown as mean ±SD. Linear fits to the data with coefficient of determination (R^2) are shown as solid lines.

Then, 10-fold diluted s-PMS was used in order to improve the detection sensitivity in serum by increasing the number of target proteins per microsphere. Hence, much more b-BSA molecules and s-MNP labels would be concentrated on s-PMS for the same b-BSA concentration levels used in previous experiments. CV analysis (Figure 4.16) was conducted for the data after removing outliers with 1% Q value for different b-BSA concentrations in FBS sample diluted 1:1 (v/v) with PBSP. Experiments revealed that the

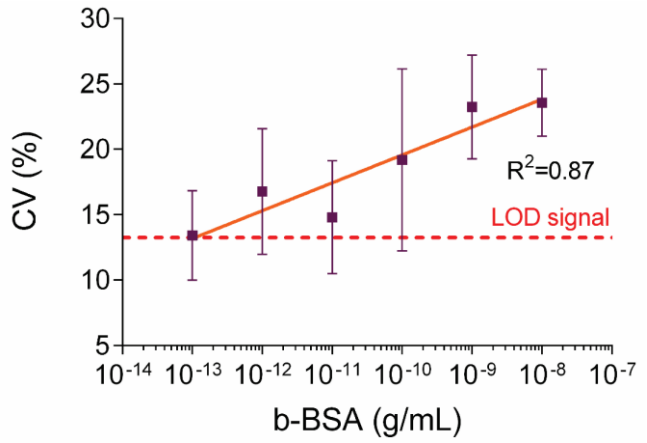

Figure 4.16. CV (%) analysis of the deviation height profiles of diluted s-PMS for different concentrations of b-BSA-spiked FBS sample prepared in PBSP. Data collected using the 30 mM Gd^{3+}-based levitation medium are shown as the mean of three replicates with error bars (±SD). A linear fit to the data with a coefficient of determination (R^2) is shown as a solid line.

LOD reached down to ~110 fg/mL levels for b-BSA in the serum sample. However, the standard deviation increased between the repeats because of the low number of microspheres. CV and deviation analysis for serum experiments with zero concentrations are presented in Figure 4.17.

4.4.6. Detection of Immunoglobulin G as a Biomarker

4.4.6.1. Optimization of the Dilution Buffer

Buffer 1 (PBSP) resulted in microsphere aggregation for the negative test in PBS containing 0 g/mL mouse IgG. Most of the microspheres were attracted at the bottom of the capillary channel during the levitation procedure. This indicated non-specific binding on microspheres. In Buffer 2 (PBSP-BSA), BSA molecules were added into the Buffer 1 at 1% (w/v) to block the surfaces and eliminate non-specific binding. By using this buffer, functionalized microspheres could be levitated with a CV (%) of 6.7 ±0.4 in PBS containing 0 g/mL mouse IgG. Therefore, Buffer 2 was decided to be used in the further experiments.

4.4.6.2. Optimization of the Magnetic Nanoparticle Concentration

1 µL magnetic nanoparticle concentration did not create a significant change in the deviation height of microspheres compared to reference for the PBS sample. Increasing magnetic nanoparticle concentration from 1 µL to 3 µL increased the deviation height difference between the reference and 1 µg/mL IgG (Figure 4.18). For the FBS sample, 3µL still gave the significant change in the deviation heights.

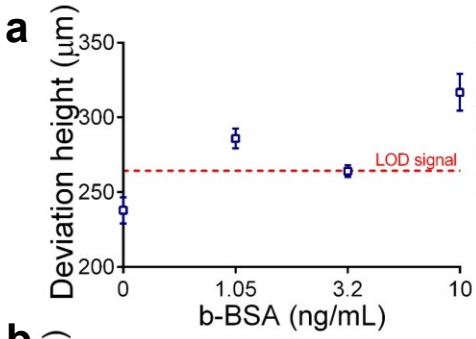

b-BSA (ng/mL)	Average height in Test 1 (µm)	Average height in Test 2 (µm)	Average height in Test 3 (µm)	Average height in all tests (µm)	± SD (µm)
0	243.9	244.3	225.5	237.9	8.8
1.05	278.4	294.5	285.0	286.0	6.6
3.2	264.5	259.1	268.7	264.1	3.9
10	315.9	302.1	332.4	316.8	12.4

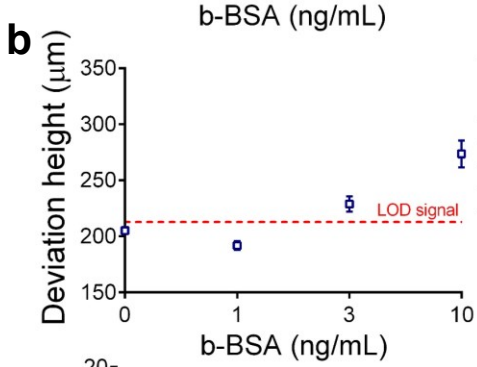

b-BSA (ng/mL)	Average height in Test 1 (µm)	Average height in Test 2 (µm)	Average height in Test 3 (µm)	Average height in all tests (µm)	± SD (µm)
0	208.7	203.2	203.6	205.2	2.5
1	186.2	194.7	194.6	191.8	4.0
3	221.2	227.5	237.7	228.8	6.8
10	260.3	270.9	289.3	273.5	12.0

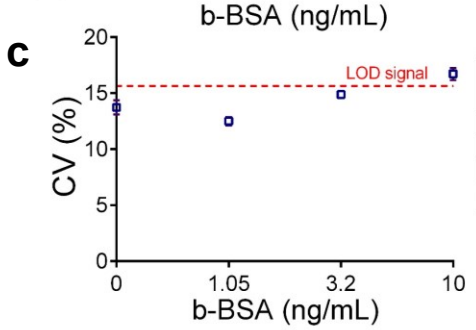

b-BSA (ng/mL)	Average height in Test 1 (µm)	Average height in Test 2 (µm)	Average height in Test 3 (µm)	Average height in all tests (µm)	± SD (µm)
0	12.9	14.3	14.0	13.7	0.6
1.05	12.4	12.1	13.0	12.5	0.4
3.2	14.5	15.2	15.0	14.9	0.3
10	17.29	16.86	16	16.7	0.5

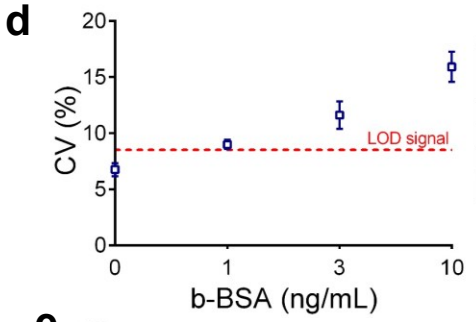

b-BSA (ng/mL)	Average height in Test 1 (µm)	Average height in Test 2 (µm)	Average height in Test 3 (µm)	Average height in all tests (µm)	± SD (µm)
0	7.5	6.1	6.7	6.8	0.6
1	8.4	9.4	9.2	9.0	0.4
3	9.9	12.0	12.9	11.6	1.2
10	17.3	16.3	14.1	15.9	1.3

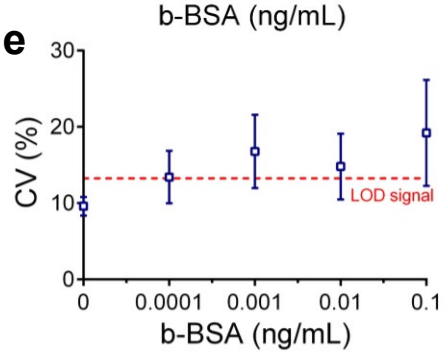

b-BSA (ng/mL)	Average height in Test 1 (µm)	Average height in Test 2 (µm)	Average height in Test 3 (µm)	Average height in all tests (µm)	± SD (µm)
0	9.7	8.1	11.0	9.6	1.2
0.0001	18.3	11.2	10.8	13.4	3.4
0.001	17.1	22.5	10.8	16.8	4.8
0.01	19.6	15.7	9.1	14.8	4.3
0.1	18.7	10.9	28.0	19.2	7.0

Figure 4.17. Data of FBS samples with zero concentration for different b-BSA concentrations using 30 mM Gd^{3+}. Deviation height and CV (%) analyses for the samples diluted with (a, c) PBST and (b, d) PBSP, respectively. (e) CV (%) analysis for 1:10 diluted s-PMS with sample diluted in PSBP buffer.

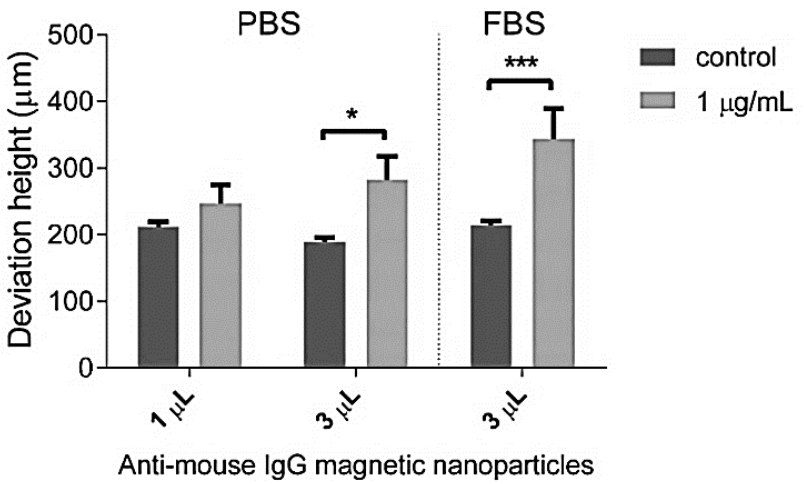

Figure 4.18. Optimization of the anti-mouse IgG magnetic nanoparticles for detection experiments in PBS and FBS. * and *** represent $P < 0.05$ and $P < 0.001$, respectively.

4.4.6.3. Measurement of IgG Concentration in Pure and Complex Media

Lastly, a sandwich immunoassay was applied to the polymer microspheres for the detection of a serological biomarker. IgG was chosen as the target biomarker to validate the method since IgG levels in the blood are indicators of neutralization of toxins and pathogens (Diem et al., 2019), and autoimmune diseases (Haroun and M El-Sayed, 2007). The normal concentrations of total IgG in human blood ranges between 8-16 mg/mL (Linder et al., 2002) and discrepancies in total IgG levels in blood relates to serious health problems. For instance, in hypogammaglobulinemia the IgG levels are significantly reduced (Pimenta et al., 2019). On the other hand, elevated levels of IgG may be the signatures of cancer (Qiu et al., 2003) or long-term infections such as HIV (McGowan et al., 2006). Moreover, antigen-specific IgG tests possess very critical role for the conformation of viral infections such as severe acute respiratory syndrome coronavirus 2 (SARS-CoV-2), in which specific IgG concentration peaks at 16.47 μg/mL after the onset of the illness and stays at 11.4 μg/mL until 31-41 days (Ma et al., 2020). In this context, microspheres and magnetic nanoparticles covered with biotinylated anti-mouse IgG antibodies were used to detect mouse IgG spiked in buffer and serum by monitoring deviation heights of anti-mouse IgG microspheres (Figure 4.19). In PBS,

LOD value was determined as 1.5 ng/mL (~ 10 pM) (Figure 4.19 a) whereas in FBS, a higher concentration (> 10 ng/mL) was detectable with CV analysis (Figure 4.19 b). LODs calculated with deviation height analysis were 1.8 ng/mL (~ 12 pM) for PBS and 31 ng/mL (~ 210 pM) for FBS (Figure 4.19 c, d). The results revealed that LOD values increased for IgG compared to that of b-BSA. This could be since the b-BSA used in this study contains multiple binding sites (i.e., 8-16 mol biotin per mol BSA) for binding onto the s-PMS and s-MNP. Moreover, the streptavidin-biotin interaction has a 10^3-10^6 times higher affinity than an antibody-antigen formation and is not easily disturbed by assay manipulations such as washing steps (Diamandis and Christopoulos, 1991). In addition, the increases in LOD when compared to b-BSA could be due to the lowered number of available target binding sites on particles since not all streptavidin molecules on their

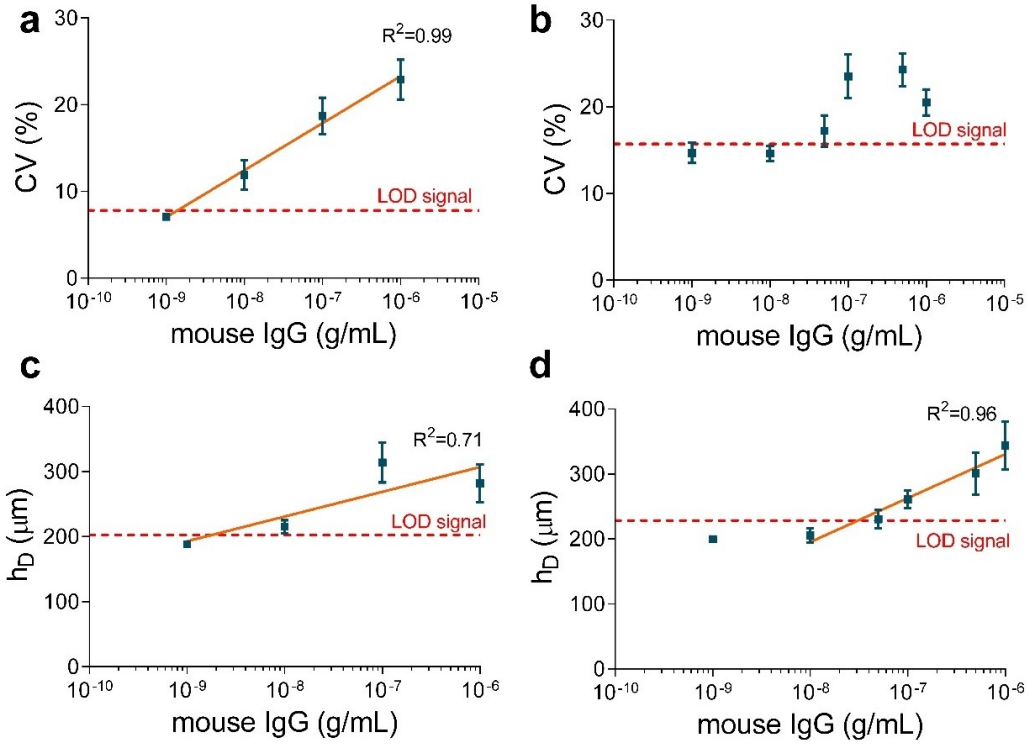

Figure 4.19. Deviation analyses of the anti-mouse IgG microspheres for different concentrations of mouse IgG. IgG was spiked in (a,c) PBS and (b,d) FBS and analyzed in terms of CV and deviation height of microspheres. Data collected using a 30 mM Gd^{3+}-based levitation medium are shown as the mean of three replicates with error bars (±SD). A linear fit to the data with a coefficient of determination (R^2) is shown as a solid line.

surface would be functionalized with the well-oriented biotinylated antibody. This can be eliminated by immobilizing capture antibody covalently onto the pre-activated solid phase, instead of using the streptavidin-biotin system. It is a complex method but may improve antibody density on the surface (Welch et al., 2017).

4.4.7. Comparison with Other Magnetic Levitation-Based Protein Detection Methods

Magnetic levitation technology has been exploited to detect different proteins. Target proteins, sample volume, detection limit, assay time, and detection principle of those studies are presented in Table 4.1. So far, the detection efforts have been based on the density change of microparticles upon binding of target molecules. This study is novel in that it has proved the applicability of magnetic susceptibility-based protein detection under magnetic levitation offering notable protein detection levels of ~ 110 fg/mL (~ 1.6 fM) in serum samples and improved the detection sensitivity of magnetic levitation technology. Since biological samples mostly have weak magnetic signals (Tao et al., 2020), the measurement based on magnetic susceptibility change can also be used to detect many other clinically important biomolecules.

Compared to the detection limits (>100 pg/mL) and assay time (>360 min) of conventional ELISA (Rissin et al., 2010), the magnetic susceptibility-based protein assay provided low detection limits for a biotinylated target protein with reasonable analysis time (~80 min). The protein analysis with the presented strategy was conducted directly on a simple brightfield microscope with a more straightforward method that does not require complex instrumentation, numerous washing, and incubation steps, unlike conventional ELISA. Moreover, magnetic nanoparticles could be adopted in ultrasensitive and automated on-chip protein analysis platforms (Cornaglia et al., 2014; Tekin et al., 2013). For a remote and portable protein analysis, this assay could be adopted to low-cost and portable imaging systems such as cellular phones (Andersen et al., 2017), lensless holographic microscopy systems (Delikoyun et al., 2019a; Sobieranski et al., 2015), and self-contained and handheld magnetic levitation devices (Yenilmez et al., 2016a; Yenilmez et al., 2016b). In addition, integration of the assay into flow-assisted magnetic levitation devices (Amin et al., 2016) could enable analyzing higher sample

Table 4.1. Summary of the magnetic levitation-based protein detection strategies

Target Molecule	**Sample**	**Sample Volume**	**Assay time**	**LOD**	**Working Principle**	**Ref.**
IL-6	PBS	Not reported	Incubation (40 min) + Levitation (Not Reported)	10 pg/mL	Density change	(Andersen et al., 2017)
Neomycin	Milk	25 µL	<1h	250 ppb	Density change	(Subramaniam et al., 2015)
Syphilis and hepatitis C antibodies	Serum	100 µL		Qualitative (+/- response)		
Bovine carbonic anhydrase (BCA)	PBS/Blood	20 µL	3-24 h	300-600 nM	Density change	(Shapiro et al., 2012a)
Anti-*T. cruzi* antibodies	Blood	<30 µL	~55 min	5 µg/mL	Density change	(Castro et al., 2018)
Biotinylated bovine serum albumin	FBS	200 µL	Incubation (~50 min) + Levitation (30 min)	110 fg/mL (1.6 fM)	Magnetic susceptibility change	This Study
Mouse immunoglobulin G	PBS/FBS			1.5 ng/mL (10 pM) (in PBS)/ 9 ng/mL (in FBS)		

sizes and hence, increasing the sensitivity of protein detection.

The proposed detection method uses centrifugation to eliminate sample matrices. Hence, the analysis is independent of the variabilities coming from the real sample composition, such as viscosity and density. Even if there are some residues of detected molecules left in the paramagnetic medium with a density of 1.016 g/mL, their effect on the medium density is very low since low concentration of molecules (≤ 1 µg/mL) were used in our study. Moreover, if the sample medium (i.e., FBS with a density of 1.025 g/mL (Durmus et al., 2015)) remains in the paramagnetic medium, its effect should also be observed in the reference tests (i.e., without the target molecule). In addition, the aggregation of the microspheres does not alter the net levitation height of microspheres since the levitation height is independent from the volume of the microspheres (Figure 4.2). It is also known that the magnetic levitation profile was not significantly affected by mild temperature changes (28-36^{o}C) (Anil-Inevi et al., 2018). Considering all, the method shown here could provide consistent readouts in the field. For more sensitive protein detection, MNPs labels with higher susceptibility can be easily adapted in the presented method so that microspheres can deviate more under the same magnetic field and create a significant levitation height change in the presence of ultra-low protein concentrations. By changing the surface properties of the particles, the unspecific adsorption can be reduced in complex media such as blood plasma, and the sensitivity of the assay can be further increased (Lichtenberg et al., 2019).

4.5. Other studies for Characterization of the Assay

4.5.1. The effect of Medium Density on Levitation of Microspheres

According to the simulation results (Figure 4.3 b), the highest deviation height with respect to magnetic nanoparticle attachment to polymer microspheres was achieved when the lowest Gd^{3+} concentration (i.e., 10 mM) was used. However, results of the previous experiments with 10 mM Gd^{3+} -based medium revealed that microspheres could only be levitated near the boundaries of the capillary channel making it impossible for

imaging their deviation in case of protein presence. On the other hand, according to the simulations made in Chapter 3; Section 3.3.2, increasing density of the solution, and therefore, the volumetric density difference between the beads and the paramagnetic medium ($\Delta\rho$) increases the levitation height of the beads. Therefore, increasing density could offer the high sensitivity obtained by the low Gd^{3+} concentration. Using this information, four different density levitation media (i.e., 1.02, 1.03, 1.04, and 1.06 g/mL) were prepared using a density-gradient medium Ficoll 400 (Sigma-Aldrich) and tested with 10 mM Gd^{3+} (Figure 4.20) to be able to levitate beads with a higher resolution. According to Figure 4.20, the reference beads (without protein) had the lowest distribution profile when the microspheres were dissolved in 1.02 g/mL density used compared to 1.04 and 1.06 g/mL. Besides increasing medium density increased the time necessary for the microspheres to equilibrate, such as a few hours. Therefore, 1.02 g/mL was chosen for further protein tests.

4.5.2. The effect of Medium on Protein Detection

For 1.02 g/mL experiments, three biotinylated BSA concentrations, i.e., 1 pg/mL, 100 pg/mL and 100 pg/mL, were tested (Figure 4.21). A small proportion of beads for 1 pg/mL b-BSA experiments were at the bottom of the capillary channel. For 10 and 100 pg/mL experiments, beads were at the bottom of the capillary channel with a higher proportion. Since the capillary channel position is variable between the experiments, this could affect the number of microspheres that could be counted in the microcapillary for each experiment. Nevertheless, deviation height analyses were made with countable microspheres.

According to the results, 10 pg/mL had the highest deviation height change compared to the reference (Figure 4.20 b), whereas 100 pg/mL had the highest microsphere distribution (Figure 4.20 c). Since some of the microspheres were at the bottom of the capillary in the case of 100 pg/mL protein concentration, the error between the experiments was increased for CV analysis.

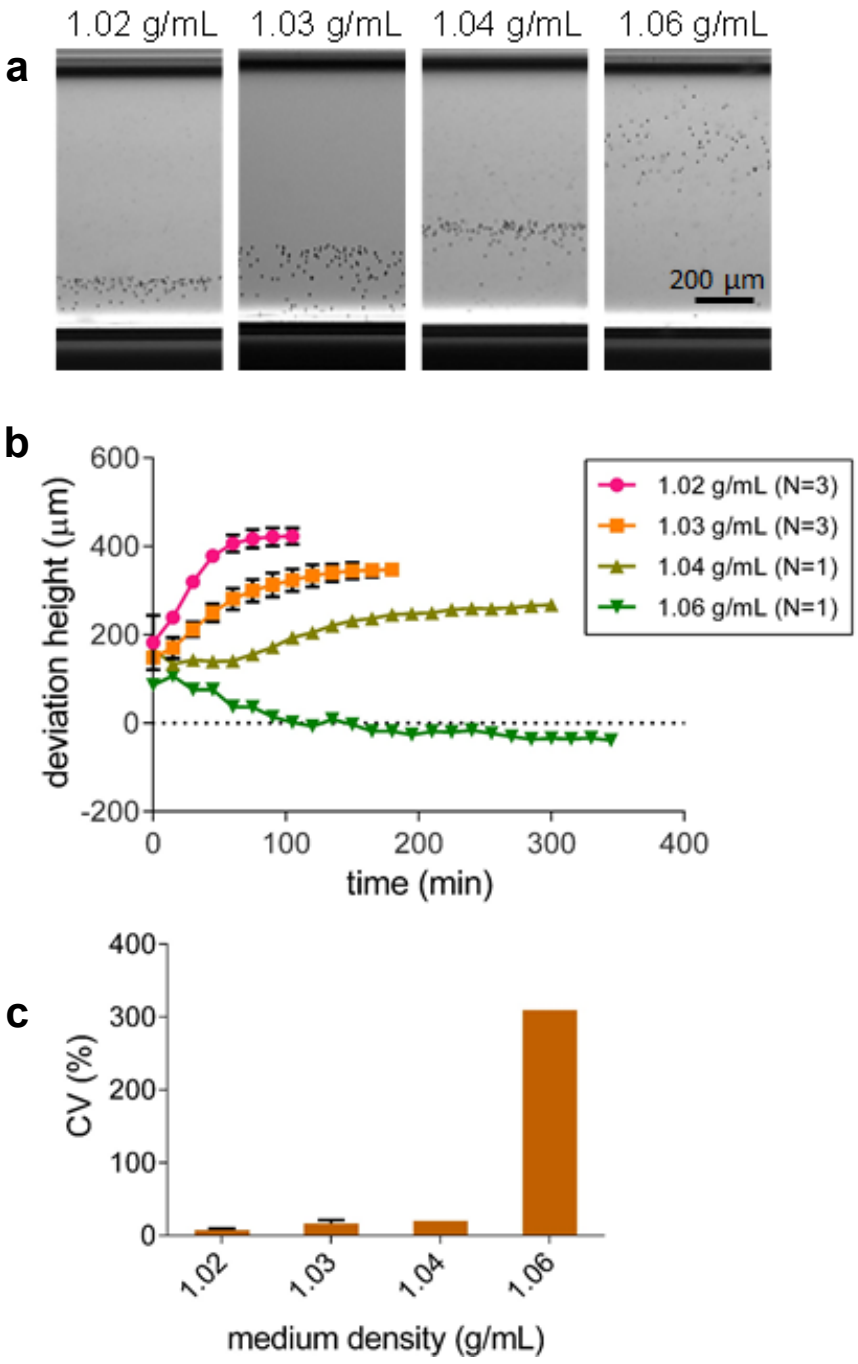

Figure 4.20. Levitation of polymer microspheres without biotinylated BSA under 10 mM Gd^{3+}-based paramagnetic medium with different medium densities. (a) The micrographs of final equilibrium images of i. 1.02, ii. 1.03, iii. 1.04 and iv. 1.06 g/mL under 5x magnification. Scale bar: 200 µm. (b) CV (%) analysis of microspheres at different density media, (c) Levitation height analysis of different density media with respect to time. The data for only 1.02 and 1.03 g/mL medium density are presented as means ± SD of triplicates (N=3). For 1.04 and 1.06, the experiments were conducted once (N=1). 0 in -y axis represents the middle of the capillary.

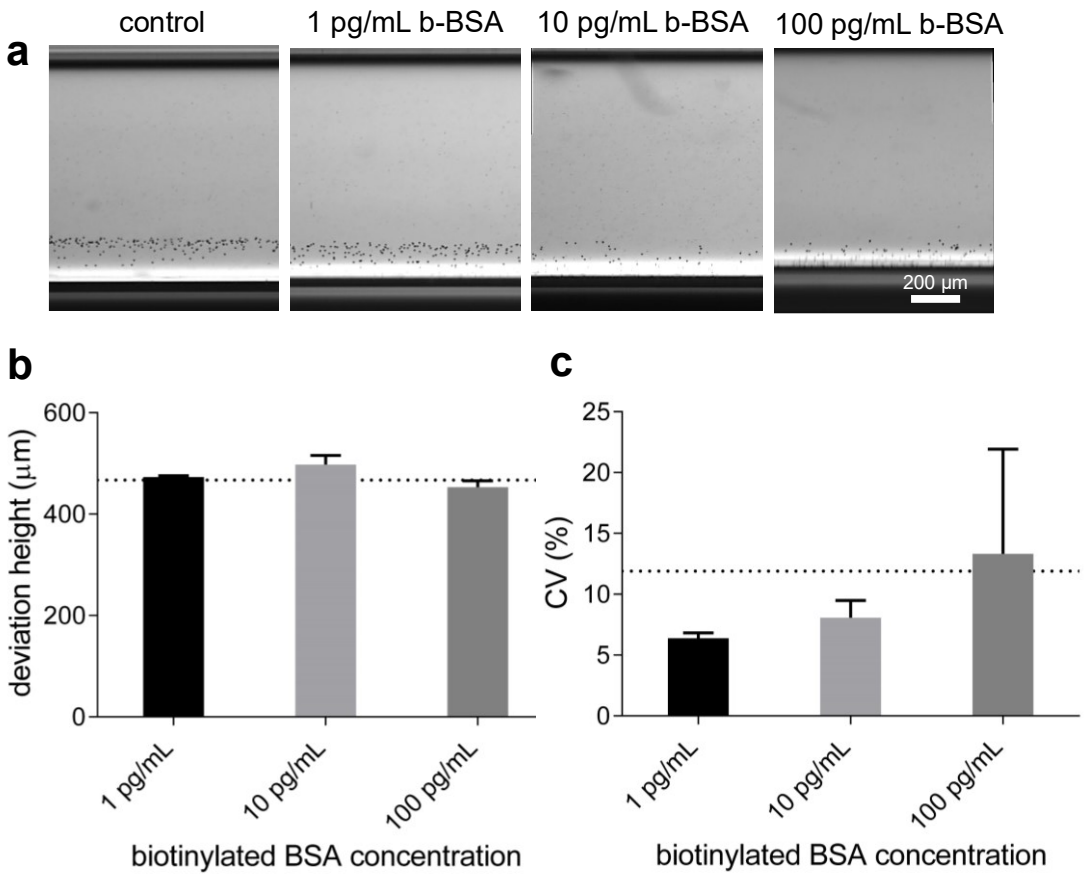

Figure 4.21. Levitation of polymer microspheres with biotinylated BSA under paramagnetic medium with 10 mM Gd^{3+} and 1.02 g/mL density. (a) Micrographs of the capillary channel after 120 min of levitation with 10 mM Gd^{3+} under 5x magnification. Scale bar represents 200 µm. (b) CV (%) analysis of microspheres at different density media.

4.5.3. Characterization of the Assay for Troponin I Detection

Cardiac troponins have revolutionized the management of patients with suspected acute myocardial infarction (AMI) due to their specificity and sensitivity to myocardial (muscular tissue of the heart) cell damage (Negahdary et al., 2016). Therefore, in this study, it was also aimed to develop sandwich immunoassay formats for recombinant human cardiac troponin I detection.

4.5.3.1. Biofunctionalization of Polymer Microspheres and Magnetic Nanoparticles for Troponin I Detection

For biofunctionalization experiments regarding Troponin I detection, streptavidin microspheres and magnetic nanoparticles were modified using recombinant biotinylated Protein G (Pierce™ 29988), biotin, and anti-cardiac Troponin I antibodies (Abcam ab47003). Biofunctionalization was conducted in PBSP-BSA buffer. Since each protocol differs in its incubation steps, the amounts of components are given as a separate list in Table 4.2 per µL of beads. Different protocols listed in Table 4.3 and 4.4 were tested for the detection of recombinant human cardiac Troponin I proteins (Abcam ab207624) spiked in PBS.

4.5.3.2. Sandwich Immunoassay Formats for Troponin I Detection

For the protocols 1-4, the streptavidin polymer microspheres and magnetic nanoparticles were biofunctionalized through the same reaction steps stated in Table 4.3. In this regard, the sandwich immunoassay after the collection of beads at the end of the listed protocols 1-4 was conducted as follows:

Table 4.2. The amount of components used for per µL of beads

	Streptavidin microsphere (1 µL)
Biotinylated Protein G (1 mg/mL)	0.5 µL
Biotin (1 mg/mL)	1 µL
Anti-cardiac Troponin I (0.9 mg/mL)	0.6 µL
	Streptavidin magnetic nanoparticle (1 µL)
Biotinylated Protein G (1 mg/mL)	0.042 µL
Biotin (1 mg/mL)	0.084 µL
Anti-cardiac Troponin I (0.9 mg/mL)	0.05 µL

Table 4.3. The protocols (1-4) tested for modification of streptavidin microspheres and magnetic nanoparticles for cardiac Troponin I detection

		Step*	Time
Protocol 1	I.	Biotinylated protein G incubation	30 min
	II.	Biotin incubation	30 min
	III.	Anti-cardiac Troponin I antibody incubation	30 min
	IV.	Washing with centrifugation	5 min x 2
Protocol 2	I.	Biotinylated protein G incubation	30 min
	II.	Anti-cardiac Troponin I antibody incubation	overnight
	III.	Biotin incubation	30 min
	IV.	Washing with centrifugation	5 min x 2
Protocol 3	I.	Biotinylated protein G incubation	30 min
	II.	Biotin incubation	30 min
	III.	Washing with centrifugation	5 min x 2
	IV.	Anti-cardiac Troponin I antibody incubation	overnight
	V.	Washing with centrifugation	5 min x 2
Protocol 4	I.	Biotinylated protein G incubation	overnight
	II.	Biotin incubation	30 min
	III.	Washing with centrifugation	5 min x 2
	IV.	Anti-cardiac Troponin I antibody incubation	overnight
	V.	Washing with centrifugation	5 min x 2

*Biofunctionalization steps are the same for microspheres and magnetic nanoparticles

1. Biofunctionalized streptavidin microspheres (anti-troponin I microspheres) were added to the PBSP-BSA buffer at a concentration of 10^6 particles per mL.

2. The sample solutions (200µL) in PBS were diluted 1:1 (v/v) using the PBSP-BSA buffer and added into the microsphere solution.

3. The solution is mixed for 30 min at room temperature.

4. The solution is centrifugated and resuspended in 200 µL of PBSP-BSA.

5. 1 µL of biofunctionalized streptavidin magnetic nanoparticles (anti-troponin I magnetic nanoparticles) was added to the sample solution and incubated for 15

min. Later, the solution is mixed with a 1M Gadolinium solution having a volume of 1.2 µL to achieve 30 mM Gd^{3+} in the final loading solution of 40 µL.

Table 4.4. The protocols (5-6) tested for modification of streptavidin microspheres and magnetic nanoparticles for cardiac Troponin I detection

		Step	Time
Protocol 5		**Polymer Microspheres**	
	I.	Biotinylated protein G incubation	30 min
	II.	Biotin incubation	30 min
	III.	Anti-cardiac Troponin I antibody incubation	30 min
	IV.	Washing with centrifugation	5 min x 2
		Magnetic Nanoparticles	
	I.	Biotinylated protein G incubation	30 min
	II.	Biotin incubation	30 min
	III.	Washing with centrifugation	5 min x 2
Protocol 6		**Polymer Microspheres**	
	I.	Biotinylated protein G incubation	30 min
	II.	Biotin incubation	30 min
	III.	Anti-cardiac Troponin I antibody incubation	30 min
	IV.	Washing with centrifugation	5 min x 2
		Magnetic Nanoparticles	
		Stock solution	

On the other hand, for the protocols 5-6 listed in Table 4.4, the biofunctionalization of magnetic nanoparticles differs. For Protocol 5, the 1-2-3 steps were the same as Protocols 1-4. The remaining steps were applied as follows:

4. Free anti-cardiac antibodies were added into the sample solution to attach captured Troponin I molecules onto the microspheres, according to the concentrations given in Table 4.2. Then, the solution is mixed for 30 min.

5. The solution is centrifugated and resuspended in 200 µL of PBSP-BSA.

6. 1 µL of protein G functionalized magnetic nanoparticles was added to the sample solution to label added anti-troponin I molecules through protein G-antibody (IgG) interaction. The resulting solution is incubated for 15 min.

7. The solution is mixed with a 1M Gadolinium solution with a volume of 1.2 µL to obtain 30 mM Gd^{3+} in the final loading solution of 40 µL.

In the case of Protocol 6 (Table 4.4), the stock magnetic nanoparticle solution was used without any modification for functionalization. In this context, 1-4 of the assay steps for Protocol 5 was continued with the following steps as follows:

5. Free biotinylated protein G molecules were added into the sample solution to attach captured Troponin I molecules onto the microspheres, according to the concentrations given in Table 4.2. Then, the solution is mixed for 30 min.

6. The solution is centrifugated and resuspended in 200 µL of PBSP-BSA.

7. 1 µL of the streptavidin magnetic nanoparticles from the stock solution was added to the sample solution to label added biotinylated protein G molecules through streptavidin-biotin interaction. The resulting solution is incubated for 15 min.

8. The solution is mixed with a 1M Gadolinium solution (1.2 µL) to achieve 30 mM Gd^{3+} in the final loading solution of 40 µL.

The protocols in Table 4.3, and 4.4 were tested for 100 ng/mL Troponin I concentration (corresponds to 4.2 nM) and the results are presented in Figures 4.19 and 4.20, respectively. The detection was achieved in terms of deviation height when Protocol 2 (Figure 4.22), which included the overnight incubation of anti-troponin I molecules, was used. In the case of the Protocols where the functionalization of magnetic nanoparticles differs, 100 ng/mL Troponin I could be detected (Figure 4.23) using Protocol 6 in which the magnetic nanoparticles are used from the stock solution.

Even though the definition of normal for plasma levels of cardiac troponins is still controversial, Venge et al. reported the range of cardiac Troponin I molecules measured in healthy subjects as 1.1-7.9 pg/mL (Venge et al., 2009) and elevations above 0.01 ng/mL levels have been considered as troponin I positive test (Dokainish et al., 2005). In this work, the measured signal levels for Troponin I molecules was low for a 100 ng/mL (~4.2 nM) concentration when compared to the assays conducted with b-BSA and IgG in this

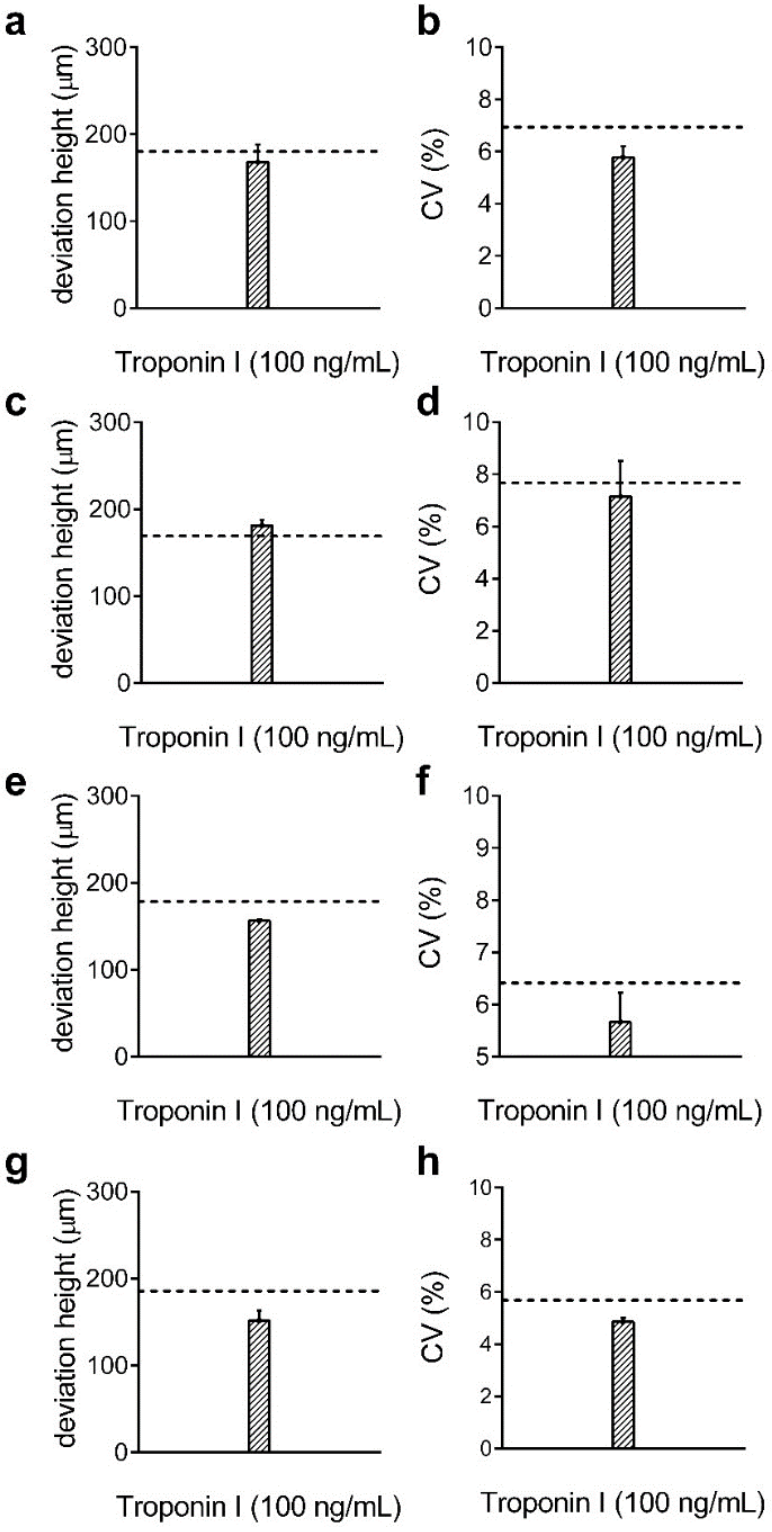

Figure 4.22. The deviation height and CV (outliers eliminated) analyses of different protocols tested (1-4) for Troponin I detection. Protocol 1, 2, 3 and 4 are represented in (a, b), (c, d), (e, f), and (g, h), respectively. Dashed lines represent the LOD signal. Data are presented as mean ± SD.

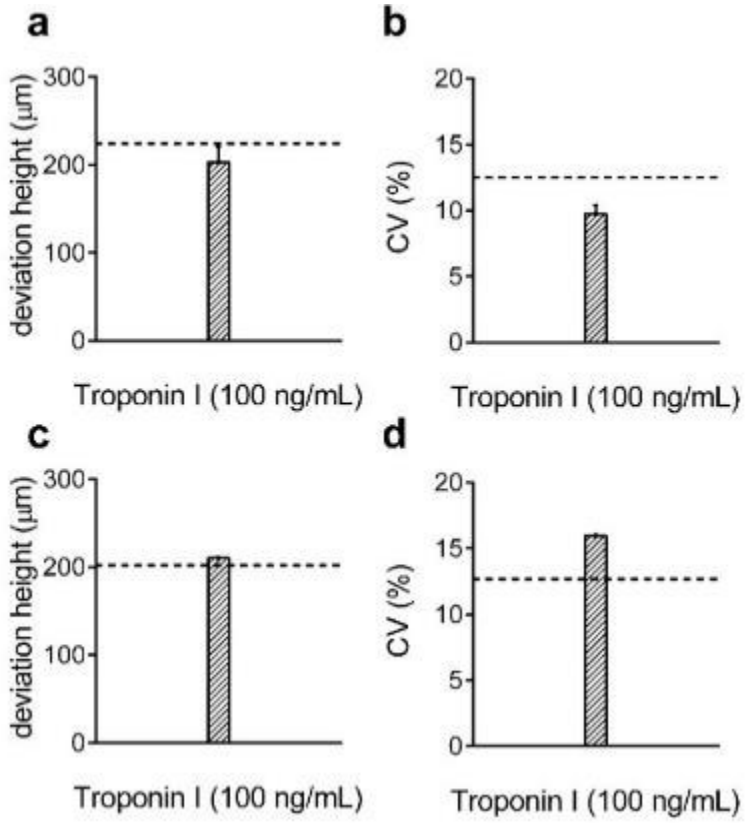

Figure 4.23. The deviation height and CV (outliers eliminated) analyses of different protocols tested (5-6) for Troponin I detection. Protocol 5 and 6 are presented in (a, b) and (c, d), respectively. Dashed lines represent the LOD signal. Data are presented as mean ± SD.

chapter. To increase this signal level and to meet the cut-off levels reported in the literature (Table 2.3), the troponin assay needs significant improvements. In this work, Troponin I detection includes the use of protein G, which is known to bind many immunoglobulin antibodies for immobilization onto solid surfaces (Nistor and Emnéus, 2005). This sandwich immunoassay format relies on using biotinylated protein G as a bridge to attach antibody molecules onto the streptavidin-coated beads increased biofunctionalization steps compared to the direct use of a biotinylated antibody. This may be the reason for decreased binding efficiency and higher LOD in Troponin I when compared to the mouse IgG experiments. For further sensitivity, the attachment of the anti-troponin I antibodies onto the beads could be optimized with other antibody bioconjugation methods to enhance the capture efficiency of the microspheres (Kausaite-Minkstimiene et al., 2010).

4.6. Conclusions

In this study, a new method of using diamagnetic microspheres as mobile assays substrates to catch the target protein and magnetic nanoparticles as labels to increase the magnetic susceptibility of protein-conjugated microspheres was developed. The increase in the magnetic susceptibility results in a significant deviation of microsphere–protein conjugates from the centerline of the two magnets compared to microspheres containing no protein. While other magnetic levitation-based protein detection methods focus on density change of particles due to binding of the target analytes, here, a method that utilizes minute magnetic-susceptibility changes upon labeling the target with magnetic nanoparticles was proposed. Hence, apart from protein detection, the method developed here could be used to estimate the magnetic susceptibility changes of particles with a resolution of 4.2×10^{-8}. The results also revealed that the sensitivity of the method could be improved using a high-density medium (e.g., Ficoll). Moreover, the assay platform does not depend on electric power to operate, and it offers a plain and low-cost design (< $30) that can be mounted easily to a regular microscope for protein measurements. The presented protein detection assay could also be adopted for the detection of any other target molecule using polymeric and magnetic micro/nanoparticles decorated with specific recognition molecules against the target molecule. This could enable the use of the assay in a broad range of applications in the field of environmental inspection, food and water safety, and drug screening tests, and medical diagnosis.

CHAPTER 5

HOMOGENEOUS BIOMOLECULE DETECTION USING MAGNETIC LEVITATION TECHNOLOGY

5.1. Background

Determining the amount of biomolecules present in a solution is a major focus in many practices such as drug screening, environmental monitoring, food safety analysis, and *in vitro* diagnostics. Hence the development of fast, accurate, and sensitive biomolecule detection with cost-effective procedures and instrumentations plays a very critical role in many biotechnological applications. In this chapter a homogeneous biomolecule detection scheme was developed where the detection signal is created within the sample solution without any signal amplification technique (i.e., fluorescent or enzymatic) and independent of washing and elution steps. Streptavidin-coated polymer microspheres and superparamagnetic particles were used for affinity-based capturing and labeling of target biomolecules, respectively. Once the labeled microspheres were loaded inside a paramagnetic solution within the magnetic levitation platform, they were attracted and captured by the magnets while non-biomolecule carrying microspheres were repelled by the magnets and levitate in the sample solution. This phenomenon decreased the total number of microspheres reside in the channel with respect to the amount of target protein present in the sample solution. The method was realized for the detection of bovine serum albumin spiked as target biomolecule and reached a detection limit of 0.43 nM and 73 nM in pure buffer (PBS) and 1:100 (v/v) diluted complex protein mixture (FBS), respectively, using a sample volume as low as 10 μL within 15 min. This approach was also applied for the quantification of mouse immunoglobulin G (IgG) molecules in PBS and provided the detection of 6.7 nM IgG.

5.2. Introduction

The precise measurement of biomolecules within pure solutions and complex matrices are vital in various fields related to the healthcare (Batrla and Jordan, 2015; DePriest et al., 2015), pharmacology (Coleman et al., 1986), environment screening (Albright et al., 2016; Dhar et al., 2019), biodefense (Jenko et al., 2014), and food safety (Samarajeewa et al., 1991). Immunoassays that capture target analytes based on *in vitro* antibody-antigen reaction are backbones of protein detection (Crowther, 2001). Detection of the analyte is achieved with measuring the signal generating labels such as radioactive (Skelley et al., 1973), fluorescent (Ozinskas, 1994), chemiluminescent (Dodeigne et al., 2000; Weeks and Woodhead, 1987) or enzyme (Lequin, 2005). Despite numerous advantages, traditional immunoassays suffer from several limitations. They require multiple steps of washing and incubation, making the whole process take several hours to two days (Lee et al., 2006). As a result, there is a need for creative and novel immunoassays that work with reduced volume, short analysis time and simple operation scheme.

Homogeneous assays in which the analysis signal is developed within the sample simplify the assay procedure (Pulli et al., 2005). There exist sensitive homogeneous protein detection methods coupled with such technologies as dynamic light scattering (Liu et al., 2008), electrochemiluminescence (Akhavan-Tafti et al., 2013) and surface plasmon resonance (Andresen et al., 2014). However, most of them require sophisticated and expensive instruments. Recently, magnetic force-based bioanalytical techniques by levitating microspheres as assay substrates have drawn notable interest owing to its simplicity and cost-effectiveness (Andersen et al., 2017; Castro et al., 2018; Shapiro et al., 2012a; Subramaniam et al., 2015).

In this study, a homogeneous, washing- and amplification-free protein detection scheme was developed using magnetic levitation technology with a minute amount of sample (10 μL). In the assay, polymer microspheres are used as 3D assay substrates. Microspheres that capture target protein are specifically labeled with a magnetic particle. The microspheres conjugated with the target proteins and magnetic particles are attracted by the magnet in the magnetic levitation platform. The developed assay enabled a LOD of 0.43 nM and 73 nM b-BSA in buffer and serum, respectively. Besides, a homogeneous

sandwich immunoassay was developed for the detection of IgG and provided a LOD of 6.7 nM in pure buffer.

5.3. Materials and Methods

5.3.1. Magnetic Levitation Platform

The homogeneous protein detection was achieved in the magnetic levitation system consists of two magnets (N52 grade neodymium magnets, 5 mm height × 2 mm width × 50 mm length) with same poles facing each other and a glass capillary channel (1 mm height × 1mm width × 50 mm length) in which the sample solution is loaded. As the platform is inserted into an inverted benchtop microscope, two side mirrors are attached at a 45° angle onto the magnetic levitation platform to observe the center of the capillary channel using an equipped camera (AxioCam 305) on the inverted microscope (Zeiss Axio Observer Z1, 5 × objective). The components of the platform are held together using 3D-printed body (Formlabs Form 2 3D printer). The detailed information about the production of the platform are presented in Chapter 3.

5.3.2. Optimization of Levitation Time and Gd^{3+} Concentration

For optimization of the assay time, polymer microspheres without target protein were levitated inside the capillary during 15 min under 25, 50, and 100 mM Gd^{3+}-based paramagnetic medium. Levitation heights and microsphere distribution (CV%) within the channel were then analyzed.

5.3.3. Biotinylated BSA Detection

Biotinylated BSA (A8549), streptavidin microspheres (24157-1, Streptavidin Fluoresbrite YG Microspheres, 6.0 μm) and streptavidin magnetic beads (88817, Pierce, 1.0 μm) were purchased from Sigma-Aldrich, Polysciences, Inc., and Thermo Scientific, respectively. In the assay, the biotinylated target proteins were captured on streptavidin microspheres through streptavidin-biotin interaction, first. Later, captured proteins on microspheres were labeled using streptavidin magnetic beads again through streptavidin-biotin binding. In this regard, protein detection protocol starts with mixing of 170 μL streptavidin microsphere solution (10^5 microspheres per mL) prepared with PBS (Gibco, pH=7.4) containing 1% (w/v) of Pluronic F-127 (Sigma-Aldrich) (PBSP) and 10 μL sample b-BSA solution during 5 min in an Eppendorf tube at room temperature (or at 37ºC). For reference tests, the microspheres were incubated with only PBS, FBS, 1:10 (v/v) diluted FBS, or 1:100 (v/v) diluted FBS. Later, 0.34 μL of streptavidin magnetic bead stock solution was spiked into the mixture and incubated for 5 min with continuous mixing. After the incubation with magnetic particles, the Gd^{3+} (Gadavist, 1M) solution was added to the tube at a 25, 50, or 100 mM final concentration and ~40 μL of the resulting solution loaded into the glass capillary channel that was treated for 4 min using a plasma device (Diener Plasma Cleaner). After sealing (Critoseal) the end of the microcapillary channel, it was inserted into the magnetic levitation platform. Even though the method does not include the removal of unbound proteins before the addition of magnetic particles, the effect of centrifugation was also investigated. In this context, the sample solution incubated with the microspheres was centrifugated under 13500 rpm during 5 min (DAIHAN Scientific CF-10) and resuspended in 180 μL of PBSP and spiked with 0.34 μL of magnetic particles.

5.3.4. Immunoglobulin G (IgG) Detection

Mouse IgG (Sigma-Aldrich, I5381) molecules were detected using anti-mouse immunoglobulin G-conjugated microspheres and magnetic beads. In this regard,

streptavidin microspheres and magnetic beads were biofunctionalized with biotinylated anti-mouse IgG molecules (Sigma-Aldrich, B7264) through streptavidin-biotin interaction. For 1 µL of streptavidin microspheres and magnetic particles, 1 µL and 1.1 µL of antibody solution (0.5 mg/mL) were added into separate Eppendorf tubes. Then the volume is completed up to 100 µL with PBS buffer containing 1% (w/v) BSA and Pluronic (PBSP-BSA). The conjugation was achieved for 30 min on a vortex at room temperature. Then, the empty streptavidin molecules on the beads were blocked by free biotin molecules (1 mg/mL) during 30 min agitation at room temperature. After biofunctionalization, the beads were washed twice by centrifugation and resuspended in 1 µL of PBSP-BSA. Anti-mouse IgG microspheres were then diluted in PBSP-BSA to a concentration of 10^5 (or 10^4) particles/mL. IgG detection protocol was conducted as follows: 10 µL of the sample solution is mixed with an anti-mouse IgG microsphere solution prepared in 170 µL of PBSP-BSA. Then, 0.34 µL (or 3.4 µL) anti-mouse IgG magnetic beads were added into the solution and mixed. 5 min, 15 min, 1 h, and 2 h of incubation were tested for IgG. Before loading into the platform, the microsphere solution was mixed with 1M of Gd^{3+} solution to achieve 100 mM Gd^{3+} in the final levitation medium. Then, ~40 µL of the resulting solution is loaded into the microcapillary. The end of the microcapillary channel was sealed (Critoseal) before it was inserted into the platform.

5.3.5. Image Analysis

Vertical position and number of each microsphere within the channel were determined from captured images using the Image J software. The levitation heights of microspheres, the distance from the top surface of the bottom magnet, were determined as explained in Chapter 3, Section 3.3.3. The number of microspheres was counted in the center of the microcapillary channel using a Cell Counter plugin. The number of microspheres was converted to percentage (%) by taking the mean microsphere number obtained for the reference test (no protein) as 100%.

5.3.6. Simulation of Microsphere Levitation

Levitation of microspheres was estimated using Equation 3.12 and magnetic induction ($\vec{B}$) values obtained with FEM simulation data in Chapter 3. In this regard, the density and volumetric magnetic susceptibility of streptavidin microspheres were taken as 1.050 g/mL and 0. For magnetic particles, the density and volumetric susceptibility were used as 2.000 g/mL and 1.6 (assumed to be the same as Dynabeads MyOne (Grob et al., 2018). The diameters of microspheres and magnetic particles were taken as 6.0 μm and 1.0 μm, respectively, in the model.

5.3.7. Statistical Analysis

All the experiments were repeated three times and the data are presented as the mean ± standard deviation (±SD) from the mean of replicates. Limit of detection (LOD) line for biomolecule detection is created by subtracting 3 × SD from the mean value. Statistical significance was determined as $P < 0.05$ and tested using an ordinary one-way ANOVA test.

5.4. Results and Discussion

Here a homogeneous assay was developed for protein detection using magnetically-levitated microspheres with a size of 6 μm and magnetic particles with a size of 1 μm. The platform developed in Chapter 3 was also used for the homogeneous assay.

5.4.1. Modeling and Characterization of Protein Detection Using b-BSA As Target Protein

The strategy for b-BSA protein detection depends on the strong affinity between streptavidin and biotin. In this regard, free b-BSA molecules are captured by streptavidin-coated microspheres with the method shown in Figure 5.1 a. Then, with the addition of magnetic particles, the microsphere-protein complex was labeled. It was previously shown that (in Chapter 4), the significant change in the levitation occurs due to the attachment of magnetic tags, rather than protein. Here, the levitation of streptavidin microsphere in the absence and conjugation of magnetic particle label were modeled. The

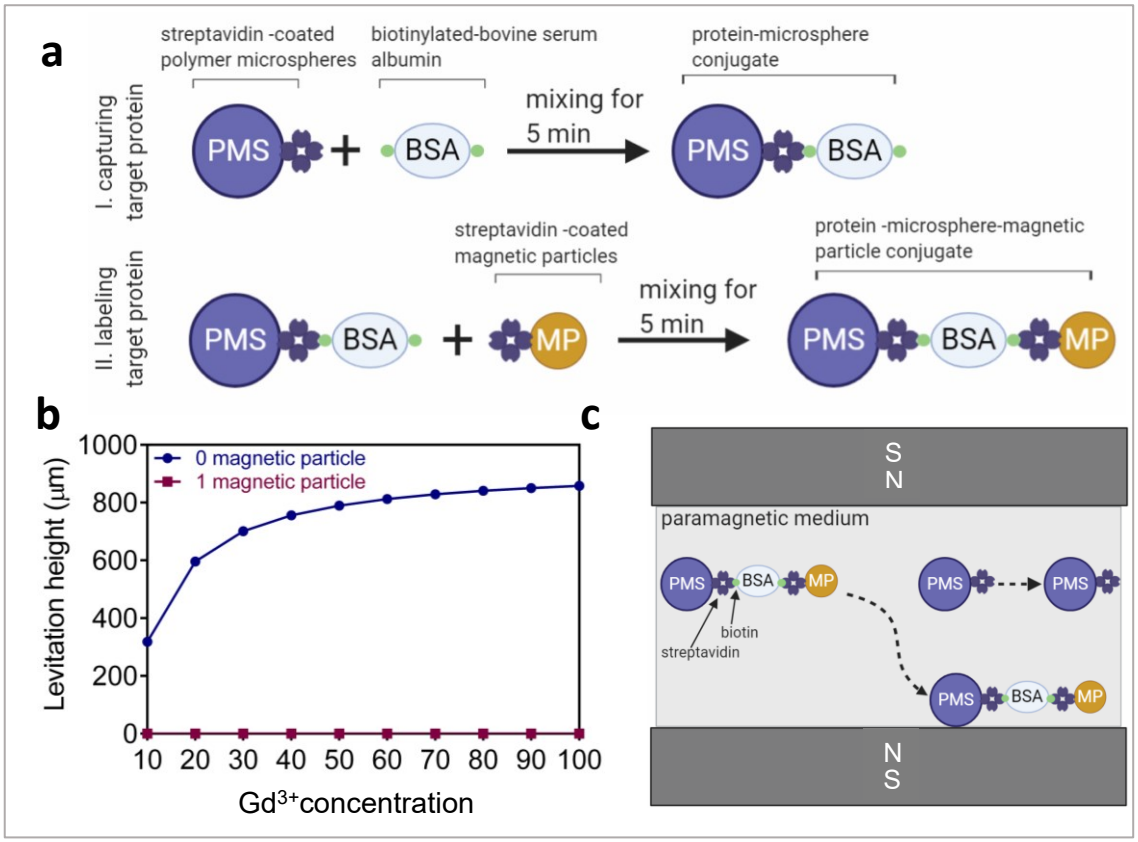

Figure 5.1. Protein detection principle using 1μm magnetic particles. (a) Schematic illustration of protein detection steps. (b) Simulated levitation height change of polymer microspheres in case of binding 1 magnetic particles under different Gd^{3+} concentrations. (c) Protein detection principle using magnetic levitation technology.

results showed that in the presence of only 1 magnetic particle attached to the microsphere, the microsphere is strongly attracted by the magnets, even at high Gd^{3+} concentrations (e.g., 100 mM) (Figure 5.1 b). Therefore, the microsphere cannot levitate. Due to this simulation results, it was hypothesized that in the presence of protein and the magnetic label attached to the microspheres, the number of microspheres levitated in the microcapillary channel would decrease (Figure 5.1 c). This decrease in the bead number could be converted into a percentage by taking the mean bead number of reference (no-protein) as 100%. The remaining microspheres that are not coupled to the protein and magnetic particles would levitate at the same levitation height as the reference.

For the characterization of the system, reference microspheres incubated with only PBS (without b-BSA) and magnetic particles were levitated during 15 min. Since it was aimed to create an assay which results fast, the range between 1-15 min of levitation in terms of levitation height and microsphere distribution were analyzed (Figure 5.2). The

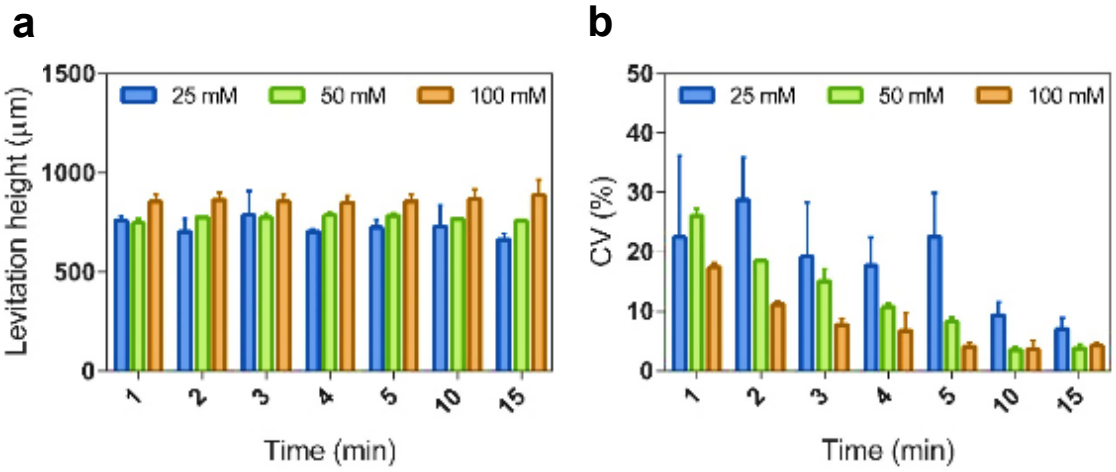

Figure 5.2. The levitation height and bead distribution (CV%) analysis of streptavidin microspheres with respect to time under different Gd^{3+} concentrations.

results revealed that microspheres levitated at higher heights for higher Gd^{3+} concentrations. The levitation height and the microsphere distribution (CV (%)) in the capillary are significantly changed over time for different Gd^{3+} concentrations. The CV of the microspheres decreases as they come to their equilibrium position. The time required for microspheres to reach the 95% of the CV of 15 min levitation was determined as 15 min, 10 min, and 5 min for 25 mM Gd^{3+}, 50 mM Gd^{3+} and 100 mM Gd^{3+}. Therefore,

protein detection experiments were conducted by levitating microspheres at 100 mM Gd^{3+} for 5 min.

The protein detection strategy was tested for b-BSA dilutions prepared in the buffer (PBS) using a very minute amount sample (10 µL). For capturing and labeling b-BSA, the sample solution is incubated with polymer microspheres for 5 min. Then, magnetic particles were added and incubated for another for 5 min. In this context, the total analysis time (offline preparations + microsphere levitation) of b-BSA detection is 15 min. The micrographs of the capillary channel for reference and 1 µg/mL b-BSA in PBS are presented in Figure 5.3. Due to the binding of protein and magnetic particles onto

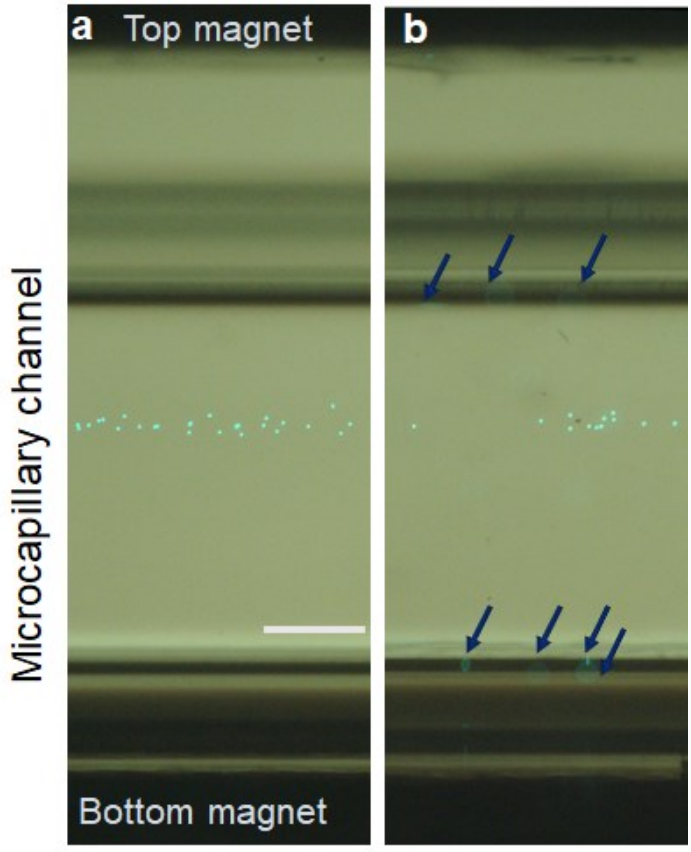

Figure 5.3. Micrographs of the capillary channel for b-BSA detection in PBS sample under fluorescent and bright-field imaging using 1 µm magnetic nanoparticles. (a) The micrograph of the reference (no b-BSA) microspheres. The number of levitated microspheres were 76 ± 2 (n=3) for the reference condition (b) The micrograph of capillary channel microspheres in the presence of 1 µg/mL b-bSA. The number of levitated microspheres were n=29 ± 2 (n=3) for 1 µg/mL b-bSA. Arrows in (b) indicate the out-of-focus microspheres that are captured by the magnets. Scale bar: 200 µm.

the polymer microspheres, the levitated microsphere number in the channel decreased. Each microsphere that levitated in the channel for every protein test was counted. The analyses were done and are shown in Figure 5.4 accordingly. The results revealed that at lower b-BSA concentrations (1ng/mL-10 ng/mL), there was no detectable change in the microsphere number. With a further increase in the b-BSA concentration (>10 ng/mL), the decrease in microsphere number occurred with a trend that was fitted into a linear curve (R^2=0.89) (i.e., semilog lines) to obtain standard equations for microsphere number versus protein concentration. This decrease continued until 1 µg/mL b-BSA concentration. Higher concentrations (> 1 µg/mL) increased the microsphere number.

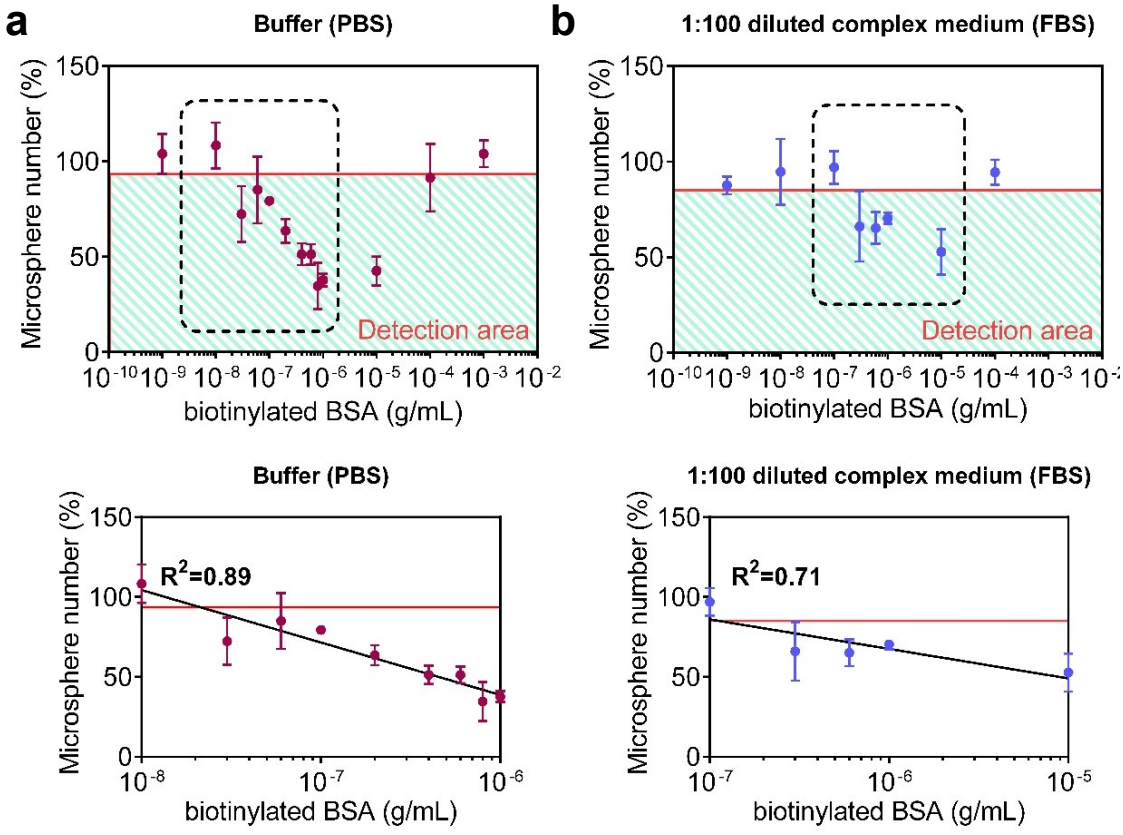

Figure 5.4. Microsphere analysis for b-BSA detection using 1 µm magnetic particles. (a) Buffer and (b) 1:100 (v/v) diluted serum samples for b-BSA. Black solid lines represent the fitting of levitated microsphere number versus protein concentration. Red solid lines represent the LOD signal. Green shaded area in (a) and (b) shows the detection frame. The linear region represented by black dashed lines in (a) and (b) are zoomed in and constructed as separate graphs. The coefficient of determination (R^2) of the fit is represented on the graphs. LOD concentration was determined to solve the linear equation obtained by the fit for the LOD line.

Later, the number of microspheres continued to increase and became very similar to the no protein test. The increase after a certain b-BSA concentration probably occurs due to the saturation of the s-PMS at high b-BSA concentrations. This phenomenon is called the high-dose Hook effect, where the excess analytes result in obtaining lower signals (Hoofnagle and Wener, 2009). When the microspheres are saturated, the unbound b-BSA remains inside the solution and makes a complex with magnetic particles preventing them to attach to the microsphere-protein complexes. Hence, there is no microparticle left to attach to the microspheres, and the bead number stays the same as the reference test. When Figure 5.4 a fitted into a linear curve, the LOD was calculated as 0.43 nM in PBS samples.

Then, the detection capacity of the assay in a complex medium containing other proteins together with the target was tested. In this regard, the dilutions of b-BSA were prepared in FBS, 1:10 (v/v) diluted FBS, and 1:100 (v/v) diluted FBS. For FBS and 1:10 diluted FBS, the microsphere did not provide any change in number at different b-BSA concentrations. This may be due to the bovine serum proteins (reported as 3.0 - 4.5 g %), immunoglobulins (≤ 1 mg/mL), and hemoglobins (reported as ≤ 0.2 mg/mL) that could bind the surface of microspheres non-specifically (e.g., hydrophobic interaction) and hinder the binding of target protein (Ahluwalia et al., 1995). This unwanted binding is associated with the concentration of serum; therefore, in many assays serum samples are diluted at the ratio of 1:100 or more (Farajollahi et al., 2012). When FBS was diluted to 1:100 (v/v), this effect was eliminated due to the lowered concentration of serum proteins (Figure 5.4 b). With increased b-BSA concentrations, the number of microspheres started to decrease after 100 ng/mL b-BSA concentration. The decrease was continued until 10 µg/mL b-BSA. With a 10-fold increase in b-BSA concentration (i.e., 100 µg/mL b-BSA), the microspheres became saturated and their number reached the point beyond the detection area. The LOD in 1:100 (v/v) diluted FBS was 73 nM (112 ng/mL).

Eliminating the Hook effect was also investigated in PBS by centrifugating the sample solution incubated with the microspheres for 5 min. The results showed that centrifugating the sample and bead solution after incubation and removing unbound b-BSA molecules avoided the saturation of magnetic particles (Figure 5.5). Unlike the homogeneous assay performed without centrifugation previously, the microspheres did not saturate at 10 µg/mL b-BSA concentration since the unbound proteins are removed from the solution. Then, the decrease in microsphere number was continued as the protein

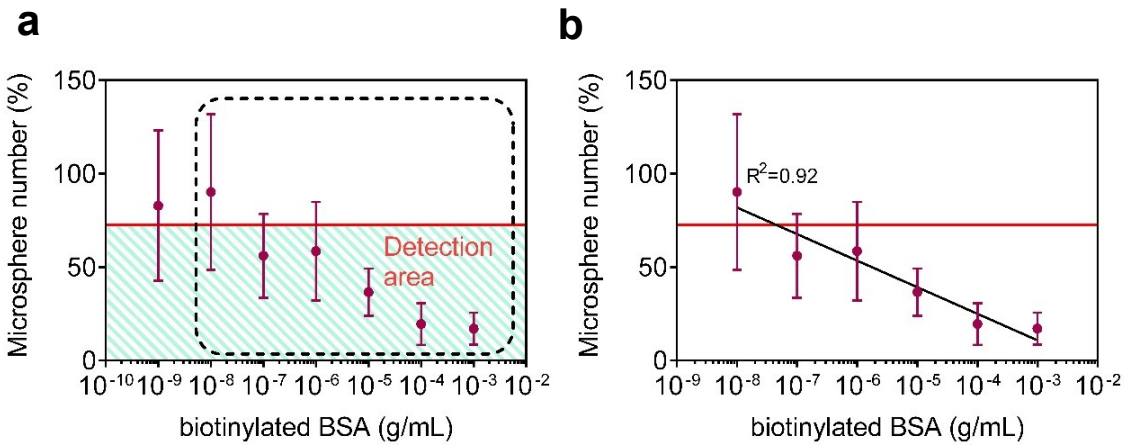

Figure 5.5. Microsphere analysis for b-BSA samples prepared in PBS and centrifugated before the addition of 1 µm magnetic particles. (a) The levitated microsphere number change with respect to protein concentration. The linear region represented by black dashed lines in (a) is zoomed in and constructed as a separate graph in (b). (b) Linear correlation of protein concentration versus microsphere number for PBS samples under centrifugation. The black solid line represents the fitting of the data. Red solid lines in both graphs represent the LOD signal. The Green shaded area in (a) shows the detection frame. The coefficient of determination (R^2) of the fit is represented on the graph (b). LOD concentration was determined to solve the linear equation obtained by the fit for the LOD line.

concentration increased (Figure 5.5 a). By the centrifugation, the range that could be measured with the linear curve was increased, however, the detection limit was not improved significantly (Figure 5.5 b) compared to the no -centrifugation condition. The LOD was calculated as 0.3 nM. Besides, centrifugation resulted in increased standard deviations between the experiments shown by error bars in Figure 5.5. This was probably due to the loss of some microspheres during the recovery of microspheres after centrifugation.

Lastly, the effect of temperature was investigated for samples spiked in PBS. In this regard, the incubation steps were carried out at 37°C under continuous mixing. According to the results (Figure 5.6), the microsphere number (%) started to decrease after 10 ng/ml b-BSA and saturate at 10 µg/mL b-BSA concentration, very similar to the condition tested at room temperature (Figure 5.4), meaning that conducting experiment at 37°C does not significantly affect the achievable LOD. Therefore, subsequent experiments continued to be carried out at room temperature.

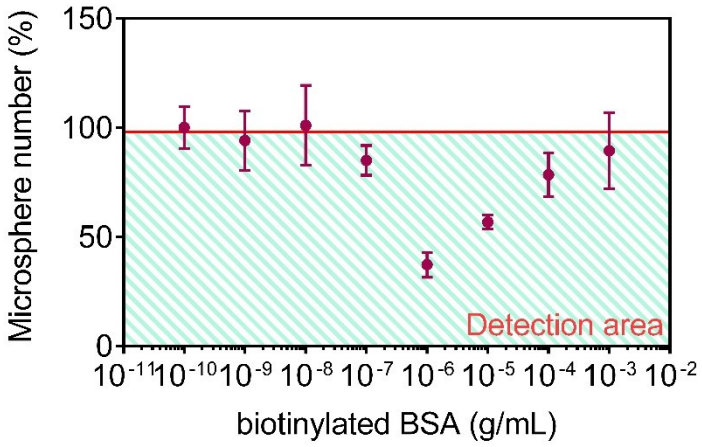

Figure 5.6. Microsphere analysis for b-BSA samples prepared in PBS and performed at 37°C using 1 µm magnetic nanoparticles. The levitated microsphere number changes with respect to protein concentration. The red solid line represents the LOD signal. The Green shaded area in shows the detection frame.

5.4.2. Serum Biomarker Detection in a Pure Medium

Until this point of the study, the developed an assay based on monitoring microsphere number in the capillary channel had been characterized using different b-BSA concentrations. Here, the strategy developed for b-BSA detection was applied for a serum biomarker, mouse IgG, in a pure buffer (PBS).

A sandwich immunoassay was developed for capturing mouse IgG onto the polymer microspheres and labeling them using magnetic particles (Figure 5.7). The same incubation and levitation protocols were applied for anti-mouse IgG microspheres and magnetic particles. For the assay performed for 5 min incubation of the sample with anti-mouse IgG microspheres and magnetic particles, there was no significant detection of mouse IgG (Figure 5.8 a). This may be due to the insufficient binding of target proteins onto the biofunctionalized beads. To concentrate the target protein onto the polymer microspheres, the microspheres were diluted to obtain 10^4 particles per mL concentration using PBSP-BSA buffer in Figure 5.8 b and c. Also, in Figure 5.8 c, the magnetic particle concentration was increased 10-fold to avoid if there was any diffusion-limited binding of magnetic particles. According to the results, diluting microspheres did not enhance the

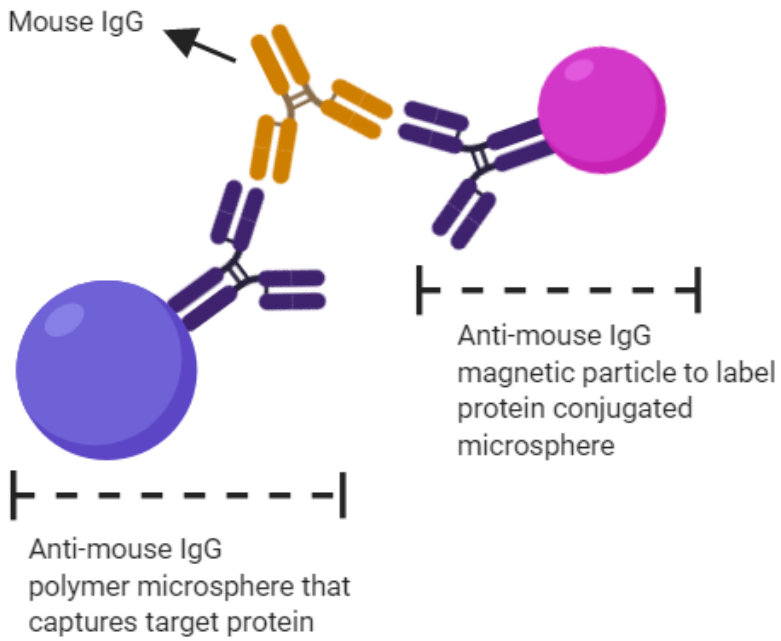

Figure 5.7. Schematic representation of sandwich immunoassay developed for mouse IgG detection.

detection of target protein (Figure 5.8 b, c). Besides, increasing magnetic particle concentration did not ensure the detection of IgG (Figure 5.8 c). Another possibility of no protein detection could be due to inefficient time for binding of target proteins onto anti-mouse IgG beads. Therefore, the effect of incubation time was investigated lastly. In this regard, three different incubation intervals (i.e., 15 min, 1 h, and 2 h) were tested (Figure 5.8 d-f) instead of 5 min. For 15 min incubation, there was no significant detection of IgG. With further increase of incubation time to 1h, a protein concentration of 1 µg/ml (6.7 nM) was observed in the detection area. However, when the incubation time increased to 2 h, no significant improvement was obtained.

A homogeneous assay simplifies the test procedure, therefore integration of the assay into the point-of-care (POC) testing platforms becomes possible (Liu et al., 2016). The homogeneous immunoassay demonstrated here offers several advantages: It does not rely on an expensive amplification technique. The measurement signal is generated directly in the sample solution. It requires a minute amount of sample (10 µL), easy to use procedure, and miniaturized experimental setup. Besides, it offers the possibility of multiplex tests if microspheres that differ in size are used simultaneously in the assay. Since these beads would be differentiated by their size on the micrographs, they can be

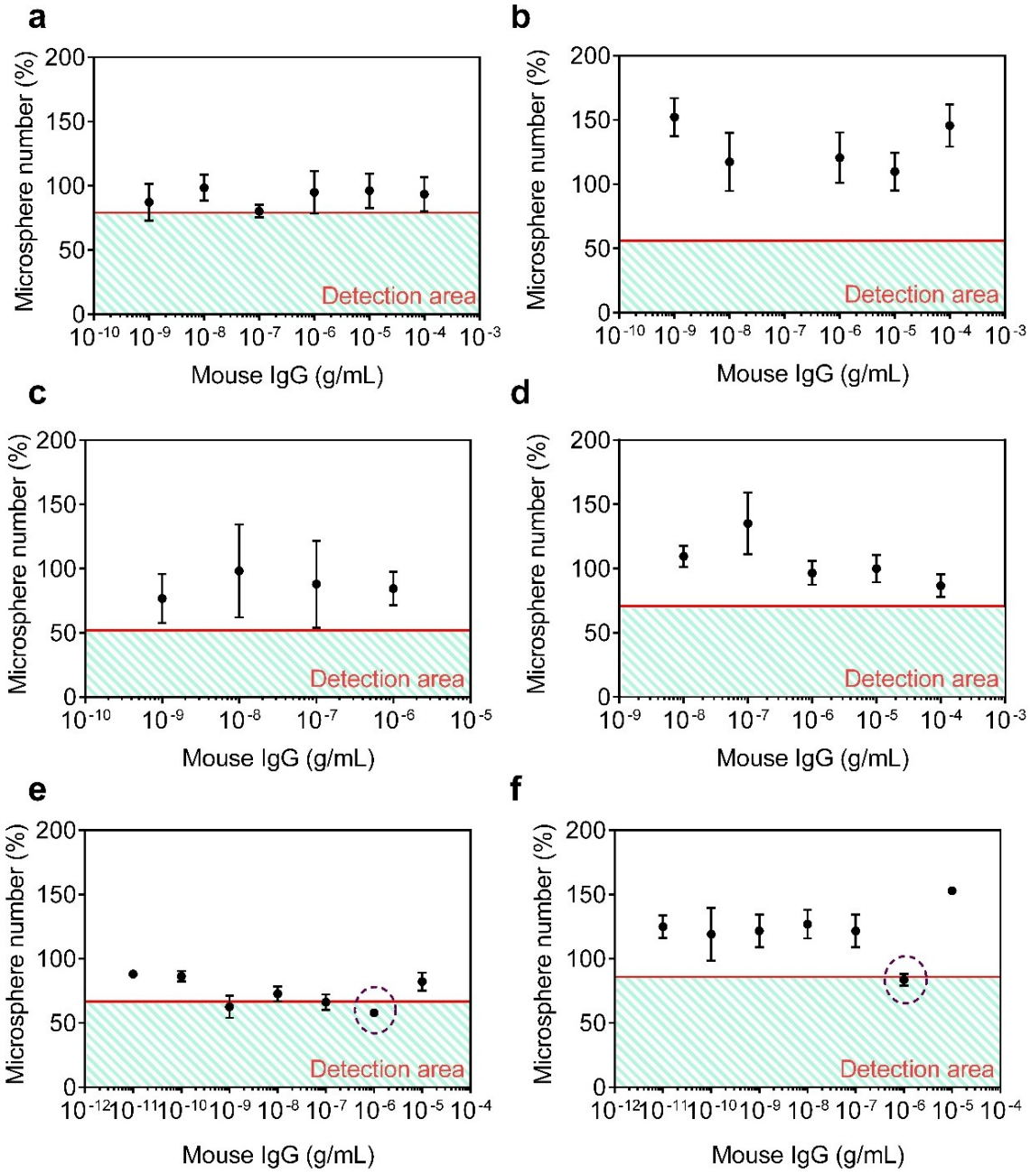

Figure 5.8. Microsphere analysis for mouse IgG samples prepared in PBS using 1 µm magnetic nanoparticles. (a) 5 min incubation with 10^5 polymer microspheres per mL. (b) 5 min incubation with 10^4 polymer microspheres per mL. (c) 5 min incubation with 10^5 polymer microspheres per mL and 10-fold mouse IgG magnetic particles. (d) 15 min incubation with 10^5 polymer microspheres per mL. (e) 1 h incubation with 10^5 polymer microspheres per mL. (f) 2 h incubation with 10^5 polymer microspheres per mL. Red solid lines represent the LOD signal. Green shaded areas show the detection frame. Black dashed circles represent detectable mouse IgG.

decorated as disparate mobile assay surfaces to capture and analyze separate target proteins present in the sample.

The protein assay developed in this chapter based on capturing magnetically-labeled microspheres in the presence of the target protein revealed reasonable LODs for a biotinylated target protein which were 0.73 nM and 43 nM for pure and complex media, respectively. However, a relatively high LOD (~ 1 μg/mL) was obtained for IgG when compared to the other magnetic levitation-based protein detection methods discussed in Table 4.2, and the method developed using 50 nm magnetic nanoparticles in Chapter 4. Besides, when working with complex matrices such as FBS, the method requires the dilution of the sample, probably due to the non-specific attachment of serum proteins at high concentrations. Moreover, a relatively long incubation time (2 h) is required for IgG detection compared to the biotinylated target protein. Since the microspheres get saturated at high protein concentrations, the detectable protein range should be determined prior to the assay. Considering the opportunities provided by this homogeneous and simple assay format, some improvements by modification of microsphere surfaces to avoid non-specific binding of proteins and obtain optimum immunorecognition (Carl et al., 2019) in a complex biological fluid may be required for future applications.

5.5. Conclusion

In this chapter, a washing-free protein detection method using microspheres as assay substrates and magnetic particles as magnetic tags was demonstrated. The increased magnetic susceptibility resulted in the capturing of microsphere-protein-magnetic label conjugate by the magnet, decreasing the remaining microsphere number in the capillary channel. The technique developed here was required a short analysis time (15 min) and a very minute amount of sample (10 μL). The analysis can be made using a simple bright-field microscope without a need for special facilities or professionals.

Following the characterization of the system was performed using a biotinylated target protein, the applicability of the method for a clinical biomarker was tested by developing a sandwich immunoassay for mouse IgG. The described method works very fast for a biotinylated target protein. However, for IgG, the detection only achieved when

the total detection time is 2 hours (for the incubation steps) and 5 min (for the levitation). Besides, it only enabled the detection down to ~ 1 μg/mL. With the improvements in microsphere chemistry and surface functionalization to avoid non-specific bindings and improve target capturing, the assay format could be more sensitive and convenient to be adopted as a portable measurement of proteins.

CHAPTER 6

CELL SEPARATION USING HOLOGRAPHIC MICROSCOPY-INTEGRATED MAGNETIC LEVITATION PLATFORM (HOLOGLEV)

6.1. Background

Separating cells of interest from a heterogeneous mixture is a necessity for many diagnostic and therapeutic applications. However, conventional techniques suffer from the use of expensive and bulky instrumentation, costly procedures, high sample and reagent volumes. Therefore, adopting cell separation into miniaturized, cost-effective, and portable platforms by utilizing physical characteristics may overcome these limitations. In this chapter, a density-based label-free separation of cells at a single cell level was demonstrated using three different cell lines. The assay platform is made up of the combination of two separate technologies, i.e., magnetic levitation and lensless holographic microscopy. Magnetic levitation module is used to levitate and focus cells at unique levitation heights based on their densities. In this regard, three different cell lines (bone marrow stem cells (D1 ORL UVA), breast cancer cells (MDA-MB-231), and human monocyte cells (U-937)) were suspended into Gadolinium-based paramagnetic medium and loaded into a glass microcapillary channel that was inserted between the magnets. Then, a lensless holography module is used to monitor and record the images of the cells. The method enables the separation of cell lines based on their density in a short time (10 min) using a small volume of sample (~40 μL).

6.2. Introduction

Separation or sorting of cells from heterogeneous populations is essential in many biological and biomedical applications such as tissue engineering (Plouffe et al., 2010), biotechnological production (Kacmar et al., 2006), regenerative medicine (Smith et al., 2017), diagnostics (Cheng et al., 2007), and therapeutics (Alhadlaq and Mao, 2004). Methods of separating cells can be divided into two groups: i. bulk sorting and ii. single-cell sorting (Orfao and Ruiz-Argüelles, 1996). In conventional methods such as filtration (Vogel and Kroner, 1999), magnetic separation (Miltenyi et al., 1990) and centrifugation (Sanderson and Bird, 1977), the average or bulk response of a cell population is measured. However, cells in cancer types have intra-tumor heterogeneity (ITH) and are highly diverse in terms of genetic, phenotypic and epigenetic levels (Chen et al., 2012; Tellez-Gabriel et al., 2016). Bulk analysis of heterogeneous cell populations, such as those of many tumors, may hinder the characteristics of a small but an important subpopulation (Hu et al., 2016). Therefore, analyzing single cells provide detailed information that could improve therapeutic decision and personalized medicine in case of diseases (Tellez-Gabriel et al., 2018). Single-cell sorters such as flow cytometry (FCM) can focus and analyze each cell individually (Greve et al., 2012). FCM devices are highly informative regarding cell size, number, and distribution of cellular macromolecules (Brehm-Stecher, 2014). However, widely used FCM devices such as fluorescence-activated cell sorters (FACS) rely on the use antibody tags (Ring et al., 2015) and expensive machinery (Emaminejad et al., 2012).

With the advances in micro and nanotechnology, the development of μTAS are currently underway to reduce the size, cost and complexity of conventional cell analysis systems (Jackson and Lu, 2013; Moon et al., 2009). Inherent mechanical and physical properties such as density (Petersson et al., 2007), magnetic susceptibility (Shen et al., 2012), refractive index (Milne et al., 2007), compressibility (Liu and Lim, 2011), size (Huang et al., 2008) and deformability (Kuo et al., 2010) have been utilized as markers for differentiating cells or particles without labels as well as biochemical characteristics based on protein expression (Ohnaga et al., 2013).

One promising way for simple, powerful, and cost-effective separation is levitating objects in a paramagnetic liquid under the balance of magnetic and buoyancy

forces inside a magnetic field gradient (Ge et al., 2019). So far, magnetic levitation has been successfully exploited for label-free separation of malaria-infected red blood cells, sickle cells (Knowlton et al., 2017b), blood (Amin et al., 2017; Knowlton et al., 2017b), tumor cells (Amin et al., 2017; Durmus et al., 2015), adipocytes (Sarigil et al., 2019), and cardiomyocytes (Puluca et al., 2020).

In this chapter, a hybrid platform (HologLev) combining lensless holographic microscopy (Sobieranski et al., 2015) and magnetic levitation modules was used for *in situ* characterization of mouse bone marrow stem cells (D1 ORL UVA), breast cancer cells (MDA-MB-231), and human monocyte cells (U-937). The magnetically-levitated cells in the HologLev are monitored using a simple illumination scheme composed of light-emitting diode (LED)-pinhole assembly and a complementary metal-oxide-semiconductor (CMOS) imaging sensor array (Sobieranski et al., 2015). Since the proposed technique does not depend on conventional optical lenses or scanning stage used in regular microscopy platforms, it could provide new aspects in portable and miniaturized imaging capacities of magnetic levitation-based cell analysis.

6.3. Materials and Methods

6.3.1. Experimental Setup

The hybrid platform used in this study consists of two modules namely magnetic levitation and lensless inline holographic microscopy. In magnetic levitation module, two block magnets (NdFeB 52 grade, 5 mm x 2 mm x 50 mm) are oriented as the same poles face each other so that cells are loaded into a square glass microcapillary channel (1 mm x 1 mm x 50 mm) inside the setup levitate by the magnetic force against gravity (Figure 6.1). Lensless inline holographic microscopy module consists of a LED in 650 nm with the power of 1 W to illuminate the capillary channel, a pinhole with a diameter of 100 μm to spatially filter the light coming from the LED. CMOS sensor (Sony IMX219) and pinhole are placed <1 mm and 5 cm away from the surface of the microcapillary channel, respectively, at the opposite sides. CMOS and LED are connected to a single-board

computer (Raspberry Pi 3 Model B+) to capture the images of holograms. The imaging area of the CMOS corresponds to 3280 (height) × 2464 (weight) pixels with a pixel size of 1.12 μm.

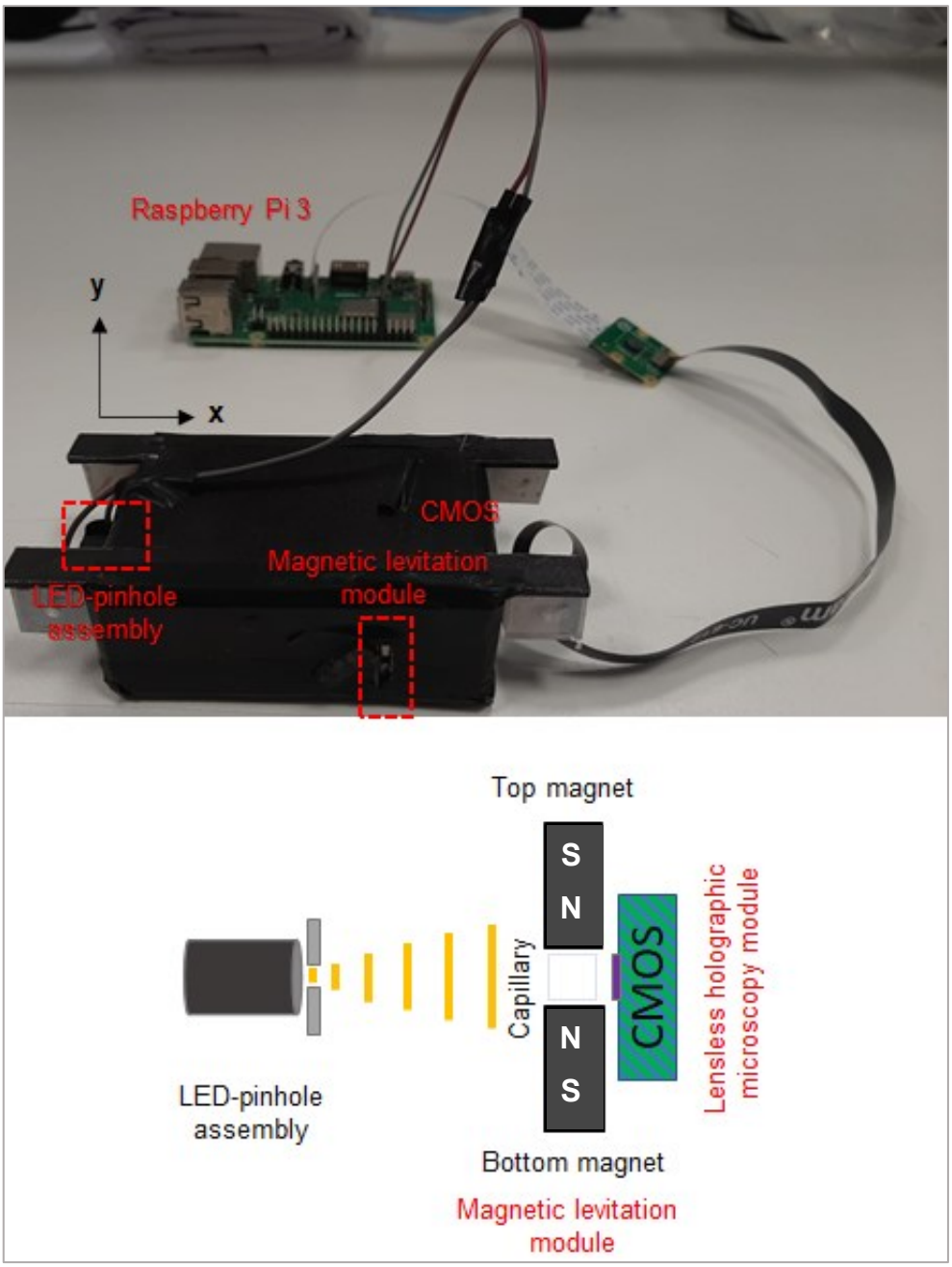

Figure 6.1. Photograph and schematic illustration of lensless holography-integrated magnetic levitation platform. The platform consists of two modules: magnetic levitation and lensless holographic microscopy. The components of the microscopy platform are connected to the single-board computer. The modules are assembled using 3D-printed parts.

6.3.2. Sample Preparation

In order to calibrate the system, diamagnetic polyethylene standard beads with a density of 1.00 g/cm^3 (10-20 μm in size), 1.026 g/cm^3 (10-20 μm in size), 1.050 g/cm^3 (45-53 μm in size), and 1.090 cm^3 (20-27 μm in size) (Cospheric, LLC) were suspended in PBS (Gibco) containing 1% (w/v) Pluronic F-127 (Sigma-Aldrich). The solution is mixed with 1 M Gadavist to achieve 25, 50, 75, and 100 mM Gd^{+3} containing levitation media. Live cells of three different cell lines, D1 ORL UVA (mouse bone marrow stem cells), U-937 (human monocyte cells), and MDA-MB-231 (breast cancer cells), are levitated in the platform with 25 mM Gd^{3+} based levitation medium. Live and dead cells of D1, U937, and MDA-MB-231 cells are also investigated in 100 mM Gd^{3+}-based medium. Dead cells were obtained with the introduction of 50% (v/v) dimethyl sulfoxide (DMSO) to the cell medium. For all experiments, cell samples are prepared at a concentration of 1×10^5 cells/mL in PBS containing 1% (w/v) Pluronic F-127.

After beads and cells were mixed with Gadavist, ~40 μL of the resulting solution was loaded into the glass capillary channel pre-treated using a plasma device for 4 min (Diener Plasma Cleaner). After sealing (Critoseal) the end of the microcapillary channel, it was inserted into the magnetic levitation module of HologLev and waited for 10 min for the levitation.

6.3.3. Measuring Levitation Heights of Microspheres and Cells

CMOS in lensless holographic microscopy module records the light reflected from the object as the object wave and the light of background illumination with custom phase as the reference wave. The resulting vawefront is the interference pattern (i.e., hologram) that shows the morphology of the object. The captured holographic images are reconstructed by the backpropagation method with spatial transfer function to obtain real images (Delikoyun et al., 2019b):

$$\Psi_P(x,y;z) = \mathcal{F}^{-1}\{\mathcal{F}\{\Psi_{Po}(x,y)\}H(k_x,k_y;z)\} \quad (6.1)$$

,where $\mathcal{F}$ is Fourier transform and $H(k_x,k_y;z)$ is the spatial transfer function defined as follows (Delikoyun et al., 2019c; Delikoyun et al., 2019a):

$$H(p,q) = exp\left[-jk_o z\sqrt{1-\frac{(p\Delta_{kx})^2}{k_o^2}-\frac{(q\Delta_{ky})^2}{k_o^2}}\right] \quad (6.2)$$

In Equation 6.2, $k_o = w_o/v$: is the wave number, where w_o: is the angular frequency (rad/s), v: is the speed of the wavefront. (x,y) and (p,q): are the indices of sample at the spatial domain and Fourier domain, respectively. $\Delta_{kx} = 2\pi/M\Delta_x$ and $\Delta_{ky} = 2\pi/N\Delta_y$: are the frequency resolutions (radian per unit of length), where Δ_x and Δ_y: are the sampling periods, M, N: is the number of samples in the direction of x and y, respectively. z is the distance between the sample and the imaging sensor.

The reconstructed holograms are used to measure the levitation heights of each cell or particle in the microcapillary region that corresponds to the imaging area of CMOS. The distance from the center of the cells (or particles) to the surface of the bottom magnet was measured using Image J software and defined as the levitation height. For distance measurements, the scale of the image was set in the software taking pixel to micrometer ratio as 1.12 according to the pixel size of the CMOS (Delikoyun et al., 2019a).

6.4. Results and Discussion

Three different cell lineages were analyzed to separate them into distinct positions within microcapillary under the principle of magnetic levitation (Figure 6.2). After sorting of cells, lensless digital inline microscopy was utilized for monitoring the

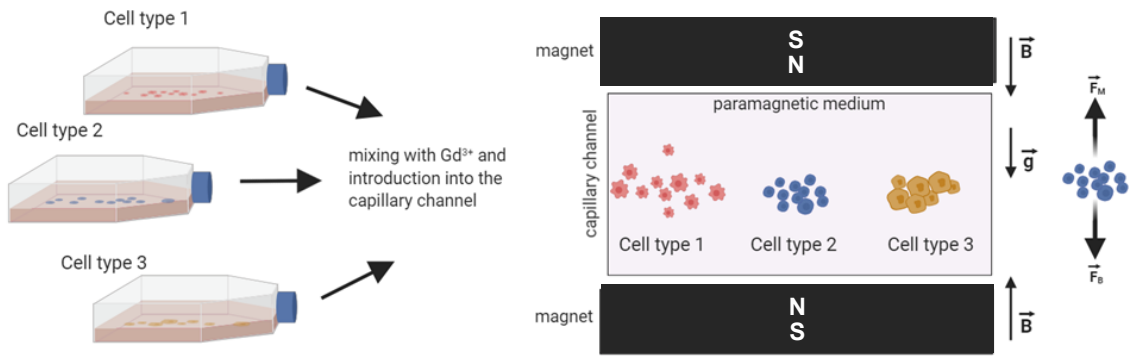

Figure 6.2. Cell separation principle used in HologLev. Different cell types suspended in a paramagnetic liquid inside the platform come to a unique equilibrium point and levitate under the balance of magnetic force $\vec{F}_M$ and buoyancy force ($\vec{F}_B$). B and g represent magnetic induction and gravity, respectively.

levitation heights with respect to the top surface of the bottom magnet in the magnetic levitation module.

The experiments in the HologLev started with the calibration of the system using standard density beads. Since these beads are diamagnetic, they tend to escape from the higher magnetic field and levitate at equilibrium heights depending on their density under magnetic the balance of magnetic ($\vec{F}_M$) and buoyancy forces ($\vec{F}_B$) based on their densities as presented previously in Equation 3.12. The images of beads and their corresponding calibration curves are presented in Figure 6.3. Using standard equations obtained by fitting the experimental data into linear curves, the density versus levitation height information was obtained. The results revealed that at increasing Gd^{3+} concentrations the standard beads levitated at higher heights as expected since increasing magnetic susceptibility of the paramagnetic solution would increase the magnetic susceptibility difference between the particles and the medium ($\chi_c - \chi_m$), therefore the magnetic force acting on the particles.

Later, the platform was tested using live cells of D1 ORL UVA, U-937, and MDA-MB-231 cell lines at 25 mM Gd^{3+} containing levitation medium (Figure 6.4). Similar to the standard beads, cells tend to levitate at the magnetic field minima under the effect of magnetic and buoyancy forces. According to results (Figure 6.4 b), the average levitation heights of D1 ORL UVA, U-937, and MDA-MB-231 cells lines were 596 ± 25 µm, 574 ±19 µm, and 588 ±8, respectively.

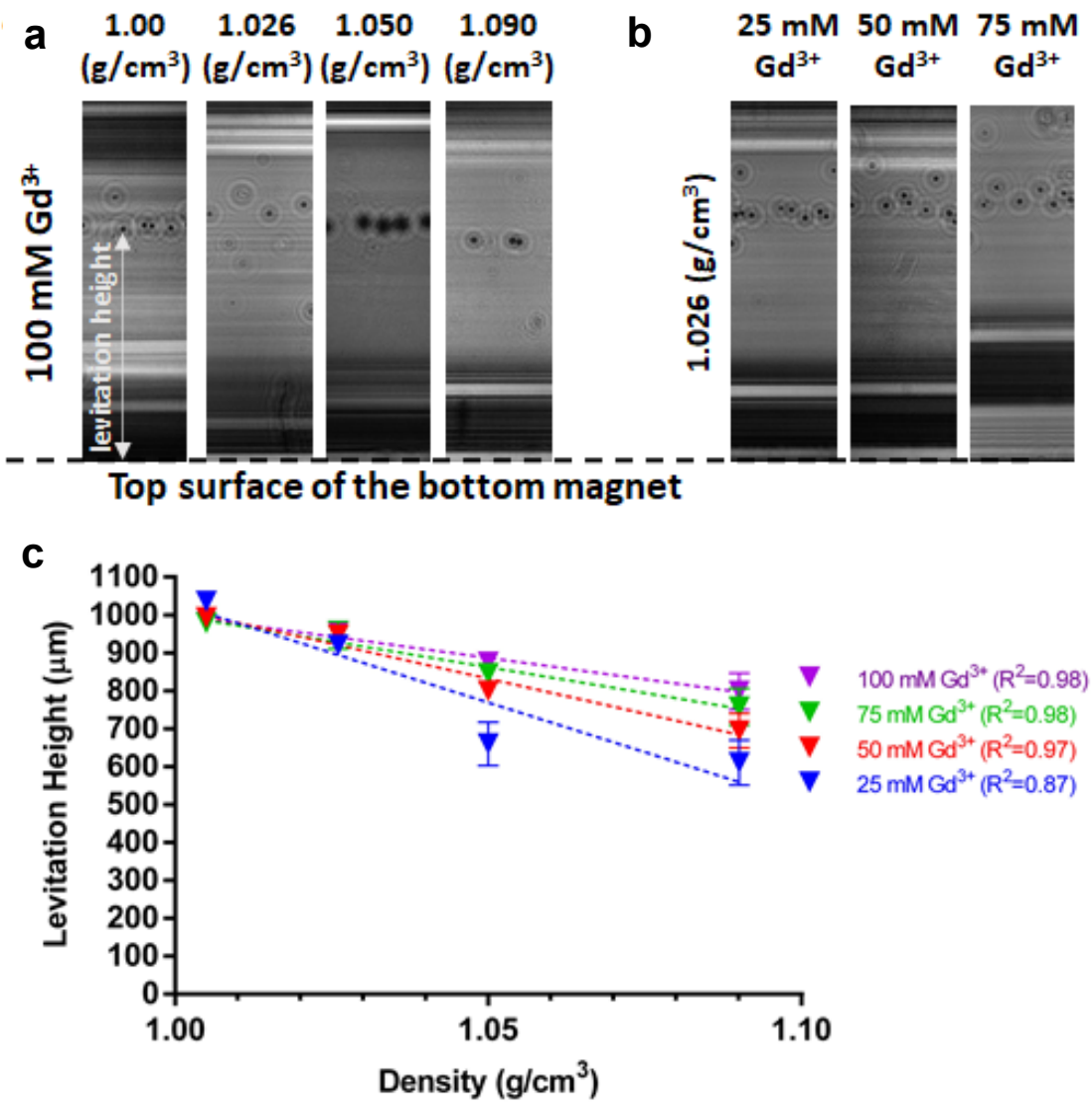

Figure 6.3. Calibration of holographic microscopy-integrated magnetic levitation system using density-standard beads at 1.00, 1.026, 1.05, and 1.09 g/cm^3 densities. (a) Reconstructed images of standard density beads at 100 mM Gd^{3+} concentrations. (b) Reconstructed images of 1.026 g/cm^3 beads at 100 mM Gd^{+3} concentration. (c) Levitation height analyses of different density beads under tested Gd^{3+} concentrations (i.e., 25, 50, 75, and 100 mM Gd^{3+}). Dashed lines represent linear fitting of density versus levitation height data. R^2 values on the graph represent the coefficient of determination for linear fits.

When dead cells are levitated in 25 mM Gd^{3+} solution, they are accumulated at the bottom of the microcapillary channel without the possibility of monitoring. Therefore, the Gd^{3+} concentration was increased to 100 mM in order to collect dead cells at higher levitation heights. At 100 mM, the levitation heights of live cells were compared with a

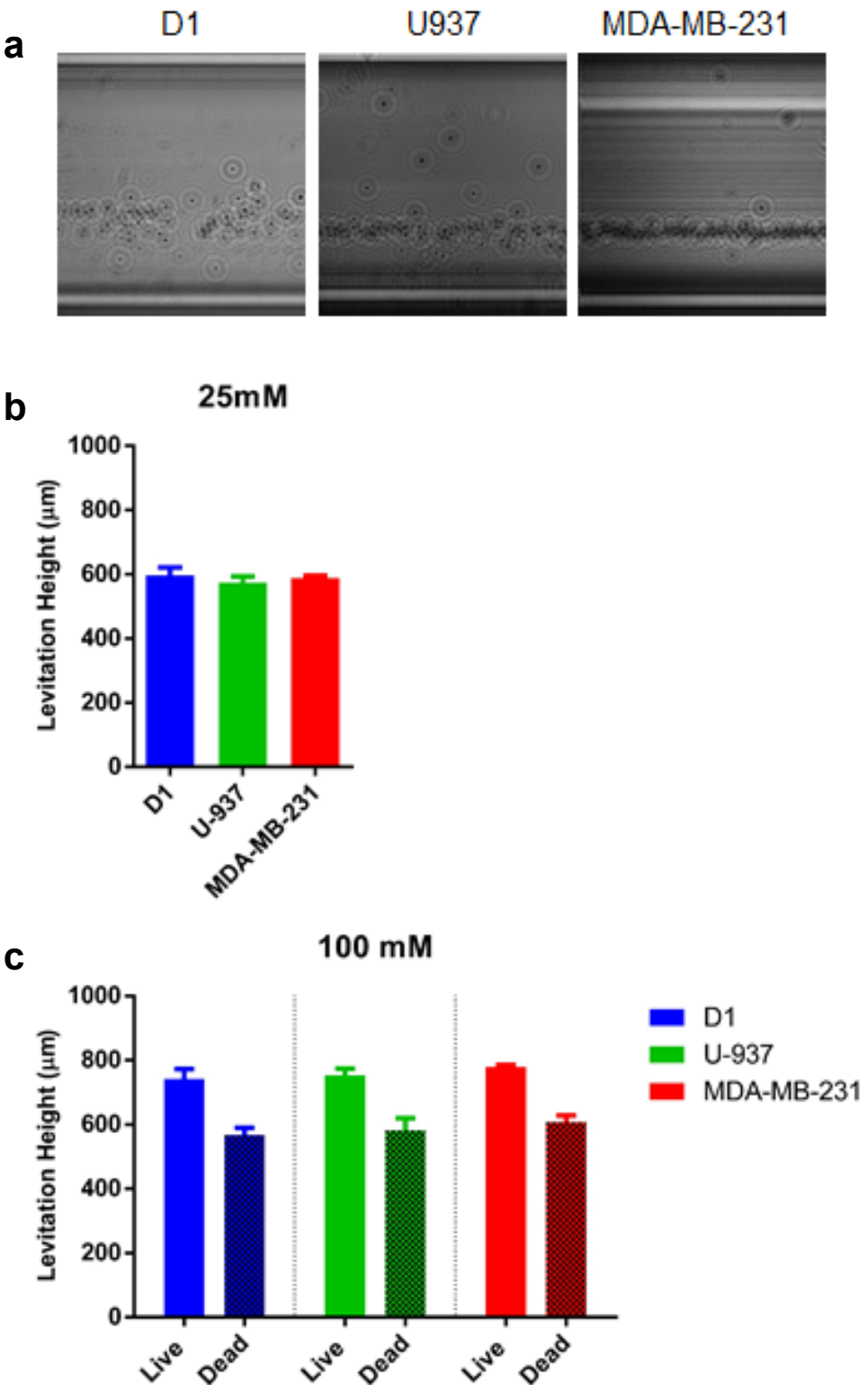

Figure 6.4. Levitation of different cell lines in the HologLev after 10 min. (a) Reconstructed holograms of D1, U937, and MDA-MB-231 cells after 10 min of levitation (b) Levitation height of live D1 ORL UVA (mouse bone marrow stem cells), U-937 (human monocyte cells), and MDA-MB-231 (breast cancer cells) cells spiked in 25 mM Gd^{3+} -based levitation medium. (c) Live and dead D1 ORL UVA, U-937, and MDA-MB-231 cells spiked in 100 mM Gd^{3+}-based levitation medium.

t-test (Welch's correction) and found as statistically different ($p = 0.0022$ for D1, $p = 0.0057$ for U-937, and $p = 0.0027$ for MDA-MB-231) than those of the dead cells. The method for obtaining dead cells includes the use of DMSO chemical which has known cytotoxic effects on cells (de Abreu Costa et al., 2017). DMSO as being an amphipathic solvent interacts with the plasma membrane of the cells and increases its permeability (Notman et al., 2006). In the case of cell death, probably due to the disintegration of cellular structure and accumulation of Gd in the cell debris, the density of the cells increased compared to the live cells. Hence, they levitate at lower heights compared to the live ones. These results showed that change in cell density due to the loss of viability can be identified based on monitoring levitation heights of cells in the channel.

For 25 mM Gd^{3+} concentration, when the cells' levitation heights were averaged, a close result was obtained (Figure 6.4 b). However, these results are not representative of individual cells of one cell line population. Therefore, each cells' density was also analyzed and presented in Figure 6.5. The calculated average cell densities (sum of the data of three replicates) with their ± deviation from the mean of all population for D1 ORL UVA, U-937, and MDA-MB-231 were 1.0830 ± 0.0138 g/cm^3, 1.0874 ± 0.0133 g/cm^3, and 1.0837 ± 0.0051 g/cm^3, respectively (Figure 6.5 a). The mean density values of D1 and MDA-MB-231 cells are very close to each other and U-937 cells had the highest mean density among the three cell lines. But also, the lowest density cell (i.e., 0.9787 g/cm^3) was observed within U937 cells. On the other hand, D1 cells showed a wider dispersion of fractions for cell densities (95% percentile: 0.16) than U937 (95% percentile: 0.25) and MDA-MB-231 (95% percentile: 0.38) (Figure 6.5 b).

Density is an important physical biomarker, as it is tightly regulated and can be used to distinguish between cell populations (Bryan et al., 2014; Grover et al., 2011). Besides, the change in cells' mass to volume ratio may be associated with cellular processes such as apoptosis (Martin et al., 1990), disease state (Mrema et al., 1979), differentiation (Maric et al., 1998). The density-based method presented here enables label-free separating of cells at the single-cell level. The FCM methods may require labeling the target cells with fluorescent molecules (Herzenberg et al., 2002) or quantum dots (Chattopadhyay, 2011) that can be costly and time-consuming. Besides, the heterogeneity of rare cells makes the finding of convenient surface markers challenging (Bhagat et al., 2010). Hence, separation techniques based on intrinsic properties of cells eliminate the bottleneck of procedures that rely on antibody labeling. Being one of the

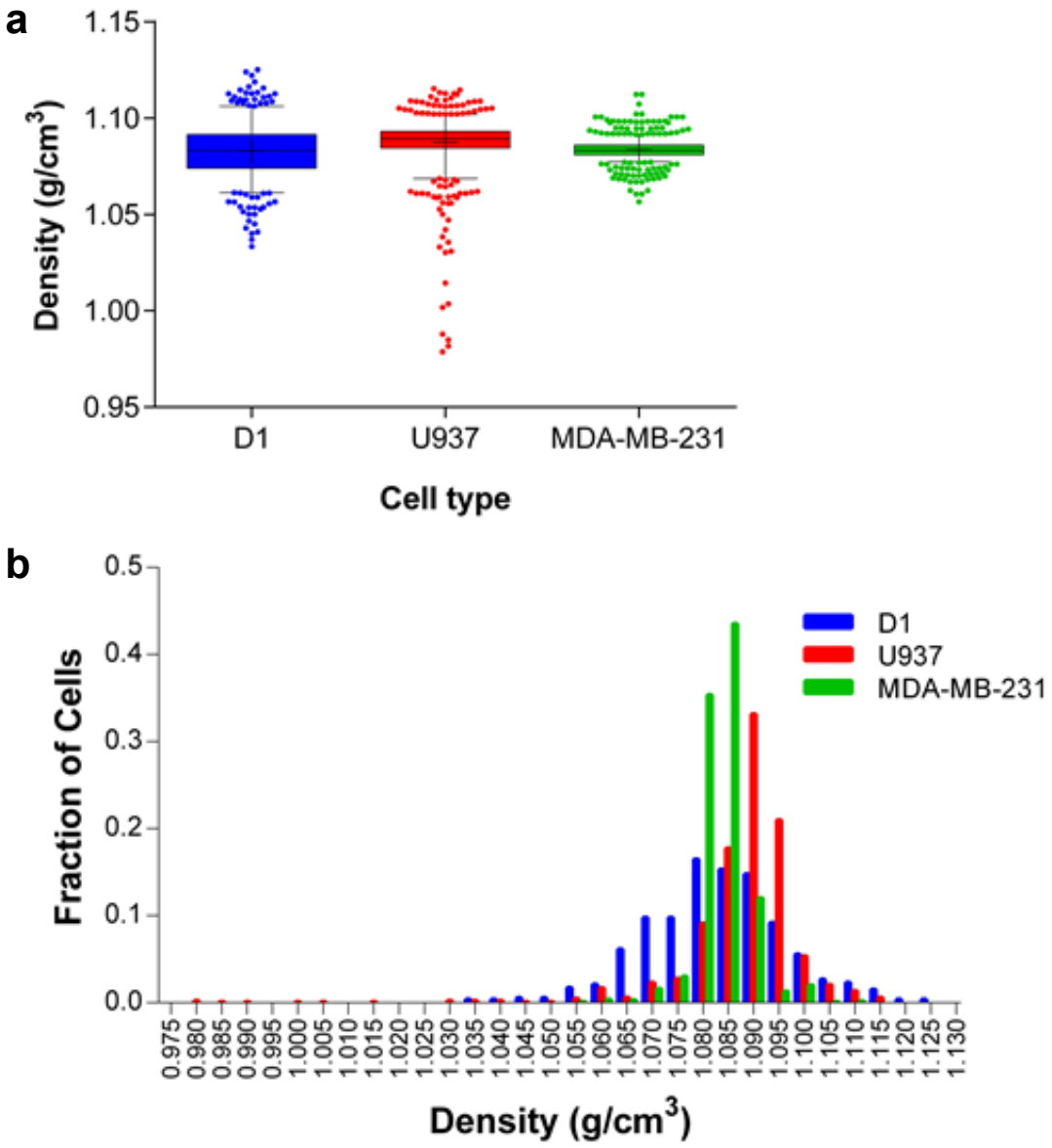

Figure 6.5. Density distribution of live D1 ORL UVA (mouse bone marrow stem cells), U-937 (human monocyte cells), and MDA-MB-231 (breast cancer cells) cells spiked in 25 mM Gd^{3+} -based levitation medium. (a) Dot-plot and (b) histogram of cell densities (N=3) for the sum of data of three replicates after 10 min of levitation. The dot plot image is constructed as a box and whiskers format with a 5-95 percentile. + shows the mean levitation height.

workhorse techniques for sorting cells, FACS provides excellent sensitivity, with the possibility of multiple parameter analysis and high throughput (>10.000 cells/s) (Ashcroft and Lopez, 2000). However, it requires expensive and machinery, a large amount of materials (Hu et al., 2016). Also, labeling with fluorophore-conjugated antibodies may damage the viability of cells (Kumar and Bhardwaj, 2008). On the other hand, the

magnetic levitation-based method proves low-cost, portable, and label-free cell monitoring. In this technique, the viability of cells is not likely affected due to the biocompatibility of the paramagnetic medium component (Gd) used for the analysis (Anil-Inevi et al., 2018). Therefore, it can eliminate viability loss after the separation of cells in conventional cytometry techniques. Moreover, this label-free technique may be also combined with the antibody-based method to discriminate labeled cells that differ in physical properties.

Magnetic levitation technique based on microscopic examination for determining levitation heights of microparticles or cells depends on bench-top microscopes which are composed of highly fragile and costly optics along with dependency of trained personnel to operate that their usage in point-of-care applications. On the other hand, the lensless holographic microscopy based on CMOS technology would provide compact and portable measurements (Adiguzel and Kulah, 2012) with high resolution (~1 μm) and ultrawide field of view (> 10 mm^2) (Delikoyun et al., 2019b) for cell analysis in MagLev platforms. Also, this system could be designed to include integrated flow components, collection and waste containers to be used as a cell cytometer in the future.

6.5. Conclusions

Here, the use of a miniaturized lensless microscopy-integrated magnetic levitation platform to monitor and analyze different cell lines was demonstrated. The method combines two separate technologies to provide low-cost, easy to use, and portable cell separation analysis. The separation works without labeling and destruction of cells which is advantageous when the separated cells should be recovered and analyzed depending on the type of application. Besides, the platform can differentiate the living cells from the non-living based on unique levitation heights. Therefore, it can be adopted to testing the *in vitro* efficiency of drugs on cells. The components of the platform (magnets, imaging sensor, light source, single-board computer, etc.) cost less than $100 and are readily accessible. With further improvements and modifications such as the integration of flow elements and separation components, the platform can be used as a low-cost and portable cell cytometer.

CHAPTER 7

CONCLUSIONS

Detection of disease-related biomarkers in bodily fluids presents valuable information regarding not only the diagnosis of diseases but also the choice of disease therapy. Effective, low-cost and simple detection methods compatible with portable measurements provide important advantages for unequipped places such as rural areas. However, traditional protein detection methods suffer from complex experimental steps, high amounts of sample, and expensive reagent use. Magnetic levitation offers low-cost, sensitive, and easy-to-handle manipulation of micro- and nano- particles or cells in small volumes and sizes by levitating them at unique heights based on their density and magnetic susceptibility under a non-homogenous magnetic field. So far, it has been a powerful tool in various applications such as label-free cell identification, 3D cell culture and protein analysis. In case of protein detection, magnetic levitation has been applied with only density-based detection schemes, so far.

This thesis has focused on the development of miniaturized assay schemes utilizing magnetic levitation. The thesis consists of two main aims: i. biomolecule detection and ii. cell separation.

For biomolecule detection, first a magnetic susceptibility-based protein detection scheme (~80 min) was developed using the magnetic levitation principle for the first time. The limit of detection (LOD) of magnetic levitation-based assays was enhanced by 100-fold (110 fg/mL) with superparamagnetic nanoparticles (50 nm) using a biotinylated protein. Target proteins were first captured on the surface of polymer microspheres (6 μm). Then, the proteins on the microspheres were labeled selectively with magnetic nanoparticles, which significantly altered the magnetic susceptibility of microsphere-protein complexes compared to the non-protein carrying microspheres. This susceptibility change resulted in the change of unique levitation heights of microspheres in the MagLev platform. Hence, target proteins could be quantified by monitoring levitation heights. Among different Gd^{3+} concentrations tested, the optimum paramagnetic medium concentration was found to be 30 mM Gd^{3+}. The method developed here can also be used

to measure the magnetic susceptibility change of microspheres with an unprecedented resolution of 4.2×10^{-8} (SI units) for sensitive protein detection. The assay methodology was adopted to the detection of two protein biomarkers, mouse immunoglobulin G and cardiac Troponin I, with the designed sandwich immunoassay formats. The results revealed that mouse immunoglobulin G could be detected at 1.5 ng/mL (~10 pM) and >10 ng/mL in pure buffer and serum, respectively. In case of cardiac troponin I, the assay requires significant improvements for a better sensitivity to meet the clinically relevant cut-off values, since the 100 ng/mL (~4.2 nM) protein concentration could only provide a low detection signal.

A magnetic susceptibility-based biomolecule detection scheme was also demonstrated with a minute amount of sample (10 μL) where the measurement signal was obtained within the sample matrix using magnetic particles with a 1500-fold higher susceptibility than the ones used in the previous magnetic susceptibility-based assay. The method is realized by directly adding and incubation polymer microspheres (6 μm) and magnetic particles (1 μm) with the sample solution. The binding of even 1 magnetic particle resulted in attracting the polymer microspheres by the magnet. Therefore, the method relied on counting the remaining beads in the capillary channel in the presence of the target protein. Even though it simplified the detection method, a higher LOD compared to the previous susceptibility-based assay was obtained. For the biotinylated target protein (~15 min) LOD was ~0.43 nM and ~73 nM for pure buffer and serum, respectively. For mouse immunoglobulin G, the detectable (~2 h) concentration was ~6.7 nM for pure buffer.

In case of cell separation, a holographic microscopy-integrated magnetic levitation platform was utilized for density-based, label-free, and portable separation of three different cell lines: bone marrow stem cells (D1 ORL UVA), breast cancer cells (MDA-MB-231), and human monocyte cells (U-937). The results revealed that each cell line showed different levitation height profiles in the capillary channel, meaning that each cell line had a different degree of distribution in their densities. Besides, the levitation of live cells is significantly different than the dead cells of the same cell line. This implies that the portable MagLev platform could be used for *in vitro* cell viability tests in the future.

Future work should focus on analyzing real samples to ensure the translation of the developed assays into clinical settings. For protein detection experiments to be compatible with portable measurements, additional work regarding the obtaining a self-

contained platform could be done. For cell separation, only static measurements have been performed in this thesis. Further modification in the HologLev system could enable separating cells under a continuous flow and using the platform as a portable and cost-effective cell cytometer in the future. To conclude, the results of the studies have revealed that low cost, sensitive and easy-to-use approaches developed in this thesis can contribute to biodiagnostic applications to be carried out on MagLev platforms.

REFERENCES

Abbas, A.K., Lichtman, A.H., Pillai, S., **2014**. *Cellular and molecular immunology* E-book. Elsevier Health Sciences.

Adiguzel, Y., Kulah, H., **2012**. CMOS Cell Sensors for Point-of-Care Diagnostics. *Sensors* (Basel) 12, 10042-10066.

Ahluwalia, A., Giusto, G., De Rossi, D., **1995**. Non-Specific Adsorption on Antibody Surfaces for Immunosensing. *Materials Science and Engineering*: C 3, 267-271.

Aho, K., Heliövaara, M., Knekt, P., Reunanen, A., Aromaa, A., Leino, A., Kurki, P., Heikkilä, R., Palosuo, T., **1997**. Serum Immunoglobulins and the Risk of Rheumatoid Arthritis. *Annals of the Rheumatic Diseases* 56, 351-356.

Akamizu, T., Shinomiya, T., Irako, T., Fukunaga, M., Nakai, Y., Nakai, Y., Kangawa, K., **2005**. Separate Measurement of Plasma Levels of Acylated and Desacyl Ghrelin in Healthy Subjects Using a New Direct ELISA Assay. *The Journal of Clinical Endocrinology and Metabolism* 90, 6-9.

Akhavan-Tafti, H., Binger, D.G., Blackwood, J.J., Chen, Y., Creager, R.S., de Silva, R., Eickholt, R.A., Gaibor, J.E., Handley, R.S., Kapsner, K.P., Lopac, S.K., Mazelis, M.E., McLernon, T.L., Mendoza, J.D., Odegaard, B.H., Reddy, S.G., Salvati, M., Schoenfelner, B.A., Shapir, N., Shelly, K.R., Todtleben, J.C., Wang, G., Xie, W., **2013**. A Homogeneous Chemiluminescent Immunoassay Method. *Journal of the American Chemical Society* 135, 4191-4194.

Albright, V.C., Hellmich, R.L., Coats, J.R., **2016**. A Review of Cry Protein Detection with Enzyme-Linked Immunosorbent Assays. *Journal of Agricultural and Food Chemistry* 64, 2175-2189.

Alhadlaq, A., Mao, J.J., **2004**. Mesenchymal Stem Cells: Isolation and Therapeutics. *Stem Cells and Development* 13, 436-448.

Alnaimat, F., Dagher, S., Mathew, B., Hilal-Alnqbi, A., Khashan, S., **2018**. Microfluidics Based Magnetophoresis: A Review. *The Chemical Recor*d 18, 1596-1612.

Altschuler, S.J., Wu, L.F., 2010. Cellular Heterogeneity: Do Differences Make a Difference? *Cell* 141, 559-563.

Amin, R., Knowlton, S., Dupont, J., Bergholz, J.S., Joshi, A., Hart, A., Yenilmez, B., Yu, C.H., Wentworth, A., Zhao, J.J., Tasoglu, S., **2017**. 3D-Printed Smartphone-Based Device for Label-Free Cell Separation. *Journal of 3D Printing in Medicine* 1, 155-164.

Amin, R., Knowlton, S., Yenilmez, B., Hart, A., Joshi, A., Tasoglu, S., **2016**. Smart-Phone Attachable, Flow-Assisted Magnetic Focusing Device. *RSC Advances* 6, 93922-93931.

Andersen, M.S., Howard, E., Lu, S., Richard, M., Gregory, M., Ogembo, G., Mazor, O., Gorelik, P., Shapiro, N.I., Sharda, A.V., Ghiran, I., **2017**. Detection of Membrane-Bound and Soluble Antigens by Magnetic levitation. *Lab on a Chip* 17, 3462-3473.

Andersen, M.S., Lu, S., Lopez, G.J., Lassen, A.T., Shapiro, N.I., Ghiran, I.C., **2019**. A Novel Implementation of Magnetic Levitation to Quantify Leukocyte Size, Morphology, and Magnetic Properties to Identify Patients With Sepsis. *Shock* 51, 147-152.

Andres, U., **1976**. *Magnetohydrodynamic and Magnetohydrostatic Methods of Mineral Separation*. Halsted Press, Wiley: New York.

Andresen, H., Mager, M., Grießner, M., Charchar, P., Todorova, N., Bell, N., Theocharidis, G., Bertazzo, S., Yarovsky, I., Stevens, M.M., 2014. Single-Step Homogeneous Immunoassays Utilizing Epitope-Tagged Gold Nanoparticles: on the Mechanism, Feasibility, and Limitations. *Chemistry of Materials* 26, 4696-4704.

Anil-Inevi, M., Yaman, S., Yildiz, A.A., Mese, G., Yalcin-Ozuysal, O., Tekin, H.C., Ozcivici, E., **2018**. Biofabrication of in situ Self Assembled 3D Cell Cultures in a Weightlessness Environment Generated Using Magnetic Levitation. *Scientific Reports* 8, 7239.

Anil-Inevi, M., Yilmaz, E., Sarigil, O., Tekin, H.C., Ozcivici, E., **2019**. Single Cell Densitometry and Weightlessness Culture of Mesenchymal Stem Cells Using Magnetic Levitation. In Kursad Turksen (Eds.) *Stem Cell Nanotechnology* pp. 15-25. Humana, New York, NY.

Araujo, M., Doi, S.Q., **2017**. Editorial: Biomarkers in CKD. *Frontiers in Medicine* 4, 168-168.

Arbuckle, M.R., McClain, M.T., Rubertone, M.V., Scofield, R.H., Dennis, G.J., James, J.A., Harley, J.B., **2003**. Development of Autoantibodies Before the Clinical Onset of Systemic Lupus Erythematosus. *The New England Journal of Medicine* 349, 1526-1533.

Armstrong, A.J., Marengo, M.S., Oltean, S., Kemeny, G., Bitting, R.L., Turnbull, J.D., Herold, C.I., Marcom, P.K., George, D.J., Garcia-Blanco, M.A., **2011**. Circulating Tumor Cells From Patients With Advanced Prostate and Breast Cancer Display Both Epithelial and Mesenchymal Markers. *Molecular Cancer Research* 9, 997-1007.

Aronson, J.K., **2005**. Biomarkers and Surrogate Endpoints. *British Journal of Clinical Pharmacology* 59, 491-494.

Ashcroft, R.G., Lopez, P.A., **2000**. Commercial High Speed Machines Open New Opportunities in High Throughput Flow Cytometry (HTFC). *Journal of Immunological Methods* 243, 13-24.

Ashkarran, A.A., Suslick, K.S., Mahmoudi, M., **2020**. Magnetically Levitated Plasma Proteins. *Analytical Chemistry* 92, 1663-1668.

Axelsson, H., **2009**. Cell Separation, Centrifugation. *Encyclopedia of Industrial Biotechnology: Bioprocess, Bioseparation, and Cell Technology*, M.C. Flickinger (Ed.) 1-21.

Balogh, E., Nass, S.J., Patlak, M., **2010**. *Extending the Spectrum of Precompetitive Collaboration in Oncology Research: Workshop Summary*. National Academies Press.

Bantikassegn, A., Song, X., Politi, K., **2015**. Isolation of Epithelial, Endothelial, and Immune Cells From Lungs of Transgenic Mice With Oncogene-Induced Lung Adenocarcinomas. *American Journal of Respiratory Cell and Molecular biology* 52, 409-417.

Barani, A., Paktinat, H., Janmaleki, M., Mohammadi, A., Mosaddegh, P., Fadaei-Tehrani, A., Sanati-Nezhad, A., **2016**. Microfluidic Integrated Acoustic Waving for Manipulation of Cells and Molecules. *Biosensors and Bioelectronics* 85, 714-725.

Batrla, R., Jordan, B.W.M., **2015**. Personalized Health Care Beyond Oncology: New Indications for Immunoassay-Based Companion Diagnostics. *Annals of the New York Academy of Sciences*1346, 71-80.

Battistoni, A., Rubattu, S., Volpe, M., **2012**. Circulating Biomarkers With Preventive, Diagnostic and Prognostic Implications in Cardiovascular Diseases. *International Journal of Cardiology* 157, 160-168.

Bauwens, C.L., Peerani, R., Niebruegge, S., Woodhouse, K.A., Kumacheva, E., Husain, M., Zandstra, P.W., **2008**. Control of Human Embryonic Stem Cell Colony and Aggregate Size Heterogeneity Influences Differentiation Trajectories. *Stem Cells* 26, 2300-2310.

Benz, L., Cesafsky, K.E., Le, T., Park, A., Malicky, D., **2012**. Employing Magnetic Levitation To Monitor Reaction Kinetics and Measure Activation Energy. *Journal of Chemical Education* 89, 776-779.

Beutler, B., Cerami, A., **1988**. Tumor Necrosis, Cachexia, Shock, and Inflammation: A Common Mediator. *Annual Review of Biochemistry* 57, 505-518.

Bhagat, A.A.S., Bow, H., Hou, H.W., Tan, S.J., Han, J., Lim, C.T., **2010**. Microfluidics for cell separation. *Medical and Biological Engineering and Computing* 48, 999-1014.

Bhuvanendran Nair Gourikutty, S., Chang, C.P., Puiu, P.D., **2016**. Microfluidic Immunomagnetic Cell Separation From Whole Blood. *Journal of Chromatography. B* 1011, 77-88.

Biomarkers Definitions Working, G., Atkinson Jr, A.J., Colburn, W.A., DeGruttola, V.G., DeMets, D.L., Downing, G.J., Hoth, D.F., Oates, J.A., Peck, C.C., Schooley, R.T., **2001**. Biomarkers and Surrogate Endpoints: Preferred Definitions and Conceptual Framework. *Clinical Pharmacology and Therapeutics* 69, 89-95.

Blennow, K., Zetterberg, H., **2015**. The Past and the Future of Alzheimer's Disease Csf Biomarkers—a Journey Toward Validated Biochemical Tests Covering the Whole Spectrum of Molecular Events. *Frontiers in Neuroscience* 9, 345.

Bojorge Ramírez, N., Salgado, A.M., Valdman, B., **2009**. The Evolution and Developments of Immunosensors for Health and Environmental Monitoring: Problems and Perspectives. *Brazilian Journal of Chemical Engineering* 26, 227-249.

Boxshall, K., Wu, M.-H., Cui, Z., Cui, Z., Watts, J.F., Baker, M.A., **2006**. Simple Surface Treatments To Modify Protein Adsorption and Cell Attachment Properties Within a Poly(dimethylsiloxane) Micro-Bioreactor. *Surface and Interface Analysis* 38, 198-201.

Bozorth, R.M., **1947**. Magnetism. *Reviews of Modern Physics* 19, 29-86.

Brehm-Stecher, B.F., **2014**. Flow Cytometry, in: Batt, C.A., Tortorello, M.L. (Eds.), *Encyclopedia of Food Microbiology* (Second Edition). Academic Press, Oxford, pp. 943-953.

Brody, T., **2016**. Chapter 19 - Biomarkers, in: Brody, T. (Ed.), *Clinical Trials* (Second Edition). Academic Press, Boston, pp. 377-419.

Bryan, A.K., Hecht, V.C., Shen, W., Payer, K., Grover, W.H., Manalis, S.R., **2014**. Measuring Single Cell Mass, Volume, and Density With Dual Suspended Microchannel Resonators. *Lab on a Chip* 14, 569-576.

Byun, S., Son, S., Amodei, D., Cermak, N., Shaw, J., Kang, J.H., Hecht, V.C., Winslow, M.M., Jacks, T., Mallick, P., Manalis, S.R., **2013**. Characterizing Deformability and Surface Friction of Cancer Cells. *Proceedings of the National Academy of Sciences* 110, 7580-7585.

Çağlayan, Z., Demircan Yalçın, Y., Külah, H., **2020**. Examination of the Dielectrophoretic Spectra of MCF7 Breast Cancer Cells and Leukocytes. *Electrophoresis* 41, 345-352.

Callister, W.D., Rethwisch, D.G., **2018**. *Materials Science and Engineering: An Introduction* pp.344-348. Wiley New York.

Candlish, A.A.G., **1991**. Immunological Methods in Food Microbiology. *Food Microbiology* 8, 1-14.

Carl, P., Ramos, I.I., Segundo, M.A., Schneider, R.J., **2019**. Antibody Conjugation to Carboxyl-Modified Microspheres Through N-Hydroxysuccinimide Chemistry for Automated Immunoassay Applications: A General Procedure. *Plos One* 14, e0218686-e0218686.

Castillo-León, J., Svendsen, W.E., (Eds.) **2014**. *Lab-on-a-Chip devices and Micro-Total Analysis Systems: A Practical Guide.* Springer.

Castillo-León, J., Svendsen, W.E., Dimaki, M., **2011**. *Micro and Nano Techniques for the Handling of Biological Samples.* CRC Press.

Castro, B., de Medeiros, M.S., Sadri, B., Martinez, R.V., **2018**. Portable and Power-Free Serodiagnosis of Chagas Disease Using Magnetic Levitating Microbeads. *Analyst* 143, 4379-4386.

Chalmers, J.J., Zhao, Y., Nakamura, M., Melnik, K., Lasky, L., Moore, L., Zborowski, M., **1999**. Instrument to Determine the Magnetophoretic Mobility of Labeled, Biological Cells and Paramagnetic Particles. *Journal of Magnetism and Magnetic Materials* 194, 231-241.

Chan, C.P., Rainer, T.H., **2013**. Pathophysiological Roles and Clinical Importance of Biomarkers in Acute Coronary Syndrome. *Advances in Clinical Chemistry* 59, 23-63.

Chattopadhyay, P.K., **2011**. Chapter 18 - Quantum Dot Technology in Flow Cytometry, in: Darzynkiewicz, Z., Holden, E., Orfao, A., Telford, W., Wlodkowic, D. (Eds.), *Methods in Cell Biology* pp. 463-477. Academic Press,

Chen, Q., Zhang, Z.-H., Wang, S., Lang, J.-H., **2019**. Circulating Cell-Free DNA or Circulating Tumor DNA in the Management of Ovarian and Endometrial Cancer. *OncoTargets and Therapy* 12, 11517-11530.

Chen, Z.-Y., Zhong, W.-Z., Zhang, X.-C., Su, J., Yang, X.-N., Chen, Z.-H., Yang, J.-J., Zhou, Q., Yan, H.-H., An, S.-J., Chen, H.-J., Jiang, B.-Y., Mok, T.S., Wu, Y.-L., **2012**. EGFR Mutation Heterogeneity and the Mixed Response to EGFR Tyrosine Kinase Inhibitors of Lung Adenocarcinomas. *The Oncologist* 17, 978-985.

Cheng, X., Irimia, D., Dixon, M., Ziperstein, J.C., Demirci, U., Zamir, L., Tompkins, R.G., Toner, M., Rodriguez, W.R., **2007**. A Microchip Approach for Practical Label-Free CD4+ T-Cell Counting of HIV-Infected Subjects in Resource-Poor Settings. *Journal of Acquired Immune Deficiency Syndromes* 45, 257-261.

Chin, C.D., Linder, V., Sia, S.K., **2007**. Lab-on-a-Chip Devices for Global Health: Past Studies and Future Opportunities. *Lab on a Chip* 7, 41-57.

Chou, J., Wong, J., Christodoulides, N., Floriano, P.N., Sanchez, X., McDevitt, J., **2012**. Porous Bead-Based Diagnostic Platforms: Bridging the Gaps in Healthcare. *Sensors* (Basel, Switzerland) 12, 15467-15499.

Christenson, R.H., Newby, L.K., Ohman, E.M., **1997**. Cardiac Markers in the Assessment of Acute Coronary Syndromes *Maryland Medical Journal* pp. 18-24 (Baltimore, Md.: 1985).

Coey, J.M., **2010**. *Magnetism and Magnetic Materials*. Cambridge University Press.

Coleman, J.W., Yeung, J.H.K., Tingle, M.D., Park, B.K., **1986**. Enzyme-Linked Immunosorbent Assay (ELISA) for Detection of Antibodies to Protein-Reactive Drugs and Metabolites: Criteria for Identification of Antibody Activity: Detection and Hapten Specificity of Anti-Dnp, Anti-Captopril and Anti-Sulphanilamidobenzoic Acid. *Journal of Immunological Methods* 88, 37-44.

Cornaglia, M., Trouillon, R., Tekin, H.C., Lehnert, T., Gijs, M.A.M., **2014**. Magnetic Particle-Scanning for Ultrasensitive Immunodetection On-Chip. *Analytical Chemistry* 86, 8213-8223.

Crowther, J.R., **2001**. *The ELISA Guidebook*. Springer Science and Business Media.

Cukauskas, E.J., Vincent, D.A., Deaver, B.S., **1974**. Magnetic Susceptibility Measurements Using a Superconducting Magnetometer. *Review of Scientific Instruments* 45, 1-6.

Cullity, B.D., Graham, C.D., **2008**. *Introduction to Magnetic Materials*. Wiley-IEEE Press.

Cullity, B.D., Graham, C.D., **2011**. *Introduction to Magnetic Materials*. John Wiley and Sons.

Cummins, B., Auckland, M.L., Cummins, P., **1987**. Cardiac-Specific Troponin-I Radioimmunoassay in the Diagnosis of Acute Myocardial Infarction. *American Heart Journal* 113, 1333-1344.

Dai, H., Zhu, J., Yang, Z., Li, J., Jiao, X., Hu, X., Wang, J., **2013**. A Paramagnetic Microspheres Based Automation-Friendly Rapid Chemiluminescent

Immunoassay Method for Sensitive Detection of Chicken Interferon-γ. *Chemical Communications* 49, 1708-1710.

Darwish, I.A., **2006**. Immunoassay Methods and their Applications in Pharmaceutical Analysis: Basic Methodology and Recent Advances. *International Journal of Biomedical Science* 2, 217-235.

Davis, J.A., Inglis, D.W., Morton, K.J., Lawrence, D.A., Huang, L.R., Chou, S.Y., Sturm, J.C., Austin, R.H., **2006**. Deterministic Hydrodynamics: Taking Blood Apart *Proceedings of the National Academy of Sciences* 103, 14779-14784.

de Abreu Costa, L., Henrique Fernandes Ottoni, M., Dos Santos, M.G., Meireles, A.B., Gomes de Almeida, V., de Fátima Pereira, W., Alves de Avelar-Freitas, B., Eustáquio Alvim Brito-Melo, G., **2017**. Dimethyl Sulfoxide (DMSO) Decreases Cell Proliferation and TNF-α, IFN-γ, and IL-2 Cytokines Production in Cultures of Peripheral Blood Lymphocytes. *Molecules* (Basel, Switzerland) 22, 1789.

Del Ben, F., Turetta, M., Celetti, G., Piruska, A., Bulfoni, M., Cesselli, D., Huck, W.T., Scoles, G., **2016**. A Method for Detecting Circulating Tumor Cells Based on the Measurement of Single-Cell Metabolism in Droplet-Based Microfluidics. *Angewandte Chemie* 128, 8723-8726.

Delikoyun, K., Yaman, S., Tekin, H.C., **2019a**. Density-Based Separation of Microparticles Using Magnetic Levitation Technology Integrated on Lensless Holographic Microscopy Platform, 2019 *Innovations in Intelligent Systems and Applications Conference (ASYU)*, pp. 1-6.

Delikoyun, K., Cine, E., Anil-Inevi, M., Ozuysal, M., Ozcivici, E., Tekin, H.C., **2019b**. Lensless Digital in-Line Holographic Microscopy for Space Biotechnology Applications, 2019 *9th International Conference on Recent Advances in Space Technologies (RAST)*, pp. 937-940.

Delikoyun, K., Yaman, S., Anil-Inevi, M., Ozcivici, E., Tekin, H.C., **2019c**. Cell Separation with Hybrid Magnetic Levitation-Based Lensless Holographic Microscopy Platform, 2019 *Medical Technologies Congress (TIPTEKNO)*, pp. 1-4.

Deng, L., Kitova, E.N., Klassen, J.S., **2013**. Dissociation Kinetics of the Streptavidin–Biotin Interaction Measured Using Direct Electrospray Ionization Mass Spectrometry Analysis. *Journal of The American Society for Mass Spectrometry* 24, 49-56.

DePriest, A.Z., Black, D.L., Robert, T.A., **2015**. Immunoassay in Healthcare Testing Applications. *Journal of Opioid Management* 11, 13-25.

Desai, M., Stockbridge, N., Temple, R., **2006**. Blood Pressure as an Example of a Biomarker That Functions as a Surrogate. *The AAPS Journal* 8, E146-E152.

Dhar, D., Roy, S., Nigam, V.K., **2019**. Chapter 10 - Advances in Protein/Enzyme-Based Biosensors for the Detection of Pharmaceutical Contaminants in the Environment, In: Kaur Brar, S., Hegde, K., Pachapur, V.L. (Eds.), *Tools, Techniques and Protocols for Monitoring Environmental Contaminants* pp. 207-229. Elsevier,

Diamandis, E.P., Christopoulos, T.K., **1991**. The Biotin-(Strept)Avidin System: Principles and Applications in Biotechnology. *Clinical Chemistry* 37, 625-636.

Diem, S., Fässler, M., Bomze, D., Ali, O.H., Berner, F., Niederer, R., Hillmann, D., Mangana, J., Levesque, M.P., Dummer, R., Risch, L., Recher, M., Risch, M., Flatz, L., **2019**. Immunoglobulin G and Subclasses as Potential Biomarkers in Metastatic Melanoma Patients Starting Checkpoint Inhibitor Treatment. *Journal of Immunotherapy* 42, 89-93.

Dodeigne, C., Thunus, L., Lejeune, R., **2000**. Chemiluminescence as Diagnostic Tool. A Review. *Talanta* 51, 415-439.

Dokainish, H., Pillai, M., Murphy, S.A., DiBattiste, P.M., Schweiger, M.J., Lotfi, A., Morrow, D.A., Cannon, C.P., Braunwald, E., Lakkis, N., 2005. Prognostic Implications of Elevated Troponin in Patients With Suspected Acute Coronary Syndrome but No Critical Epicardial Coronary Disease: A TACTICS-TIMI-18 Substudy. *Journal of the American College of Cardiology* 45, 19-24.

Duffy, M.J., Crown, J., **2008**. A Personalized Approach to Cancer Treatment: How Biomarkers Can Help. *Clinical Chemistry* 54, 1770-1779.

Dunbar, S.A., **2006**. Applications of Luminex xMAP Technology for Rapid, High-Throughput Multiplexed Nucleic Acid Detection. *Clinica Chimica Acta* 363, 71-82.

Durmus, N.G., Tekin, H.C., Guven, S., Sridhar, K., Arslan Yildiz, A., Calibasi, G., Ghiran, I., Davis, R.W., Steinmetz, L.M., Demirci, U., **2015**. Magnetic Levitation of Single Cells. *Proceedings of the National Academy of Sciences* 112, 1-8.

Dzoyem, J.P., Kuete, V., Eloff, J.N., **2014**. 23 - Biochemical Parameters in Toxicological Studies in Africa: Significance, Principle of Methods, Data Interpretation, and Use in Plant Screenings, in: Kuete, V. (Ed.) T*oxicological Survey of African Medicinal Plants* pp. 659-715. Elsevier.

Eberwine, J., Yeh, H., Miyashiro, K., Cao, Y., Nair, S., Finnell, R., Zettel, M., Coleman, P., **1992**. Analysis of gene expression in single live neurons. *Proceedings of the National Academy of Sciences* 89, 3010-3014.

Eisen, H.N., Chakraborty, A.K., **2010**. Evolving Concepts of Specificity in Immune Reactions. *Proceedings of the National Academy of Sciences* 107, 22373-22380.

Elshal, M.F., McCoy, J.P., **2006**. Multiplex Bead Array Assays: Performance Evaluation and Comparison of Sensitivity to ELISA. *Methods* (San Diego, Calif.) 38, 317-323.

Emaminejad, S., Javanmard, M., Dutton, R.W., Davis, R.W., **2012**. Microfluidic Diagnostic Tool for the Developing World: Contactless Impedance Flow Cytometry. *Lab on a Chip* 12, 4499-4507.

Engvall, E., Perlmann, P., **1971**. Enzyme-Linked Immunosorbent Assay (ELISA). Quantitative Assay of Immunoglobulin G. *Immunochemistry* 8, 871-874.

Ersoy, H., Rybicki, F.J., **2007**. Biochemical Safety Profiles of Gadolinium-Based Extracellular Contrast Agents and Nephrogenic Systemic Fibrosis. *Journal of Magnetic Resonance Imaging* 26, 1190-1197.

Farajollahi, M.M., Cook, D.B., Hamzehlou, S., Self, C.H., **2012**. Reduction of Non-Specific Binding in Immunoassays Requiring Long Incubations. *Scandinavian Journal of Clinical and Laboratory Investigation* 72, 531-539.

Felton, E.J., Velasquez, A., Lu, S., Murphy, R.O., ElKhal, A., Mazor, O., Gorelik, P., Sharda, A., Ghiran, I.C., **2016**. Detection and Quantification of Subtle Changes in Red Blood Cell Density Using a Cell Phone. *Lab on a Chip* 16, 3286-3295.

Filatov, V.L., Katrukha, A.G., Bulargina, T.V., Gusev, N.B., **1999**. Troponin: Structure, Properties, and Mechanism of Functioning. *Biochemistry* (Moscow) 64, 969-985.

Foner, S., **1959**. Versatile and Sensitive Vibrating-Sample Magnetometer. *Review of Scientific Instruments* 30, 548-557.

Frei, K., Bernstein, H.J., **1962**. Method for Determining Magnetic Susceptibilities by NMR. *The Journal of Chemical Physics* 37, 1891-1892.

Füzéry, A.K., Levin, J., Chan, M.M., Chan, D.W., **2013**. Translation of Proteomic Biomarkers Into FDA Approved Cancer Diagnostics: Issues and Challenges. *Clinical Proteomics* 10, 13-13.

Gao, D., Jin, F., Zhou, M., Jiang, Y., **2019a**. Recent Advances in Single Cell Manipulation and Biochemical Analysis on Microfluidics. *Analyst* 144, 766-781.

Gao, Q.-H., Zhang, W.-M., Zou, H.-X., Li, W.-B., Yan, H., Peng, Z.-K., Meng, G., **2019b**. Label-Free Manipulation via the Magneto-Archimedes Effect: Fundamentals, Methodology and Applications. *Materials Horizons* 6, 1359-1379.

Garcia, J., Liu, S.Z., Louie, A.Y., **2017**. Biological Effects of MRI Contrast Agents: Gadolinium Retention, Potential Mechanisms and a Role for Phosphorus. *Philosophical Transactions. Series A, Mathematical, Physical, and Engineering Sciences* 375, 20170180.

Gaster, R.S., Hall, D.A., Nielsen, C.H., Osterfeld, S.J., Yu, H., Mach, K.E., Wilson, R.J., Murmann, B., Liao, J.C., Gambhir, S.S., Wang, S.X., **2009**. Matrix-Insensitive Protein Assays Push the Limits of Biosensors in Medicine. *Nature Medicine* 15, 1327-1332.

Ge, S., Nemiroski, A., Mirica, k.A., Mace, C.R., Hennek, J.W., Kumar, A.A., Whitesides, G.M., **2019**. Magnetic Levitation in Chemistry, Materials Science, and Biochemistry. *Angewandte Chemie International Edition*.

Ge, S., Wang, Y., Deshler, N.J., Preston, D.J., Whitesides, G.M., **2018**. High-Throughput Density Measurement Using Magnetic Levitation. *Journal of the American Chemical Society* 140, 7510-7518.

Ge, S., Whitesides, G.M., **2018**. "Axial" Magnetic Levitation Using Ring Magnets Enables Simple Density-Based Analysis, Separation, and Manipulation. *Analytical Chemistry* 90, 12239-12245.

Gijs, M.A.M., **2004**. Magnetic Bead Handling On-Chip: New Opportunities for Analytical Applications. *Microfluidics and Nanofluidics* 1, 22-40.

Giljohann, D.A., Mirkin, C.A., **2009**. Drivers of Biodiagnostic Development. *Nature* 462, 461-464.

Gohring, J.T., Dale, P.S., Fan, X., **2010**. Detection of HER2 Breast Cancer Biomarker Using the Opto-Fluidic Ring Resonator Biosensor. *Sensors and Actuators B: Chemical* 146, 226-230.

Gómez-Pastora, J., Karampelas, I.H., Bringas, E., Furlani, E.P., Ortiz, I., **2019**. Numerical Analysis of Bead Magnetophoresis from Flowing Blood in a Continuous-Flow Microchannel: Implications to the Bead-Fluid Interactions. *Scientific Reports* 9, 7265.

Gorodeski, E.Z., Ishwaran, H., Kogalur, U.B., Blackstone, E.H., Hsich, E., Zhang, Z.-m., Vitolins, M.Z., Manson, J.E., Curb, J.D., Martin, L.W., **2011**. Use of Hundreds of Electrocardiographic Biomarkers for Prediction of Mortality in Postmenopausal Women: The Women's Health Initiative. *Circulation: Cardiovascular Quality and Outcomes* 4, 521-532.

Gosho, M., Nagashima, K., Sato, Y., **2012**. Study Designs and Statistical Analyses for Biomarker Research. *Sensors* (Basel, Switzerland) 12, 8966-8986.

Gossett, D.R., Weaver, W.M., MacH, A.J., Hur, S.C., Tse, H.T.K., Lee, W., Amini, H., Di Carlo, D., **2010**. Label-Free Cell Separation and Sorting in Microfluidic Systems. *Analytical and Bioanalytical Chemistry* 397, 3249-3267.

Greve, B., Kelsch, R., Spaniol, K., Eich, H.T., Götte, M., **2012**. Flow Cytometry in Cancer Stem Cell Analysis and Separation. *Cytometry Part A* 81, 284-293.

Grier, D.G., **2003**. A Revolution in Optical Manipulation. *Nature* 424, 810-816.

Grob, D.T., Wise, N., Oduwole, O., Sheard, S., **2018**. Magnetic Susceptibility Characterisation of Superparamagnetic Microspheres. *Journal of Magnetism and Magnetic Materials* 452, 134-140.

Grover, W.H., Bryan, A.K., Diez-Silva, M., Suresh, S., Higgins, J.M., Manalis, S.R., **2011**. Measuring Single-Cell Density. *Proceedings of the National Academy of Sciences* 108, 10992-10996.

Haisler, W.L., Timm, D.M., Gage, J.A., Tseng, H., Killian, T., Souza, G.R., **2013**. Three-Dimensional Cell Culturing by Magnetic Levitation. *Nature Protocols* 8, 1940.

Hall, D.A., Gaster, R.S., Lin, T., Osterfeld, S.J., Han, S., Murmann, B., Wang, S.X., **2010**. GMR Biosensor Arrays: A System Perspective. *Biosensors and Bioelectronics* 25, 2051-2057.

Haroun, M., M El-Sayed, M., **2007**. Measurement of IgG Levels Can Serve as a Biomarker in Newly Diagnosed Diabetic Children. *Journal of Clinical Biochemistry and Nutrition* 40, 56-61.

Hejazian, M., Nguyen, N.T., **2016**. Magnetofluidic Concentration and Separation of Non-Magnetic Particles Using Two Magnet Arrays. *Biomicrofluidics* 10, 044103.

Henry, N.L., Hayes, D.F., **2012**. Cancer Biomarkers. *Molecular Oncology* 6, 140-146.

Herzenberg, L.A., Parks, D., Sahaf, B., Perez, O., Roederer, M., Herzenberg, L.A., **2002**. The History and Future of the Fluorescence Activated Cell Sorter and Flow Cytometry: A View From Stanford. *Clinical Chemistry* 48, 1819-1827.

Heyman, M., Darmon, N., Dupont, C., Dugas, B., Hirribaren, A., Blaton, M.A., Desjeux, J.F., **1994**. Mononuclear Cells From Infants Allergic to Cow's Milk Secrete Tumor Necrosis Factor Alpha, Altering Intestinal Function. *Gastroenterology* 106, 1514-1523.

Honardoost, M., Rajabpour, A., Vakili, L., **2018**. Molecular Epidemiology; New But Impressive. *Medical Journal of the Islamic Republic of Iran* 32, 53-53.

Hoofnagle, A.N., Wener, M.H., **2009**. The Fundamental Flaws of Immunoassays and Potential Solutions Using Tandem Mass Spectrometry. *Journal of Immunological Methods* 347, 3-11.

Hosseini, S., Aeinehvand, M.M., Uddin, S.M., Benzina, A., Rothan, H.A., Yusof, R., Koole, L.H., Madou, M.J., Djordjevic, I., Ibrahim, F., **2015**. Microsphere Integrated Microfluidic Disk: Synergy of Two Techniques for Rapid and Ultrasensitive Dengue Detection. *Scientific Reports* 5, 16485.

Hosseini, S., Vázquez-Villegas, P., Rito-Palomares, M., Martinez-Chapa, S.O., **2018**. Advantages, Disadvantages and Modifications of Conventional ELISA, In: Hosseini, S., Vázquez-Villegas, P., Rito-Palomares, M., Martinez-Chapa, S.O. (Eds.), *Enzyme-linked Immunosorbent Assay (ELISA): From A to Z* pp. 67-115. Springer Singapore.

Hu, P., Zhang, W., Xin, H., Deng, G., **2016**. Single Cell Isolation and Analysis. *Frontiers in Cell and Developmental* Biology 4, 116.

Huang, R., Barber, T.A., Schmidt, M.A., Tompkins, R.G., Toner, M., Bianchi, D.W., Kapur, R., Flejter, W.L., **2008**. A Microfluidics Approach for the Isolation of Nucleated Red Blood Cells (Nrbcs) From the Peripheral Blood of Pregnant Women. *Prenatal Diagnosis* 28, 892-899.

Islam, S., Zeisel, A., Joost, S., La Manno, G., Zajac, P., Kasper, M., Lönnerberg, P., Linnarsson, S., **2014**. Quantitative Single-Cell RNA-Seq With Unique Molecular Identifiers. *Nature Methods* 11, 163-166.

Issa, B., Obaidat, I.M., Albiss, B.A., Haik, Y., **2013**. Magnetic Nanoparticles: Surface Effects and Properties Related to Biomedicine Applications. *International Journal of Molecular Sciences* 14, 21266-21305.

Jackson, E.L., Lu, H., **2013**. Advances in Microfluidic Cell Separation and Manipulation. *Current Opinion in Chemical Engineering* 2, 398-404.

Jacofsky, D., Jacofsky, E.M., Jacofsky, M., **2020**. Understanding Antibody Testing for COVID-19. *The Journal of Arthroplasty* 35, 74-81.

Jamison, D.T., Breman, J.G., Measham, A.R., Alleyne, G., Claeson, M., Evans, D.B., Jha, P., Mills, A., Musgrove, P., **2006**. *Disease Control Priorities in Developing Countries.* The World Bank.

Jamshaid, T., Neto, E.T.T., Eissa, M.M., Zine, N., Kunita, M.H., El-Salhi, A.E., Elaissari, A., **2016**. Magnetic Particles: From Preparation to Lab-On-A-Chip, Biosensors, Microsystems and Microfluidics Applications. *TrAC - Trends in Analytical Chemistry* 79, 344-362.

Jenko, K.L., Zhang, Y., Kostenko, Y., Fan, Y., Garcia-Rodriguez, C., Lou, J., Marks, J.D., Varnum, S.M., **2014**. Development of an Elisa Microarray Assay for the Sensitive and Simultaneous Detection of Ten Biodefense Toxins. *Analyst* 139, 5093-5102.

Ji, T., Liu, D., Liu, F., Li, J., Ruan, Q., Song, Y., Tian, T., Zhu, Z., Zhou, L., Lin, H., **2016**. A Pressure-Based Bioassay for the Rapid, Portable and Quantitative Detection of C-Reactive Protein. *Chemical Communications* 52, 8452-8454.

Jin, Z., Hahn, Y.K., Oh, E., Kim, Y.-P., Park, J.-K., Moon, S.H., Jang, J.-T., Cheon, J., Kim, H.-S., **2009**. Magnetic Nanoclusters for Ultrasensitive Magnetophoretic Assays. *Small* 5, 2243-2246.

Johannsson, A., **1991**. Heterogeneous Enzyme Immunoassay, In: Price, C.P., Newman, D.J. (Eds.), *Principles and Practice of Immunoassay pp.* 295-325. Palgrave Macmillan UK, London.

Jones, E.A., Kinsey, S.E., English, A., Jones, R.A., Straszynski, L., Meredith, D.M., Markham, A.F., Jack, A., Emery, P., McGonagle, D., **2002**. Isolation and Characterization of Bone Marrow Multipotential Mesenchymal Progenitor Cells. *Arthritis and Rheumatism* 46, 3349-3360.

Kacmar, J., Carlson, R., Balogh, S.J., Srienc, F., **2006**. Staining and Quantification of Poly-3-hydroxybutyrate in Saccharomyces cerevisiae and Cupriavidus necator Cell Populations Using Automated Flow Cytometry. *Cytometry Part A* 69A, 27-35.

Kamat, H.A., Adhia, M., Koppikar, G.V., Parekh, B.K., **1999**. Detection of Antibodies to HIV in Saliva. T*he National Medical Journal of India* 12, 159-161.

Kan, C.W., Tobos, C.I., Rissin, D.M., Wiener, A.D., Meyer, R.E., Svancara, D.M., Comperchio, A., Warwick, C., Millington, R., Collier, N., Duffy, D.C., **2020**. Digital Enzyme-Linked Immunosorbent Assays With Sub-Attomolar Detection Limits Based on Low Numbers of Capture Beads Combined With High Efficiency Bead Analysis. *Lab on a Chip* 20, 2122-2135.

Kashevskii, B.E., Kashevskii, S.B., Prokhorov, I.V., Aleksandrova, E.N., Istomin, Y.P., **2006**. Magnetophoresis and the Magnetic Susceptibility of Hela Tumor Cells. *Biophysics* 51, 902-907.

Katsurada, A., Hagiwara, Y., Miyashita, K., Satou, R., Miyata, K., Ohashi, N., Navar, L.G., Kobori, H., **2007**. Novel Sandwich ELISA for Human Angiotensinogen. *American Journal of Physiology-Renal Physiology* 293, F956-F960.

Katus, H.A., Remppis, A., Looser, S., Hallermeier, K., Scheffold, T., Kübler, W., **1989**. Enzyme Linked Immuno Assay of Cardiac Troponin T for the Detection of Acute Myocardial Infarction in Patients. *Journal of Molecular and Cellular Cardiology* 21, 1349-1353.

Kaufmann, S.H.E., **2017**. Remembering Emil von Behring: From Tetanus Treatment to Antibody Cooperation with Phagocytes. *mBio* 8, e00117-00117.

Kausaite-Minkstimiene, A., Ramanaviciene, A., Kirlyte, J., Ramanavicius, A., **2010**. Comparative Study of Random and Oriented Antibody Immobilization Techniques on the Binding Capacity of Immunosensor. *Analytical Chemistry* 82, 6401-6408.

Kecili, S., Tekin, H.C., **2020**. Adhesive Bonding Strategies to Fabricate High-Strength and Transparent 3d Printed Microfluidic Device. *Biomicrofluidics* 14, 024113.

Kern, P., Hemmer, C.J., Van Damme, J., Gruss, H.-J., Dietrich, M., **1989**. Elevated Tumor Necrosis Factor Alpha and Interleukin-6 Serum Levels as Markers for Complicated Plasmodium Falciparum Malaria. *The American Journal of Medicine* 87, 139-143.

Kharisov, B.I., Kharissova, O.V., Ortiz-Mendez, U., **2016**. *CRC Concise Encyclopedia of Nanotechnology.* CRC Press.

Kim, P., Ong, E.H., Li, K.H.H., Yoon, Y.J., Ng, S.H.G., Puttachat, K., **2016**. Low-Cost, Disposable Microfluidics Device for Blood Plasma Extraction Using Continuously Alternating Paramagnetic and Diamagnetic Capture Modes. *Biomicrofluidics* 10, 024110.

Knowlton, S.M., Sencan, I., Aytar, Y., Khoory, J., Heeney, M.M., Ghiran, I.C., Tasoglu, S., **2015a**. Sickle Cell Detection Using a Smartphone. *Scientific Reports* 5, 1-11.

Knowlton, S., Yu, C.H., Jain, N., Ghiran, I.C., Tasoglu, S., **2015b**. Smart-Phone Based Magnetic Levitation for Measuring Densities. *Plos One* 10, e0134400-e0134400.

Knowlton, S., Joshi, A., Syrrist, P., Coskun, A.F., Tasoglu, S., **2017a**. 3D-Printed Smartphone-Based Point of Care Tool for Fluorescence- and Magnetophoresis-Based Cytometry. *Lab on a Chip* 17, 2839-2851.

Knowlton, S.M., Yenilmez, B., Amin, R., Tasoglu, S., **2017b**. Magnetic Levitation Coupled with Portable Imaging and Analysis for Disease Diagnostics. *Journal of Visualized Experiments* 120, e55012.

Ko, Y.J., Maeng, J.H., Ahn, Y., Hwang, S.Y., Cho, N.G., Lee, S.H., **2008**. Microchip-Based Multiplex Electro-Immunosensing System for the Detection of Cancer Biomarkers. *Electrophoresis* 29, 3466-3476.

Krentz, A.J., Hompesch, M., **2016**. Glucose: Archetypal Biomarker in Diabetes Diagnosis, Clinical Management and Research. *Biomarkers in Medicine* 10, 1153-1166.

Kristiansen, G., **2012**. Diagnostic and Prognostic Molecular Biomarkers for Prostate Cancer. *Histopathology* 60, 125-141.

Kumar, A., Bhardwaj, A., **2008**. Methods in Cell Separation for Biomedical Application: Cryogels as a New Tool. *Biomedical Materials* (Bristol, England) 3, 034008.

Kumar, M., Sarin, S.K., **2009**. Biomarkers of Diseases in Medicine. *Current Trends in Science* 70, 403-417.

Kummari, E., Guo-Ross, S.X., Eells, J.B., **2015**. Laser Capture Microdissection--A Demonstration of the Isolation of Individual Dopamine Neurons and the Entire Ventral Tegmental Area. *Journal of Visualized Experiments* 96, e52336.

Kuo, J.S., Zhao, Y., Schiro, P.G., Ng, L., Lim, D.S.W., Shelby, J.P., Chiu, D.T., **2010**. Deformability Considerations in Filtration of Biological Cells. *Lab on a Chip* 10, 837-842.

Laborde, J.M., Sguazza, G.H., Fuentealba, N.A., Corva, S.G., Carbone, C., Galosi, C.M., **2017**. Indirect ELISA (iELISA) for Routine Detection of Antibodies Against Minute Virus of Mice (MVM) in Mice Colonies. *Revista Argentina de Microbiologia* 49, 210-215.

Lam, S.W., Jimenez, C.R., Boven, E., **2014**. Breast Cancer Classification by Proteomic Technologies: Current State of Knowledge. *Cancer Treatment Reviews* 40, 129-138.

Lee, L.J., Yang, S.T., Lai, S., Bai, Y., Huang, W.C., Juang, Y.J., **2006**. Microfluidic Enzyme-Linked Immunosorbent Assay Technology. *Advances in Clinical Chemistry* pp. 255-295. Elsevier.

Lequin, R.M., **2005**. Enzyme Immunoassay (EIA)/Enzyme-Linked Immunosorbent Assay (ELISA). *Clinical Chemistry* 51, 2415-2418.

Li, J., Wu, N., **2013**. *Biosensors Based on Nanomaterials and Nanodevices*. CRC Press.

Li, Y., Fang, X., Li, Q.-Z., **2013a**. Biomarker Profiling for Lupus Nephritis. *Genomics, Proteomics and Bioinformatics* 11, 158-165.

Li, F.-q., Ma, C.-f., Shi, L.-n., Lu, J.-f., Wang, Y., Huang, M., Kong, Q.-q., **2013b**. Diagnostic Value of Immunoglobulin G Antibodies Against Candida Enolase and Fructose-Bisphosphate Aldolase for Candidemia. *BMC Infectious Diseases* 13, 253.

Liang, L., Xuan, X., **2012**. Diamagnetic Particle Focusing Using Ferromicrofluidics With a Single Magnet. *Microfluidics and Nanofluidics* 13, 637-643.

Lichtenberg, J.Y., Ling, Y., Kim, S., **2019**. Non-Specific Adsorption Reduction Methods in Biosensing. *Sensors* (Basel, Switzerland) 19, 2488.

Lim, S.B., Lim, C.T., Lim, W.-T., **2019**. Single-Cell Analysis of Circulating Tumor Cells: Why Heterogeneity Matters. *Cancers* (Basel) 11, 1595.

Lin, C.-C., Wang, J.-H., Wu, H.-W., Lee, G.-B., **2010**. Microfluidic Immunoassays. *Journal of the Association for Laboratory Automation* 15, 253-274.

Linder, V., Verpoorte, E., de Rooij, N.F., Sigrist, H., Thormann, W., **2002**. Application of Surface Biopassivated Disposable Poly(Dimethylsiloxane)/Glass Chips to a Heterogeneous Competitive Human Serum Immunoglobulin G Immunoassay With Incorporated Internal Standard. *Electrophoresis* 23, 740-749.

Liu, H., Rong, P., Jia, H., Yang, J., Dong, B., Dong, Q., Yang, C., Hu, P., Wang, W., Liu, H., Liu, D., **2016**. A Wash-Free Homogeneous Colorimetric Immunoassay Method. *Theranostics* 6, 54-64.

Liu, X., Dai, Q., Austin, L., Coutts, J., Knowles, G., Zou, J., Chen, H., Huo, Q., **2008**. A One-Step Homogeneous Immunoassay for Cancer Biomarker Detection Using Gold Nanoparticle Probes Coupled with Dynamic Light Scattering. *Journal of the American Chemical Society* 130, 2780-2782.

Liu, X., Jiang, H., **2017**. Construction and Potential Applications of Biosensors for Proteins in Clinical Laboratory Diagnosis. *Sensors* (Basel, Switzerland) 17, 2805.

Liu, Y., Lim, K.-M., **2011**. Particle Separation in Microfluidics Using a Switching Ultrasonic Field. *Lab on a Chip* 11, 3167-3173.

Ludwig, J.A., Weinstein, J.N., **2005**. Biomarkers in Cancer Staging, Prognosis and Treatment Selection. *Nature reviews Cancer* 5, 845-856.

Luo, J., He, X., d'Avignon, D.A., Ackerman, J.J.H., Yablonskiy, D.A., **2010**. Protein-Induced Water 1H MR Frequency Shifts: Contributions From Magnetic Susceptibility and Exchange Effects. *Journal of Magnetic Resonance* 202, 102-108.

Luzza, F., Maletta, M., Imeneo, M., Marcheggiano, A., Iannoni, C., Biancone, L., Pallone, F., **1995**. Salivary-Specific Immunoglobulin G in the Diagnosis of Helicobacter Pylori Infection in Dyspeptic Patients. *American Journal of Gastroenterology* (Springer Nature) 90.

Ma, H., Zeng, W., He, H., Zhao, D., Yang, Y., Jiang, D., Zhou, P., Qi, Y., He, W., Zhao, C., Yi, R., Wang, X., Wang, B., Xu, Y., Yang, Y., Kombe Kombe, A.J., Ding, C., Xie, J., Gao, Y., Cheng, L., Li, Y., Ma, X., Jin, T., **2020**. COVID-19 Diagnosis and Study of Serum Sars-Cov-2 Specific IgA, IgM and IgG by Chemiluminescence Immunoanalysis. *medRxiv* 2020.2004.2017.20064907.

Mair, J., Jaffe, A., Apple, F., Lindahl, B., **2015**. *Cardiac Biomarkers* Hindawi.

Manole, E., Bastian, A.E., Popescu, I.D., Constantin, C., Mihai, S., Gaina, G.F., Codrici, E., Neagu, M.T., **2018**. Immunoassay Techniques Highlighting Biomarkers in Immunogenetic Diseases. In *Immunogenetics* IntechOpen.

Maric, D., Maric, I., Barker, J.L., **1998**. Buoyant Density Gradient Fractionation and Flow Cytometric Analysis of Embryonic Rat Cortical Neurons and Progenitor Cells. *Methods* (San Diego, Calif.) 16, 247-259.

Martin, S.J., Bradley, J.G., Cotter, T.G., **1990**. HL-60 Cells Induced to Differentiate Towards Neutrophils Subsequently Die via Apoptosis. *Clinical and Experimental Immunology* 79, 448-453.

Martínez-Sagasti, F., Velasco-López, E., Domingo-Marín, S., Gil-Perdomo, J.M., **2018**. Usefulness of Biomarkers on Infection Management: With or Without Them? *Revista Española de Quimioterapia* 31 (Suppl 1), 43-46.

Mayeux, R., **2004**. Biomarkers: Potential Uses and Limitations. *NeuroRx* 1, 182-188.

McElhinny, M.W., McFadden, P.L., **1999**. *Paleomagnetism: Continents and Oceans*. Elsevier.

McGowan, J.P., Shah, S.S., Small, C.B., Klein, R.S., Schnipper, S.M., Chang, C.J., Rosenstreich, D.L., **2006**. Relationship of Serum Immunoglobulin and Igg Subclass Levels to Race, Ethnicity and Behavioral Characteristics in HIV Infection. *Medical Science Monitor* 12, Cr11-16.

Milne, G., Rhodes, D., MacDonald, M., Dholakia, K., **2007**. Fractionation of Polydisperse Colloid With Acousto-Optically Generated Potential Energy Landscapes. *Optics Letters* 32, 1144-1146.

Miltenyi, S., Müller, W., Weichel, W., Radbruch, A., **1990**. High Gradient Magnetic Cell Separation With MACS. *Cytometry* 11, 231-238.

Mirica, K.A., Phillips, S.T., Mace, C.R., Whitesides, G.M., **2010**. Magnetic Levitation in the Analysis of Foods and Water. *Journal of Agricultural and Food Chemistry* 58, 6565-6569.

Mirica, K.A., Phillips, S.T., Shevkoplyas, S.S., Whitesides, G.M., **2008**. Using Magnetic Levitation To Distinguish Atomic-Level Differences in Chemical Composition of Polymers, and To Monitor Chemical Reactions on Solid Supports. *Journal of the American Chemical Society* 130, 17678-17680.

Mirica, K.A., Shevkoplyas, S.S., Phillips, S.T., Gupta, M., Whitesides, G.M., **2009**. Measuring Densities of Solids and Liquids Using Magnetic Levitation: Fundamentals. *Journal of the American Chemical Society* 131, 10049-10058.

Mishriki, S., Abdel Fattah, A.R., Kammann, T., Sahu, R.P., Geng, F., Puri, I.K., **2019**. Rapid Magnetic 3D Printing of Cellular Structures with MCF-7 Cell Inks. *Research* 2019, 13.

Moon, S., Keles, H.O., Ozcan, A., Khademhosseini, A., Hæggstrom, E., Kuritzkes, D., Demirci, U., **2009**. Integrating Microfluidics and Lensless Imaging for Point-of-Care Testing. *Biosensors and Bioelectronics* 24, 3208-3214.

Motulsky, H.J., Brown, R.E., **2006**. Detecting Outliers When Fitting Data With Nonlinear Regression – A New Method Based on Robust Nonlinear Regression and the False Discovery Rate. *BMC Bioinformatics* 7, 123.

Mrema, J.E., Campbell, G.H., Miranda, R., Jaramillo, A.L., Rieckmann, K.H., **1979**. Concentration and Separation of Erythrocytes Infected with Plasmodium falciparum by Gradient Centrifugation. *Bull World Health Organ* 57, 133-138.

Nathamgari, S.S., Dong, B., Zhou, F., Kang, W., Giraldo-Vela, J.P., McGuire, T., McNaughton, R.L., Sun, C., Kessler, J.A., Espinosa, H.D., **2015**. Isolating Single Cells in a Neurosphere Assay Using Inertial Microfluidics. *Lab on a Chip* 15, 4591-4597.

Negahdary, M., Namayandeh, S.M., Behjati-Ardekani, M., Ghobadzadeh, S., Dehghani, H., Soltani, M.H., **2016**. The Importance of the Troponin Biomarker in Myocardial Infarction. *Journal of Biology and Today's World*, ISSN, 2322-3308.

Nemiroski, A., Soh, S., Kwok, S.W., Yu, H.-D., Whitesides, G.M., **2016**. Tilted Magnetic Levitation Enables Measurement of the Complete Range of Densities of Materials with Low Magnetic Permeability. *Journal of the American Chemical Society* 138, 1252-1257.

Neto, E.C., Rubin, R., Schulte, J., Giugliani, R., **2004**. Newborn Screening for Congenital Infectious Diseases. *Emerging Infectious Diseases* 10, 1068-1073.

Neurohr, G.E., Amon, A., **2020**. Relevance and Regulation of Cell Density. *Trends in Cell Biology* 30, 213-225.

Nistor, C., Emnéus, J., **2005**. Chapter 9 Immunoassay: Potentials and Limitations, *Comprehensive Analytical Chemistry* pp. 375-427. Elsevier.

Notman, R., Noro, M., O'Malley, B., Anwar, J., **2006**. Molecular Basis for Dimethylsulfoxide (DMSO) Action on Lipid Membranes. *Journal of the American Chemical Society* 128, 13982-13983.

Novis, D.A., Jones, B.A., Dale, J.C., Walsh, M.K., **2004**. Biochemical Markers of Myocardial Injury Test Turnaround Time: A College of American Pathologists Q-Probes Study of 7020 Troponin and 4368 Creatine Kinase-MB Determinations in 159 Institutions. *Archives of Pathology and Laboratory Medicine* 128, 158-164.

Oersted, H.C., **1820**. Experiments on the Effect of a Current of Electricity on the Magnetic *Needle Annals of Philosophy* 16, 273-276.

Ohnaga, T., Shimada, Y., Moriyama, M., Kishi, H., Obata, T., Takata, K., Okumura, T., Nagata, T., Muraguchi, A., Tsukada, K., **2013**. Polymeric Microfluidic Devices Exhibiting Sufficient Capture of Cancer Cell Line for Isolation of Circulating Tumor Cells. *Biomedical Microdevices* 15, 611-616.

Orfao, A., Ruiz-Argüelles, A., **1996**. General Concepts About Cell Sorting Techniques. *Clinical Biochemistry* 29, 5-9.

Organization, W.H., **1993**. *Biomarkers and Risk Assessment: Concepts and Principles-Environmental Health Criteria 155*.

Otieno, B.A., Krause, C.E., Rusling, J.F., **2016**. Bioconjugation of Antibodies and Enzyme Labels onto Magnetic Beads. *Methods in Enzymology* 571, 135-150.

Overdevest, J.B., Theodorescu, D., Lee, J.K., **2009**. Utilizing the Molecular Gateway: The Path to Personalized Cancer Management. *Clinical Chemistry* 55, 684-697.

Ozefe, F., Yildiz, A.A., **2020**. Magnetic Levitation Based Applications in Bioscience, In *Magnetic Levitation*. IntechOpen.

Ozinskas, A.J., **1994**. Principles of Fluorescence Immunoassay, In: Lakowicz, J.R. (Ed.), *Topics in Fluorescence Spectroscopy: Probe Design and Chemical Sensing* pp. 449-496. Springer US, Boston, MA.

Palmirotta, R., Lovero, D., Cafforio, P., Felici, C., Mannavola, F., Pellè, E., Quaresmini, D., Tucci, M., Silvestris, F., **2018**. Liquid Biopsy of Cancer: A Multimodal Diagnostic Tool in Clinical Oncology. *Therapeutic Advances in Medical Oncology* 10, 1758835918794630.

Pamme, N., **2006**. Magnetism and Microfluidics. *Lab on a Chip* 6, 24-38.

Petersson, F., Aberg, L., Sward-Nilsson, A.-M., Laurell, T., **2007**. Free Flow Acoustophoresis: Microfluidic-Based Mode of Particle and Cell Separation. *Analytical Chemistry* 79, 5117-5123.

Petracic, O., **2010**. Superparamagnetic Nanoparticle Ensembles. *Superlattices and Microstructures* 47, 569-578.

Piazza, R., **2008**. Thermophoresis: Moving Particles with Thermal Gradients. *Soft Matter* 4, 1740-1744.

Picó, C., Serra, F., Rodríguez, A.M., Keijer, J., Palou, A., **2019**. Biomarkers of Nutrition and Health: New Tools for New Approaches. *Nutrients* 11, 1092.

Pimenta, F.M.C.A., Palma, S.M.U., Constantino-Silva, R.N., Grumach, A.S., **2019**. Hypogammaglobulinemia: A Diagnosis That Must Not Be Overlooked. *Brazilian Journal of Medical and Biological Research* 52, e8926-e8926.

Plouffe, B., Green, J., Murthy, S., **2010**. Microfluidic Cell Separation: Applications and Challenges in Tissue Engineering. In *Microfluidics, BioMEMS, and Medical Microsystems VIII* SPIE vol. 7593, p. 75930P. International Society for Optics and Photonics.

Podaru, G., Chikan, V., **2017**. Chapter 1 Magnetism in Nanomaterials: Heat and Force from Colloidal Magnetic Particles, Magnetic Nanomaterials. *The Royal Society of Chemistry* 2017, 1-24.

Popescu, M., Staton, D., Dorrell, D., Marignetti, F., Hawkins, D., **2013**. Study of the Thermal Aspects in Brushless Permanent Magnet Machines Performance, In *2013 IEEE Workshop on Electrical Machines Design, Control and Diagnosis (WEMDCD)* pp. 60-69. IEEE.

Proczek, G., Gassner, A.-L., Busnel, J.-M., Girault, H.H., **2012**. Total Serum IgE Quantification by Microfluidic ELISA Using Magnetic Beads. *Analytical and Bioanalytical Chemistry* 402, 2645-2653.

Pulli, T., Höyhtyä, M., Söderlund, H., Takkinen, K., **2005**. One-Step Homogeneous Immunoassay for Small Analytes. *Analytical Chemistry* 77, 2637-2642.

Puluca, N., Durmus, N.G., Lee, S., Belbachir, N., Galdos, F.X., Ogut, M.G., Gupta, R., Hirano, K.I., Krane, M., Lange, R., Wu, J.C., Wu, S.M., Demirci, U., **2020**. Levitating Cells to Sort the Fit and the Fat. *Advanced Biosystems* 4, e1900300.

Qian, C., Huang, H., Chen, L., Li, X., Ge, Z., Chen, T., Yang, Z., Sun, L., **2014**. Dielectrophoresis for Bioparticle Manipulation. *International Journal of Molecular Sciences* 15, 18281-18309.

Qiu, X., Zhu, X., Zhang, L., Mao, Y., Zhang, J., Hao, P., Li, G., Lv, P., Li, Z., Sun, X., Wu, L., Zheng, J., Deng, Y., Hou, C., Tang, P., Zhang, S., Zhang, Y., **2003**. Human Epithelial Cancers Secrete Immunoglobulin G with Unidentified Specificity to Promote Growth and Survival of Tumor Cells. *Cancer Research* 63, 6488-6495.

Qureshi, A., Gurbuz, Y., Niazi, J.H., **2012**. Biosensors for Cardiac Biomarkers Detection: A Review. *Sensors and Actuators B: Chemical* 171-172, 62-76.

Raez, J., Blais, D.R., Zhang, Y., Alvarez-Puebla, R.A., Bravo-Vasquez, J.P., Pezacki, J.P., Fenniri, H., **2007**. Spectroscopically Encoded Microspheres for Antigen Biosensing. *Langmuir* 23, 6482-6485.

Ramsey, J.M., **2015**. Central and Peripheral Molecular Profiling of Sex Differences in Schizophrenia, Major Depressive Disorder, and Controls. PhD diss., University of Cambridge.

Recktenwald, D., **1997**. *Cell Separation Methods and Applications*. CRC Press.

Ring, A., Mineyev, N., Zhu, W., Park, E., Lomas, C., Punj, V., Yu, M., Barrak, D., Forte, V., Porras, T., Tripathy, D., Lang, J.E., **2015**. EpCAM Based Capture Detects and Recovers Circulating Tumor Cells From All Subtypes of Breast Cancer Except Claudin-Low. *Oncotarget* 6, 44623-44634.

Rissin, D.M., Kan, C.W., Campbell, T.G., Howes, S.C., Fournier, D.R., Song, L., Piech, T., Patel, P.P., Chang, L., Rivnak, A.J., Ferrell, E.P., Randall, J.D., Provuncher, G.K., Walt, D.R., Duffy, D.C., **2010**. Single-Molecule Enzyme-Linked Immunosorbent Assay Detects Serum Proteins at Subfemtomolar Concentrations. *Nature Biotechnology* 28, 595.

Roberts, N.A., **2015**. The Immune System. *Yale Journal of Biology and Medicine* 88, 99.

Roberts, R., Sobel, B.E., Parker, C.W., **1976**. Radioimmunoassay for Creatine Kinase Isoenzymes. *Science* 194, 855-857.

Rosenweig, R.E., **1985**. *Ferrohydrodynamics*. Cambridge University Press.

Russell, A.P., Evans, C.H., Westcott, V.C., **1987**. Measurement of the Susceptibility of Paramagnetically Labeled Cells With Paramagnetic Solutions. *Analytical Biochemistry* 164, 181-189.

Salazar, A., Velázquez-Soto, H., Ayala-Balboa, J., Jiménez-Martínez, M.C., **2017**. Allergen-Based Diagnostic: Novel and Old Methodologies With New Approaches. *Allergen* 77.

Samarajeewa, U., Wei, C.I., Huang, T.S., Marshall, M.R., **1991**. Application of Immunoassay in the Food Industry. *Critical Reviews in Food Science and Nutrition* 29, 403-434.

Sanderson, R., Bird, K.E., **1977**. Cell Separations by Counterflow Centrifugation, In *Methods in Cell Biology* pp. 1-14. Academic Press.

Sarigil, O., Anil-Inevi, M., Yilmaz, E., Mese, G., Tekin, H.C., Ozcivici, E., **2019**. Label-Free Density-Based Detection of Adipocytes of Bone Marrow Origin Using Magnetic Levitation. *Analyst* 144, 2942-2953.

Schroeder, H.W., Jr., Cavacini, L., **2010**. Structure and Function of Immunoglobulins. *Journal of Allergy and Clinical Immunology* 125, S41-S52.

Self, C.H., Cook, D.B., **1996**. Advances in Immunoassay Technology. *Current Opinion in Biotechnology* 7, 60-65.

Selleck, M.J., Senthil, M., Wall, N.R., **2017**. Making Meaningful Clinical Use of Biomarkers. *Biomark Insights* 12, 1177271917715236.

Seumois, G., Vijayanand, P., **2019**. Single-Cell Analysis to Understand the Diversity of Immune Cell Types That Drive Disease Pathogenesis. *Journal of Allergy and Clinical Immunology* 144, 1150-1153.

Shapiro, N.D., Mirica, K.A., Soh, S., Phillips, S.T., Taran, O., Mace, C.R., Shevkoplyas, S.S., Whitesides, G.M., **2012a**. Measuring Binding of Protein to Gel-Bound Ligands Using Magnetic Levitation. *Journal of the American Chemical Society* 134, 5637-5646.

Shapiro, N.D., Soh, S., Mirica, K.A., Whitesides, G.M., **2012b**. Magnetic Levitation as a Platform for Competitive Protein–Ligand Binding Assays. *Analytical Chemistry* 84, 6166-6172.

Sharma, S., Zapatero-Rodríguez, J., Estrela, P., O'Kennedy, R., **2015**. Point-of-Care Diagnostics in Low Resource Settings: Present Status and Future Role of Microfluidics. *Biosensors* 5, 577-601.

Shen, F., Hwang, H., Hahn, Y.K., Park, J.-K., **2012**. Label-Free Cell Separation Using a Tunable Magnetophoretic Repulsion Force. *Analytical Chemistry* 84, 3075-3081.

Shields, C.W., Reyes, C.D., López, G.P., **2015**. Microfluidic Cell Sorting: A Review of the Advances in the Separation of Cells from Debulking to Rare Cell Isolation. *Lab on a Chip* 15, 1230-1249.

Shrivastava, A., Gupta, V., **2011**. Methods for the Determination of Limit of Detection and Limit of Quantitation of the Analytical Methods. *Chronicles of Young Scientists* 2, 21-25.

Signorelli, S.S., Fiore, V., Malaponte, G., **2014**. Inflammation and Peripheral Arterial Disease: The Value of Circulating Biomarkers. *International Journal of Molecular Medicine* 33, 777-783.

Sikorski, D.J., Caron, N.J., VanInsberghe, M., Zahn, H., Eaves, C.J., Piret, J.M., Hansen, C.L., **2015**. Clonal Analysis of Individual Human Embryonic Stem Cell Differentiation Patterns in Microfluidic Cultures. *Biotechnology Journal* 10, 1546-1554.

Šimúth, J., Bíliková, K., Kováčová, E., Kuzmová, Z., Schroder, W., **2004**. Immunochemical Approach to Detection of Adulteration in Honey: Physiologically Active Royal Jelly Protein Stimulating TNF-α Release Is a

Regular Component of Honey. *Journal of Agricultural and Food Chemistry* 52, 2154-2158.

Skelley, D.S., Brown, L.P., Besch, P.K., **1973**. Radioimmunoassay. *Clinical Chemistry* 19, 146-186.

Sliker, L., Ciuti, G., Rentschler, M., Menciassi, A., **2015**. Magnetically Driven Medical Devices: A Review. *Expert Review of Medical Devices* 12, 737-752.

Smith, A.J., O'Rorke, R.D., Kale, A., Rimsa, R., Tomlinson, M.J., Kirkham, J., Davies, A.G., Wälti, C., Wood, C.D., **2017**. Rapid Cell Separation With Minimal Manipulation for Autologous Cell Therapies. *Scientific Reports* 7, 41872.

Sobieranski, A.C., Inci, F., Tekin, H.C., Yuksekkaya, M., Comunello, E., Cobra, D., von Wangenheim, A., Demirci, U., **2015**. Portable Lensless Wide-Field Microscopy Imaging Platform Based on Digital Inline Holography and Multi-Frame Pixel Super-Resolution. *Light, Science and Applications* 4, e346.

Sörman, A., Zhang, L., Ding, Z., Heyman, B., **2014**. How Antibodies Use Complement to Regulate Antibody Responses. *Molecular Immunology* 61, 79-88.

Spain, E., Venkatanarayanan, A., **2014**. Review of Physical Principles of Sensing and Types of Sensing Materials, In *Comprehensive Materials Processing* pp.5-46. Elsevier.

Spaldin, N.A., **2010**. *Magnetic Materials: Fundamentals and Applications*, 2 ed. Cambridge University Press, Cambridge.

Spees, W.M., Yablonskiy, D.A., Oswood, M.C., Ackerman, J.J.H., **2001**. Water Proton MR Properties of Human Blood at 1.5 Tesla: Magnetic Susceptibility, T1, T2, T, and Non-Lorentzian Signal Behavior. *Magnetic Resonance in Medicine* 45, 533-542.

Staks, T., Schuhmann-Giampieri, G., Frenzel, T., Weinmann, H.J., Lange, L., Platzek, J., **1994**. Pharmacokinetics, Dose Proportionality, and Tolerability of Gadobutrol After Single Intravenous Injection in Healthy Volunteers. *Investigative Radiology* 29, 709-715.

Stern, M., Cohen, M., Danielli, A., **2019**. Configuration and Design of Electromagnets for Rapid and Precise Manipulation of Magnetic Beads in Biosensing Applications. *Micromachines* 10, 784.

Stone, M.J., Willerson, J.T., Gomez-Sanchez, C.E., Waterman, M.R., **1975**. Radioimmunoassay of Myoglobin in Human Serum. Results in Patients With Acute Myocardial Infarction. *The Journal of Clinical Investigation* 56, 1334-1339.

Strimbu, K., Tavel, J.A., **2010**. What Are biomarkers? *Current Opinion in HIV and AIDS* 5, 463-466.

Strzelecka, P.M., Ranzoni, A.M., Cvejic, A., **2018**. Dissecting Human Disease With Single-Cell Omics: Application in Model Systems and in the Clinic. *Disease models and mechanisms* 11.

Subramaniam, A.B., Gonidec, M., Shapiro, N.D., Kresse, K.M., Whitesides, G.M., **2015**. Metal-amplified Density Assays, (MADAs), Including a Density-Linked Immunosorbent Assay (DeLISA). *Lab on a Chip* 15, 1009-1022.

Talasaz, A.H., Powell, A.A., Huber, D.E., Berbee, J.G., Roh, K.-H., Yu, W., Xiao, W., Davis, M.M., Pease, R.F., Mindrinos, M.N., **2009**Isolating Highly Enriched Populations of Circulating Epithelial Cells and Other Rare Cells From Blood Using a Magnetic Sweeper Device. *Proceedings of the National Academy of Sciences* 106, 3970-3975.

Tan, H.T., Low, J., Lim, S.G., Chung, M.C., **2009**. Serum Autoantibodies as Biomarkers for Early Cancer Detection. *The FEBS journal* 276, 6880-6904.

Tao, Q., Zhang, L., Han, X., Chen, H., Ji, X., Zhang, X., **2020**. Magnetic Susceptibility Difference-Induced Nucleus Positioning in Gradient Ultrahigh Magnetic Field. *Biophysical Journal* 118, 578-585.

Tasoglu, S., Khoory, J.A., Tekin, H.C., Thomas, C., Karnoub, A.E., Ghiran, I.C., Demirci, U., **2015**. Levitational Image Cytometry with Temporal Resolution. *Advanced Materials* (Deerfield Beach, Fla.) 27, 3901-3908.

Tekin, H.C., Cornaglia, M., Gijs, M.A.M., **2013**. Attomolar Protein Detection Using a Magnetic Bead Surface Coverage Assay. *Lab on a Chip* 13, 1053-1059.

Tekin, H.C., Gijs, M.A., **2013**. Ultrasensitive Protein Detection: A Case for Microfluidic Magnetic Bead-Based Assays. *Lab on a Chip* 13, 4711-4739.

Tellez-Gabriel, M., Cochonneau, D., Cadé, M., Jubellin, C., Heymann, M.-F., Heymann, D., **2018**. Circulating Tumor Cell-Derived Pre-Clinical Models for Personalized Medicine. *Cancers* (Basel) 11, 19.

Tellez-Gabriel, M., Ory, B., Lamoureux, F., Heymann, M.-F., Heymann, D., **2016**. Tumour Heterogeneity: The Key Advantages of Single-Cell Analysis. *International Journal of Molecular Sciences* 17, 2142.

Timbrell, J.A., **1998**. Biomarkers in Toxicology. *Toxicology* 129, 1-12.

Tomás, A.L., de Almeida, M.P., Cardoso, F., Pinto, M., Pereira, E., Franco, R., Matos, O., **2019**. Development of a Gold Nanoparticle-Based Lateral-Flow Immunoassay

for Pneumocystis Pneumonia Serological Diagnosis at Point-of-Care. *Frontiers in Microbiology* 10, 2917.

Tombach, B., Heindel, W., **2002**. Value of 1.0- M Gadolinium Chelates: Review of Preclinical and Clinical Data on Gadobutrol. *European Radiology* 12, 1550-1556.

Tongdee, M., Yamanishi, C., Maeda, M., Kojima, T., Dishinger, J., Chantiwas, R., Takayama, S., **2020**. One-Incubation One-Hour Multiplex Elisa Enabled by Aqueous Two-Phase Systems. *Analyst* 145, 3517-3527.

Tracey, K.J., Cerami, A., **1994**. Tumor Necrosis Factor: A Pleiotropic Cytokine and Therapeutic Target. *Annual Review of Medicine* 45, 491-503.

Tran, H.T., Liu, Y., Zurita, A.J., Lin, Y., Baker-Neblett, K.L., Martin, A.M., Figlin, R.A., Hutson, T.E., Sternberg, C.N., Amado, R.G., Pandite, L.N., Heymach, J.V., **2012**. Prognostic or Predictive Plasma Cytokines and Angiogenic Factors for Patients Treated With Pazopanib for Metastatic Renal-Cell Cancer: A Retrospective Analysis of Phase 2 and Phase 3 Trials. *The Lancet Oncology* 13, 827-837.

Turker, E., Arslan-Yildiz, A., **2018**. Recent Advances in Magnetic Levitation: A Biological Approach from Diagnostics to Tissue Engineering. *ACS Biomaterials Science and Engineering* 4, 787-799.

Turner, N.C., Reis-Filho, J.S., **2012**. Genetic Heterogeneity and Cancer Drug Resistance. The Lancet Oncology 13, e178-e185.

Urusov, A.E., Petrakova, A.V., Zherdev, A.V., Dzantiev, B.B., **2017**. Application of Magnetic Nanoparticles in Immunoassay. *Nanotechnologies in Russia* 12, 471-479.

van der Wal, F.J., Bergervoet, J.H.W., Achterberg, R.P., Haasnoot, W., **2014**. Bead-based immunoassays, Novel Approaches in Immunoassays pp. 52-71. Future Medicine Ltd.

Vasan, R.S., **2006**. Biomarkers of Cardiovascular Disease. *Circulation* 113, 2335-2362.

Venge, P., Johnston, N., Lindahl, B., James, S., **2009**. Normal Plasma Levels of Cardiac Troponin I Measured by the High-Sensitivity Cardiac Troponin I Access Prototype Assay and the Impact on the Diagnosis of Myocardial Ischemia. *Journal of the American College of Cardiology* 54, 1165-1172.

Vogel, J.H., Kroner, K.-H., **1999**. Controlled Shear Filtration: A Novel Technique for Animal Cell Separation. *Biotechnology and Bioengineering* 63, 663-674.

Wang, L., **2017**. Early Diagnosis of Breast Cancer. *Sensors* (Basel, Switzerland) 17, 1572.

Weeks, I., Woodhead, J.S., **1987**. Chemiluminescence Immunoassay: A New Diagnostic Technology, In: Scheving, L.E., Halberg, F., Ehret, C.F. (Eds.), *Chronobiotechnology and Chronobiological Engineering* pp. 373-379. Springer Netherlands, Dordrecht.

Welch, N.G., Scoble, J.A., Muir, B.W., Pigram, P.J., **2017**. Orientation and Characterization of Immobilized Antibodies for Improved Immunoassays. *Biointerphases* 12, 02D301.

Weston, M.C., Gerner, M.D., Fritsch, I., **2010**. Magnetic Fields for Fluid Motion. *Analytical Chemistry* 82, 3411-3418.

WHO, **2001**. International Programme on Chemical Safety. *Biomarkers in Risk Assessment: Validity and Validation.*World Health Organization.

Wild, D., **2005**. *The immunoassay handbook.* Gulf Professional Publishing.

Wojciechowski, J.C., Narasipura, S.D., Charles, N., Mickelsen, D., Rana, K., Blair, M.L., King, M.R., **2008**. Capture and Enrichment of CD34-Positive Haematopoietic Stem and Progenitor Cells From Blood Circulation Using P-Selectin in an Implantable Device. *British Journal of Haematology* 140, 673-681.

Wolff, A., Perch-Nielsen, I.R., Larsen, U.D., Friis, P., Goranovic, G., Poulsen, C.R., Kutter, J.P., Telleman, P., **2003**. Integrating Advanced Functionality in a Microfabricated High-Throughput Fluorescent-Activated Cell Sorter. *Lab on a Chip* 3, 22-27.

Xia, F., Jin, W., Yin, X., Fang, Z., **2005**. Single-Cell Analysis by Electrochemical Detection With a Microfluidic Device. *Journal of Chromatography A* 1063, 227-233.

Xiao, Y.-D., Paudel, R., Liu, J., Ma, C., Zhang, Z.-S., Zhou, S.-K., **2016**. MRI Contrast Agents: Classification and Application. *International Journal of Molecular Medicine* 38, 1319-1326.

Xu, F., Finley, T.D., Turkaydin, M., Sung, Y., Gurkan, U.A., Yavuz, A.S., Guldiken, R.O., Demirci, U., **2011**. The Assembly of Cell-Encapsulating Microscale Hydrogels Using Acoustic Waves. *Biomaterials* 32, 7847-7855.

Yagiela, J.A., Dowd, F.J., Johnson, B., Mariotti, A., Neidle, E.A., **2010**. *Pharmacology and Therapeutics for Dentistry*. Elsevier Health Sciences.

Yalow, R.S., Berson, S.A., **1960**. Immunoassay of Endogenous Plasma Insulin in Man. *Journal of Clinical Investigation* 39, 1157-1175.

Yamada, M., Harada, M., Okada, T., **2009**. Electrophoretic Levitation and Focusing of Particles by Field Switching. *Analytical Sciences* 25, 279-284.

Yamaguchi, M., Tanimoto, Y., Yamaguchi, M., **2006**. *Magneto-Science: Magnetic Field Effects on Materials: Fundamentals and Applications* pp. 3433-3436. Springer.

Yaman, S., Anil-Inevi, M., Ozcivici, E., Tekin, H.C., **2018**. Magnetic Force-Based Microfluidic Techniques for Cellular and Tissue Bioengineering. *Frontiers in Bioengineering and Biotechnology* 6. 192.

Yang, Y., Nam, S.-W., Lee, N.Y., Kim, Y.S., Park, S., **2008**. Superporous Agarose Beads as a Solid Support for Microfluidic Immunoassay. *Ultramicroscopy* 108, 1384-1389.

Yang, Z., Min Zhou, D., **2006**. Cardiac Markers and Their Point-of-Care Testing for Diagnosis of Acute Myocardial Infarction. *Clinical Biochemistry* 39, 771-780.

Yenilmez, B., Knowlton, S., Tasoglu, S., **2016a**. Self-Contained Handheld Magnetic Platform for Point of Care Cytometry in Biological Samples. *Advanced Materials Technologies* 1, 1600144.

Yenilmez, B., Knowlton, S., Yu, C.H., Heeney, M.M., Tasoglu, S., **2016b**. Label-Free Sickle Cell Disease Diagnosis Using a Low-Cost, Handheld Platform. *Advanced Materials Technologies* 1, 1600100.

You, W.S., Park, J.J., Jin, S.M., Ryew, S.M., Choi, H.R., **2014**. Point-of-Care Test Equipment for Flexible Laboratory Automation. *Journal of Laboratory Automation* 19, 403-412.

Yuan, G.-C., Cai, L., Elowitz, M., Enver, T., Fan, G., Guo, G., Irizarry, R., Kharchenko, P., Kim, J., Orkin, S., Quackenbush, J., Saadatpour, A., Schroeder, T., Shivdasani, R., Tirosh, I., **2017**. Challenges and Emerging Directions in Single-Cell Analysis. *Genome Biology* 18, 84.

Yusuf, S., Pearson, M., Sterry, H., Parish, S., Ramsdale, D., Rossi, P., Sleight, P., **1984**. The Entry ECG in the Early Diagnosis and Prognostic Stratification of Patients With Suspected Acute Myocardial Infarction. *European Heart Journal* 5, 690-696.

Zborowski, M., Chalmers, J.J., Lowrie, W.G., **2017**. Magnetic Cell Manipulation and Sorting, In: Lee, W., Tseng, P., Di Carlo, D. (Eds.), *Microtechnology for Cell Manipulation and Sorting* pp. 15-55. Springer International Publishing, Cham.

Zeegers, D., Venkatesan, S., Koh, S.W., Low, G.K.M., Srivastava, P., Sundaram, N., Sethu, S., Banerjee, B., Jayapal, M., Belyakov, O., Baskar, R., Balajee, A.S., Hande, M.P., **2017**. Biomarkers of Ionizing Radiation Exposure: A Multiparametric Approach. *Genome Integrity* 8, 6-6.

Zhang, C., Zhao, P., Tang, D., Xia, N., Zhang, X., Nie, J., Gu, F., Zhou, H., Fu, J., **2020**. Axial Magnetic Levitation: A High-Sensitive and Maneuverable Density-Based Analysis Device. *Sensors and Actuators B: Chemical* 304, 127362.

Zhang, H., Moore, L.R., Zborowski, M., Williams, P.S., Margel, S., Chalmers, J.J., **2005**. Establishment and Implications of a Characterization Method for Magnetic Nanoparticle Using Cell Tracking Velocimetry and Magnetic Susceptibility Modified Solutions. *Analyst* 130, 514-527.

Zhao, L.-J., Yu, R.-J., Ma, W., Han, H.-X., Tian, H., Qian, R.-C., Long, Y.-T., **2017**. Sensitive Detection of Protein Biomarkers Using Silver Nanoparticles Enhanced Immunofluorescence Assay. *Theranostics* 7, 876-883.

Zhou, L., Zhou, J., Feng, Z., Wang, F., Xie, S., Bu, S., **2016a**. Immunoassay for Tumor Markers in Human Serum Based on Si Nanoparticles and SiC@ AG SERS-Active Substrate. *Analyst* 141, 2534-2541.

Zhou, Y., Basu, S., Laue, E., Seshia, A.A., **2016b**. Single Cell Studies of Mouse Embryonic Stem Cell (mESC) Differentiation by Electrical Impedance Measurements in a Microfluidic Device. *Biosensors and Bioelectronics* 81, 249-258.

Zhu, G.-P., Hejiazan, M., Huang, X., Nguyen, N.-T., **2014**. Magnetophoresis of Diamagnetic Microparticles in a Weak Magnetic Field. *Lab on a Chip* 14, 4609-4615.

VITA

PERSONAL INFORMATION

Name and Surname: Sena Yaman

E-mail: senaymn [at] gmail.com

EDUCATION

Degree	Institution	Year
PhD	İzmir Institute of Technology	2020
MSc	Middle East Technical University	2014
BSc	Ege University	2011

ACADEMIC EMPLOYMENT

Research Assistant, Department of Biotechnology and Bioengineering IZTECH, 2013-2020

SELECTED PUBLICATIONS AND CONFERENCE PAPERS

-Delikoyun, K., **Yaman, S.**, Anil-Inevi, Ozcivici, E. and Tekin, H. C., **2019**. Cell Separation with Hybrid Magnetic Levitation-Based Lensless Holographic Microscopy Platform. Medical Technologies National Congress (TIPTEKNO). Izmir, Turkey

-**Yaman, S.**, Delikoyun, K., Tekin, H.C., **2019**. Magnetic Levitation-Based Protein Detection Using Lensless Digital Inline Holographic Microscopy. 23rd International Conference on Miniaturized Systems for Chemistry and Life Sciences (μTAS). Basel, Switzerland.

-**Yaman, S**. and Tekin H.C., **2018**. Magnetic Levitation-Based Protein Detection Using Magnetic Nanoparticle Labels in a Microcapillary. 44th International Conference on Micro and Nanoengineering (MNE). Copenhagen, Denmark.

-Yaman, S., Anil-Inevi, M., Ozcivici, E., & Tekin, H. C., **2018**. Magnetic Force-Based Microfluidic Techniques For Cellular and Tissue Bioengineering. *Frontiers in Bioengineering and Biotechnology*, 6, 192.

-Anil-Inevi, M., **Yaman, S.**, Yildiz, A. A., Mese, G., Yalcin-Ozuysal, O., Tekin, H. C., & Ozcivici, E., **2018**. Biofabrication of In Situ Self-Assembled 3D Cell Cultures in a Weightlessness Environment Generated Using Magnetic Levitation. *Scientific Reports*, 8, 7239

-**Yaman, S.** and Tekin, H. C., **2020**. Magnetic Susceptiblity-Based Protein Detection Using Magnetic Levitation. *Analytical Chemisty*, DOI: 10.1021/acs.analchem.0c02479.